2015

Investigation of Cavitating Flow Luminescence for Analytical Spectroscopy

Claire Margaret Frances Whitfield

Recommended Citation

Whitfield, C. (2015) *Investigation of Cavitating Flow Luminescence for Analytical Spectroscopy.* Thesis. University of Plymouth. Retrieved from https://pearl.plymouth.ac.uk/fose-theses-other/17

PEARL

PHD

Investigation of Cavitating Flow Luminescence for Analytical Spectroscopy

Whitfield, Claire Margaret Frances

Award date:
2015

Awarding institution:
University of Plymouth

Link to publication in PEARL

All content in PEARL is protected by copyright law.

The author assigns certain rights to the University of Plymouth including the right to make the thesis accessible and discoverable via the British Library's Electronic Thesis Online Service (EThOS) and the University research repository (PEARL), and to undertake activities to migrate, preserve and maintain the medium, format and integrity of the deposited file for future discovery and use.

Copyright and Moral rights arising from original work in this thesis and (where relevant), any accompanying data, rests with the Author unless stated otherwise*.

Re-use of the work is allowed under fair dealing exceptions outlined in the Copyright, Designs and Patents Act 1988 (amended), and the terms of the copyright licence assigned to the thesis by the Author.

In practice, and unless the copyright licence assigned by the author allows for more permissive use, this means,

That any content or accompanying data cannot be extensively quoted, reproduced or changed without the written permission of the author / rights holder

That the work in whole or part may not be sold commercially in any format or medium without the written permission of the author / rights holder

* Any third-party copyright material in this thesis remains the property of the original owner. Such third-party copyright work included in the thesis will be clearly marked and attributed, and the original licence under which it was released will be specified . This material is not covered by the licence or terms assigned to the wider thesis and must be used in accordance with the original licence; or separate permission must be sought from the copyright holder.

Investigation of Cavitating Flow Luminescence for Analytical Spectroscopy

By

Claire Margaret Frances Whitfield, BSc (Hons)

A thesis submitted to Plymouth University

in partial fulfilment for the degree of

DOCTOR OF PHILOSOPHY

Earth and Environmental Sciences Doctoral Training Centre

This thesis is dedicated to John Briggs for his enthusiasm, inspiration and encouragement.

Abstract

Claire Margaret Frances Whitfield

Investigation of Cavitating Flow Luminescence for Analytical Spectroscopy

Cavitating Flow Luminescence (CFL) is spontaneous photon emission associated with hydrodynamic cavitation which occurs when a flowing liquid passes through a Venturi.[1] In this work, cavitation and micro-plasma generation in a flowing liquid, using a micro-Venturi, has been investigated. A bench-top system was designed and constructed to study CFL in a variety of liquids. The system comprised a high flow, liquid handling manifold and micro-Venturi with a variety of orifice sizes ranging from 160 – 220 µm i.d. The CFL was detected for the first time on a micro-scale using a PMT. The effect of various parameters such as temperature, flow rate (a proxy for the pressure differential) and orifice diameter were investigated to optimise the system. Studies were carried out using DDW and the effect of temperature, pressure and orifice size on CFL; it was found that low temperatures and high pressures resulted in more intense CFL. The effect of re-gassing with different noble gases was investigated and resulted in a large increase in CFL. Investigations in to the effect of solute concentration on CFL were performed using dimethylsulphoxide, polyethyleneglycol-200, isopropanol, diethyleneglycol and Triton X 100 & titanium sulphate nano-particles. Solutes with low vapour pressures resulted in an increase in CFL whereas solutes with a high vapour pressure supressed CFL, due to quenching effects. Low resolution spectra were produced using bandwidth filters to identify wavelength areas of strong emission from CFL.

Contents

LIST OF CONTENTS

List of Figures

Acknowledgments

First and foremost I would like to thank my supervisor Dr. E. Hywel Evans for his superb supervision, encouragement and support, throughout this project. Your guidance and patience have been vital and I could not have asked for a better advisor.

I would also like to thank my second supervisor Dr. Mike Foulkes for his constant encouragement and enlightening chats.

Thank you to Andy Fisher, Claire Williams, Andrew Tonkin, Andy Arnold, and Ian Doidge for their invaluable help scavenging/fixing/jerry-rigging or if all else failed buying equipment for my research. I would like to thank Roy Lowry for all the rambling conversations, silly email exchanges and generally attempting to keep me sane, despite the odds.

I would like to thank all the people who have made life in Plymouth during my PhD better for being a part of it, in particular: Charlotte, Morwenna, Neil, Nick, Lauren and Leoni – thank you for all the proof reading! Thank you to my family especially my Mum and Auntie Patricia for all your ongoing support and love, without you I would be lost.

Author's Declaration

At no time during the registration for the degree of Doctor of Philosophy has the author been registered for any other University award.

Work submitted for this research degree at the Plymouth University has not formed part of any other degree either at Plymouth University or at another establishment

This study was financed with the aid of a studentship from Plymouth University.

A programme of advanced study was undertaken, with relevant scientific seminars and conferences at which work was presented.

Presentation and Conferences Attended:

Whitfield, C.M.F., Evans E.H., Foulkes M.E. Cavitating Flow Luminescence (CFL) A Potential Source for Analytical Spectroscopy? (Oral presentation) 2nd Annual Biogeochemistry Conference, Plymouth University, UK, December 2010.

Whitfield, C.M.F., Evans E.H., Foulkes M.E. Cavitating Flow Luminescence (CFL) A Potential Source for Analytical Spectroscopy? (Oral presentation) Analytical Research Forum 2011, University of Manchester, UK, July 2011.

Whitfield, C.M.F., Evans E.H., Foulkes M.E. Cavitation Flow Luminescence (CFL) for Analytical Spectroscopy (Oral presentation) 4th Annual Biogeochemistry Conference, Plymouth University, UK, December 2012.

Whitfield, C.M.F., Evans E.H., Foulkes M.E. Cavitation Flow Luminescence (CFL) for Analytical Spectroscopy (Oral presentation) Biennial National Atomic Spectroscopy Symposium TraceSpec tandem conference 2014, University of Aberdeen, UK, August 2014.

Word count of main body of thesis: 15121

Signed……………………………………………….

Dated……………………………………………….

Glossary

Adiabatic	A change where there is no loss or gain of heat
Atomic emission	Emission of light at discrete wavelengths wave lengths by atoms which have been electronically excited.
Attenuation	The decrease with distance in the amplitude of a signal.
Bulbous	A spherical swelling.
Cavitation	The disruption of a liquid into a 2 phase system of liquid and gas.
Cavitation Flow Luminescence	The effect observed when light is emitted from the plasma generated by cavitating flow.
Cohesive forces	The forces between atoms / molecules holding them together.
Filamentous	Thread like.
Flow coefficient	An experimentally determined proportionality, relating the actual velocity of fluid flow in a pipe to the theoretical velocity.
Fluorescence	Emission of electromagnetic radiation that is caused by the flow of some form of energy into the emitting body and which ceases abruptly when the excitation ceases.
Free radical	An atom or molecule which possesses an unpaired electron.
Heat capacity	The quantity of heat required to raise the temperature of a system 1 degree.
Hydraulic shock	Momentary pressure increase in a piping system
Hydrodynamic	The motion of a fluid and the interactions with its boundaries.
Incipient	Just appearing.
Ionisation temperature	The temperature at which a neutral atom or molecule either loses or gains electrons.

Le Chatelier’s Principle	When an external force is applied the system adjusts to minimise the impact of the applied force.
Luminescence	Light emission that cannot be attributed only to the temperature of the emitting body.
Macro-Scale	Large enough to be seen by the human eye.
Mass flow rate	The mass of fluid that flows through a pipe per unit time.
Metastable	An excited but stationary energy state.
Micro-Scale	Extremely small.
Molecular emission	Emission of light at discrete wavelengths wave lengths by molecules which have been electronically excited.
Nucleation	The formation of vapour bubbles
Plasma	A highly ionised gas.
Raoult’s Law	The vapour pressure of a system of a solution equals the product of the vapour pressure of the pure solvent and the mole fraction of the solvent.
Rarefaction	Local reduction in pressure.
Scaling Effects	An effect that changes depending on the scale it is observed at.
Sonoluminescence	Luminescence caused by high frequency sound waves.
Sparge	Forcing a gas through liquid.
Spectra	A display of intensity of radiation as a function of a quantity.
Static pressure	The background pressure ie atmospheric pressure.
Steady state	The point when the conditions in a system do not change with time.
Tensile strength	The maximum stress a material can withstand before it tears.
Thermodynamics	Relates methods that heat can be changed into different forms of energy.

Total internal reflection	The effect when light in a given medium which incident to on the boundary with a less dense medium at an angle less than the critical angle is completely reflected from the boundary.
Turbulent	Where local velocities and pressure fluctuate irregularly.
Ultrasonic	Frequencies above 20,000 Hz.
Vapour pressure	The pressure of the vapour in equilibrium with the liquid.
Venturi	A pipe with a constriction in it.

1 Introduction

1.1 Cavitation

Cavitation[1] is the term given to the process of *nucleation*, growth and collapse (or diminution) of gas filled cavities within a liquid.[2-5] It is assumed that cavitation bubbles originate at microscopic bubble nuclei.[6] Bubble nuclei are tiny but distinct bubbles of gas contained within the water body. These tiny bubbles can take from minutes (bubbles with diameters in the region 100 µm) to many hours[7] (bubbles with diameters in the region of 10 µm) to escape. If the water is in *turbulent* conditions the movement stops the bubble nuclei from escaping as the movement keeps the nuclei permanently mixed. Water contains 1×10^6 bubbles per millilitre it is unknown why water is the only liquid to have so many bubble nuclei.[7, 8] Water is also probably the only liquid to contain bubble nuclei[6] therefore gas nuclei may aid cavitation but are not a prerequisite to cavitation although dissolved gases in the liquid are. Dissolved gases are essential for cavitation and dissolved gases diffuse into the water and do not affect the *tensile strength* of the liquid[7] whereas impurities in water reduce the tensile strength as they reduce the cohesive forces between the water molecules.[7] Dissolved gases therefore do not encourage or discourage the formation of cavitation however the nature of the dissolved gas does affect the chemistry of the bubble collapse.[9, 10] Cavitation bubbles form when the *static pressure* falls below the *vapour pressure* of the liquid. When the static pressure rises again the cavity starts to shrink and if the pressure changes are dramatic enough the cavity can implode and form a momentary *plasma*. The

---

[1] See Glossary

intensity of the implosion is dependent on the physical and chemical properties of the liquid as well as the pressure changes. Cavitation, under fine control, has a number of different applications including but not limited to *ultrasonic* cleaning, treatment of kidney stones,[11] destruction of salmonella and targeted weight loss. The shockwave associated with a cavitating water jet is used to increase the erosion power of liquid jets.[11]

There are 4 main types of cavitation as follow:

1. *Hydrodynamic* Cavitation

   Hydrodynamic cavitation occurs when a liquid flows through a tube with an orifice in it, this orifice causes velocity and pressure changes which cause cavitation.

2. Ultrasonic Cavitation

   Ultrasonic cavitation is the use of ultrasound to induce cavitation within a liquid.

3. Conical bubble

   Conical bubble cavitation is caused by the pressure-induced collapse of a conical bubble trapped at the end of a specially machined U-tube. [12-15]

4. Water Hammer

   Water hammer cavitation is caused by mechanical oscillation in a water column. [9]

1.2 Cavitation Luminescence

When cavitation is accompanied by the emission of light this is known as cavitation *luminescence*. An example of this which occurs in the natural world is the phenomenon of shrimpoluminesence, which is the term coined for cavitation luminescence (CL) generated by the pistol shrimp (*Alpheus heterochaelis*) during snapping of its overdeveloped claw to produce a high velocity water jet containing a cavitating bubble. This type of CL results from hydrodynamic cavitation, or cavitating flow, so will be referred to as cavitating flow luminescence (CFL). The phenomenon of CFL forms the basis for the research contained in this thesis, there are several types of CL which occur as a result of the different types of cavitation and these will be discussed in turn.

1.2.1 Cavitating flow luminesence

Cavitating flow is the term given to cavitation which takes place in a liquid flowing through a tube of changing diameter, for example an orifice plate or *Venturi*. Cavitating flow luminescence (CFL) using a Venturi tube was investigated during the 1960s by Jarman and Taylor.[16] A Venturi tube is a tube with a varying internal diameter. In the case of Jarman and Taylor they used a Venturi with an internal diameter of 9.5 mm which narrowed to 4.8 mm at the orifice and then widened gradually. The process of CL within a Venturi can be broken down into the following processes:

1. Fluid flows through the Venturi at a constant velocity and pressure until it encounters an orifice;

2. When the fluid enters the Venturi orifice the velocity of the fluid increases and the pressure decreases in accordance with the law of conservation of momentum[17]. These sudden changes result in dissolved gases being pulled out of solution forming cavitation bubbles;

3. The bubbles exit the Venturi and the velocity slows, accompanied by a sudden increase in pressure. This increase in pressure causes the small cavitation bubbles to implode. Depending on the nature of the gas inside the bubbles high temperature plasmas can form and photons can be produced and potentially analysed.

The process of CFL is shown schematically in Figure 1-1, the cavitation itself takes place predominately where the fluid passes from the orifice into the pipe.

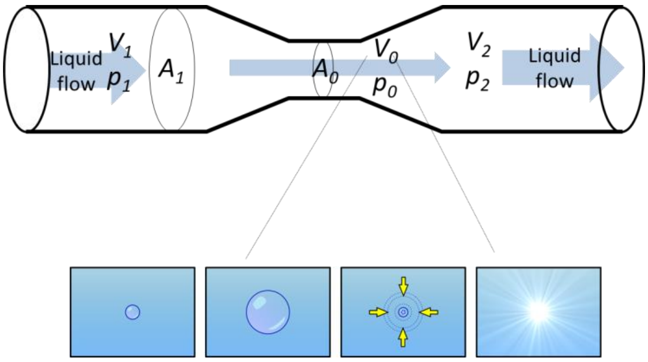

Figure 1-1 Caviation luminescnce through a Venturi tube (image adapted from *World Heritage Encyclopedia* [18] and *Ivanov* [19]) showing the process of nucleation to implosion of a cavitation bubble.

Where:

V_1 = upstream velocity

p_1 = upstream pressure

A_1 = cross-sectional area of the pipe

V_0 = orifice velocity

p_0 = orifice pressure

A_0 = cross-sectional area of the orifice

V_2 = downstream velocity

p_2 = downstream velocity

There are three sub-types of cavitating flow, these are as follows:

1. Transient cavitation, this is the type under investigation here. It is the most reliable and the most stable form of cavitation. It occurs as shown in Figure 1-1, cavitation bubbles form and implode as the changing physical conditions affect them, producing photons.
2. Sheet cavitation occurs when conditions are stable, enabling cavities to form on a solid boundary.[20] This is also known as *steady state* cavitation.
3. Super cavitation is an extreme form of cavitation where a single large bubble forms, this is problematic on the *micro-scale* as a large bubble can choke an orifice.

Flow through a Venturi is influenced by properties such as the length of the orifice, the inlet/outlet angles and diameter of the orifice. Cavitation bubble formation is highly dependent on the geometry of the orifice.[17] Cavitation starts when the liquid flowing detaches from the vessel walls this is facilitated by a sufficiently sharp inlet angle to the orifice.[3] In Figure 1-2 cavitation is shown as it occurs in a *macro-scale* example there is a jet of liquid extending from the mouth of the Venturi stretching into the main body of the tube. The cavitating bubbles around the edge of this jet are shown.

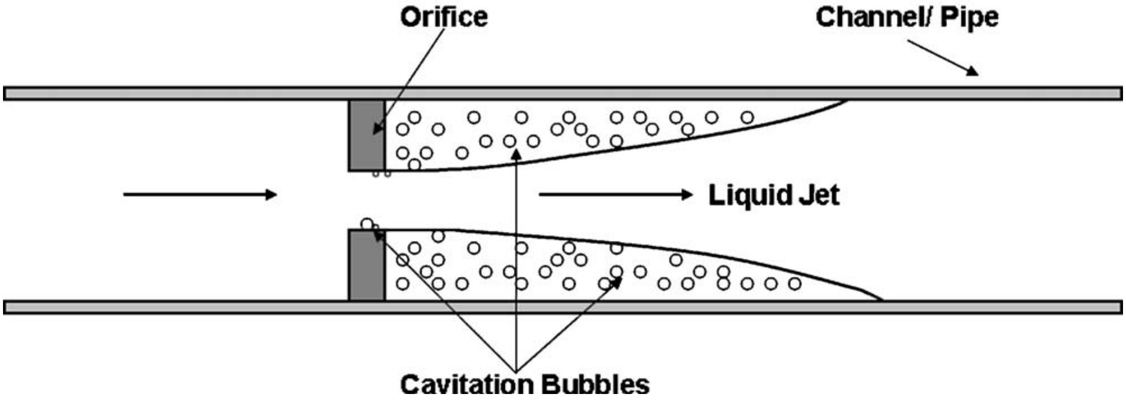

Figure 1-2 Schematic showing a cavitating orifice[21]

Given that cavitation is a physical process it is possible to calculate the point at which cavitation starts this is known as the cavitation inception point and can be given a cavitation number (see Ch. 2.2 Equation 16). The size of the Venturi has a large impact on the cavitation effect exhibited, whether it is transient cavitation, sheet cavitation or super cavitation. Size *scaling effects* have been noted when observing and calculating the cavitation number.[22-25] It has been noted that liquids behave differently when travelling through micro-orifices than when they travel through macro-orifices. This makes simply scaling down experiments in order to investigate micro-scale CFL difficult.[24] The transition from *incipient* to choking on a macro-scale takes an approximate 59% increase in inlet flow.[25] Whereas in a micro-scale system the flow increase to take the cavitation from incipient to choking is 1-2%.[25] This indicates there is an optimal set of conditions to promote transient cavitation.

1.2.1.1 Luminesence mechanisms

Possible explanations for CFL are as follows:

1. *Scattering* of stray light by cavitating bubbles (see section 6.4.2.)
2. *Free radical* reactions at the bubble-solvent interface. This has been proposed as a mechanism for alkali metal excitation in sonoluminescence of aqueous and non-aqueous solvents.[26]

   $H_2O \rightarrow H^{\bullet} + HO^{\bullet}$

   $ROH \rightarrow H^{\bullet} + HO^{\bullet} + R^{\bullet} + RO^{\bullet} + O$

   These types of free radical reactions are responsible for the extensive application in sonochemistry for synthetic reactions, so it is reasonable to expect that a range of free radicals species ($P^{\bullet}$, $Q^{\bullet}$) will form in aqueous solutions of organic compounds. These will be available for reduction and excitation of atomic and molecular species, a process known to occur in flames:

   $P^{\bullet} + Q^{\bullet} + M \rightarrow M^{*} + PQ$
3. *Atomic and/or molecular emission* resulting from plasma formation in the imploding bubble which creates a high temperature environment with associated photon emission (see section 2.1.3)

1.2.2 Ultrasonic luminescence

Ultrasonic luminescence occurs when ultrasound of the correct amplitude is applied to a liquid, the formation, subsequent implosion and photon emission is shown in Figure 1-3.

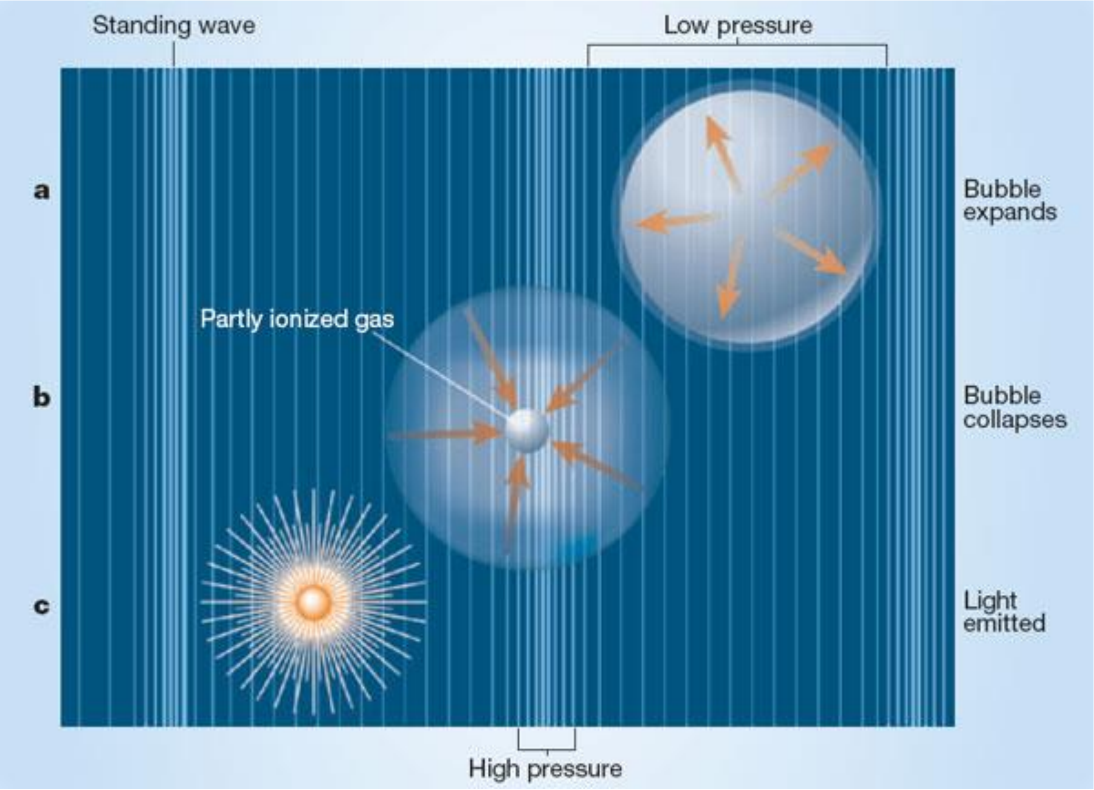

Figure 1-3 Ultrasonic Cavitation luminescence[27]

The process of ultrasonic cavitation can be broken into the following steps:

1. ultrasound is applied and the waves affect the liquid in cycles of compression and *rarefaction*;
2. during the rarefaction phase of the ultrasound waves cavities form in the liquid;

3. during the compression phase the cavities collapse violently with the emission of photons so called *sonoluminescence*.

Sonoluminescence is split into two types, single bubble sonoluminescence and multi-bubble sonoluminescence.

1.2.2.1 Single bubble

Single-bubble sonoluminescence (SBSL) occurs when ultrasound is used to cause a single gas bubble to oscillate violently enough to promote violent bubble collapse resulting in photon emission. The bubble is subjected to regular compression and rarefaction, cyclically generating short flashes of light. The flashes of light last in the region of 100 ps.[28] Sulphuric acid has been used as an ideal medium to generate sonoluminescence due to several properties including: low vapour pressure (in the region of 0.199 Pa) and the decomposition products are either solid or highly water soluble meaning they will not enter the cavitation bubble and quench light emission.[29] When a bubble is generated in 85 %wt H_2SO_4 using this method pressures and temperatures in excess of 4000 atm and 15,000 K respectively have been quantified.[30] Light intensity from 85 %wt H_2SO_4 is approximately 3 orders of magnitude greater than that observed in water from SBSL.[31] Single bubble sonoluminescence in 85 %wt H_2SO_4 has been used to create *spectra* containing molecular, ionic and atomic emission.[31, 32] These spectra demonstrate there is an ionised plasma core during SBSL.[33] Wallace *et al.*[34] investigated the analytical potential of single-bubble sonoluminescence. They observed cavitation luminescence for solutions containing the fluorescing molecules fluorescein and quinine, and also sodium, potassium and copper salts, which showed reproducible signals related directly to the concentration of the species present in the solution. The results for the molecular species were compared with those obtained by *fluorescence* spectroscopy and, in the case of quinine, parallel determinations of concentration in a test solution yielded consistent results.[34] Single-bubble sonoluminescence signals were also observed to exhibit a linear correlation with the concentration of metal salts introduced in to the solution in the measurement cell allowing some quantitative analysis.[34]

1.2.2.2 Multi bubble

Multi-bubble sonoluminescence (MBSL) occurs when light is emitted from clouds of bubbles produced during ultrasonic cavitation.[35] There are three types of MBSL which emit light; the most intense light is observed from *filamentous* cloud emission[33] and it is only from filamentous emission that spectra are observed.[33] The other types of MBSL are *bulbous* emission and cone emission shown in Figure 1-4.

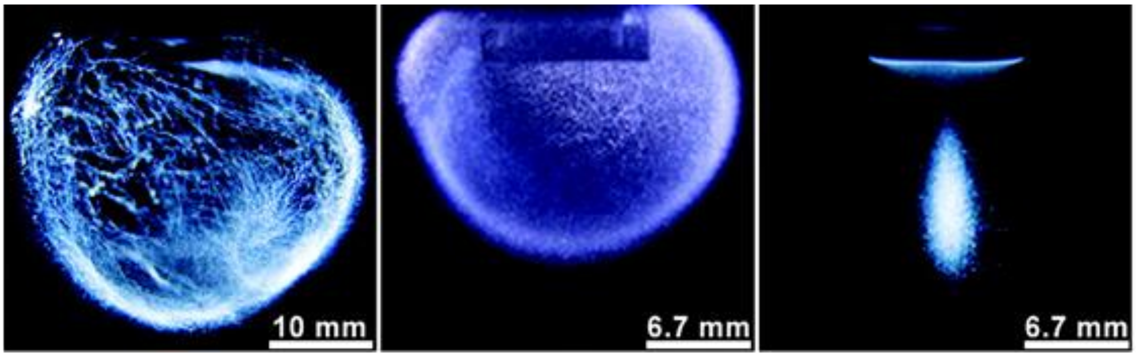

Figure 1-4 MBSL of 95% wt H_2SO_4 at increasing acoustic powers. Photographs with 10 s exposures of different light emitting regimes of MBSL in H_2SO_4, from left to right, filamentous (14 W/cm^2), bulbous (22 W/cm^2), and cone shaped emission (30 W/cm^2).[33]

The type of MBSL depends upon the acoustic pressure; as the acoustic pressure increases the cavitation changes from filamentous to bulbous to cone shaped. This can be compared to cavitation through a Venturi and the change from transient to sheet to super cavitation as the flow rate therefore pressure through the Venturi is increased. The conditions for maximum light intensity to be observed have to be carefully controlled in both methods.

Multi-bubble sonoluminescence has been observed in aqueous and alcohol solutions containing metal salts, and their emission spectra are characteristic of atomic emission from metal atoms in their excited states.[36] The spectra are analogous to those produced using flame emission.[36] Spectra generated from metal carbonyls has been used to quantify the conditions with the collapsing bubbles,[36] quantification of the metal in solution has yet to be fully explored.

1.2.3 Conical bubble luminescence

Conical bubble cavitation is a very controlled method of producing cavitation luminescence. The basic apparatus (Figure 1-5 Apparatus consisting of a U-bend pipe terminating in a PMMA block and linked to a vacuum pump comprises) consists of a steel U-tube with a 6 cm internal diameter this is filled with degassed water the system is then sealed and the pressure manipulated using a sprung top and a connected vacuum pump.

The shorter leg of the U-tube terminates in a transparent block of polymethylmethacrylate which has a hollow cone forming the tip of the apparatus. A very small bubble (around 1-2 mm) is introduced into the polymethylmethacrylate cone and the pressure is reduced using a vacuum pump, thereby causing the bubble to grow inside the tip of the cone. The pressure is released by suddenly lifting the top plate and equalising the pressure to atmospheric, causing the bubble to implode, emitting photons which can be detected by a correctly positioned charge coupled device (CCD).[14] The pressure pulse which is generated by the sudden repressurisation to atmospheric pressure within the U-tube by lifting the top plate drives this cavitation effect.[14]

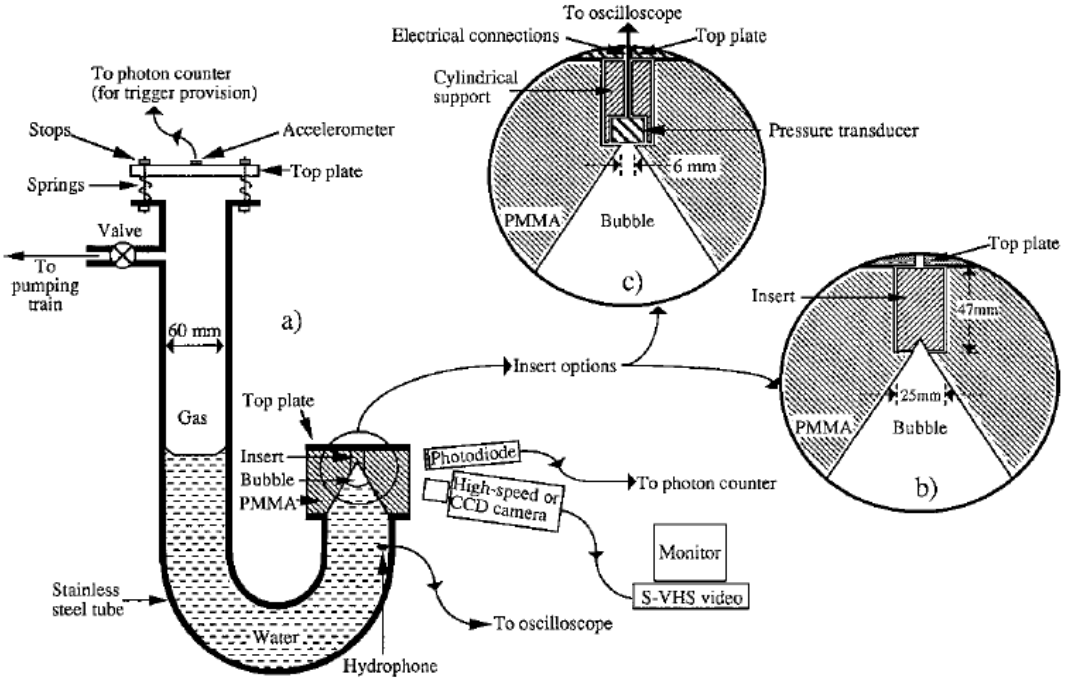

Figure 1-5 Apparatus consisting of a U-bend pipe terminating in a PMMA block and linked to a vacuum pump comprises conical bubble cavitation generation system explored by Leighton *et al.*[14]

Leighton *et al.* observed photons which coincided with the initial collapse of the cavitation bubble.[14] The luminescence generated using this apparatus was observed at 2 mm from the apex of the cone using a CCD.[15]

1.2.4 Water hammer luminescence

Water hammer cavitation is caused by *hydraulic shock* and is commonly observed in plumbing systems. When moving water is stopped suddenly the water keeps moving in the original direction, causing a pressure increase and a subsequent pressure decrease on rebound. It is this pressure change which enables cavitation to occur.

Figure 1-6 shows the apparatus which has been used to generate water hammer cavitation. A transducer was used to vibrate either a quartz or polycarbonate tube to produce the cavitation effect. In configuration (a) there is a free surface of the liquid within the cylindrical container, whereas in configuration (b) the free surface is eliminated by attaching a reservoir. The aim of this was to eliminate the surface turbulence and stabilise the increase in the threshold for luminescence. The result of this was to enable the set up to produce cyclic emissions of photons for prolonged periods of time.[9] Set up (a) with a free surface and no reservoir produced a more intense light emission.[9]

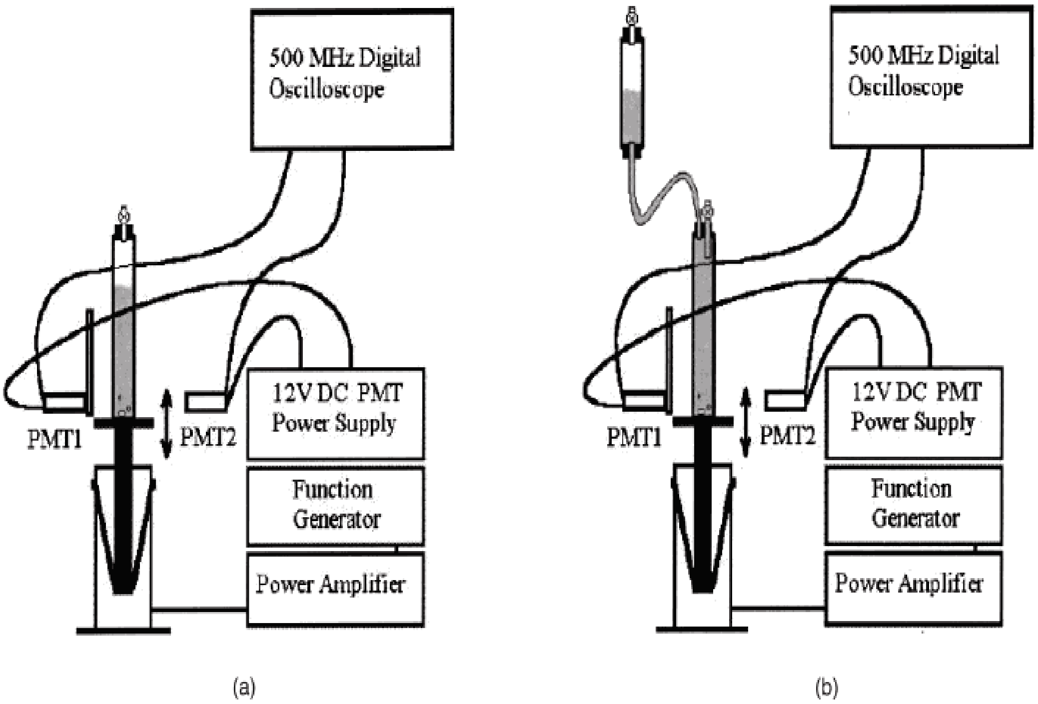

Figure 1-6 Experimental set up of water hammer apparatus, (a) the water column has a free surface. (b) The free surface of liquid is eradicated by the introduction of a reservoir. [9]

Studies utilising both partially filled and entirely filled tubes of water, vibrating at frequencies between 5 to 20 Hz, have been undertaken.[9] Bright flashes of light were observed when xenon gas was dissolved in the flowing liquid (at pressures between 5 – 60 mm Hg). [9]

1.3 Factors which affect cavitation luminescence

1. Solvent vapour pressure

   Fluids with a lower vapour pressure cavitate more easily as the change in pressure can be less extreme and still fulfil the conditions required to induce cavitation. Fluids with a high vapour pressure require a greater change in pressure as it passes through the Venturi in order for the static pressure to drop below the vapour pressure and cavitation can be initiated. A fluid has a higher vapour pressure at higher temperatures therefore a colder fluid will cavitate more easily.[28, 33]

2. Tensile strength

   The liquids tensile strength also determines how easily it will cavitate. Pure water has a tensile strength of 27.7 MPa[7] and will not cavitate due to this incredibly high tensile strength. Pure water is very difficult to manufacture and impurities in water reduce the tensile strength as they reduce the cohesive force between the water molecules. Liquids with a lower tensile strength will cavitate more easily. A fluid has a lower tensile strength with an increase in temperature.

3. Dissolved gas

   Dissolved gases such as argon, helium and xenon provide nucleation sites and aid the formation of cavitation bubbles. It has been noted that liquids which have been *sparged* with noble gases produce brighter light and more intense atomic and molecular and ionic emission.[28] There is some contention as to whether dissolved gases impact the tensile strength of the liquid. Some researchers maintain that dissolved gases do not affect the tensile strength of a liquid[7] whereas other researchers maintain that dissolved gases reduce the tensile strength of the liquid, making it easier for bubbles to form, and stating that dissolved gasses act as nuclei for cavitation bubbles to form around.[37] This can even weaken the tensile strength of the liquid to the point where a cavitation bubble will grow at pressures greater than the liquid vapour pressure.[38] However it is widely agreed that dissolved noble gases such as argon and xenon promote more extreme conditions within the cavitating bubbles, and an increase in light emissions has been observed.[9, 10] The higher the pressure and the temperature within the bubbles the higher the intensity of emitted light.[28] The conditions within the bubble can be controlled by changing the contents of the bubble, for example the addition of gaseous hydrocarbons will cause the temperature to decrease significantly.[36]

1.4 Aim and Objectives

1.4.1 Aim

The main aim of this research is to investigate the phenomenon of cavitation luminescence as a proof-of-concept for its use as an excitation method in analytical emission spectrometry. The cavitation phenomenon presents the opportunity to use the intrinsic properties of a flowing stream of liquid to generate atomic and molecular emission in the sample itself without the need for an extraneous excitation source, and is therefore ideal for use in micro-fluidic and lab-on-a-chip applications.

1.4.2 Objectives

Specific objectives are:

1. Construction of a micro-Venturi, fluid handling manifold, sample introduction and light detection system. The experimental setup is to be kept simple and built with maximum flexibility in mind to allow for changes

to be easily made. The main apparatus required are a spectrometer, venturi, sample introduction and fluidic manifold. The detection of light emitted will be carried out initially using a photo multiplier tube and amplifier.

2. Computational fluid dynamic modelling of the micro-Venturi to determine the effect of pressure and flow conditions.
3. Investigation of cavitating flow luminescence in the micro-Venturi with the specific focus of establishing the practical conditions under which optimal luminescence occurs. This will be based on work done previously by Jarman and Taylor in the 1960's,[1, 16] who achieved cavitation using tap water.
4. Investigation of the effect of dissolved gases, solutes and solvents on CFL. Volatility and pressure are important to consider when inducing cavitation. Luminescence is increased with less volatile liquids, heat capacity and ionisation energy of dissolved gases. Heat capacity and the energy of ionisation of gases dissolved in the liquid stream play an important role in determining the excitation temperature in the plasma which is formed within the micro bubble during the cavitation collapse.
5. Establish figures of merit for selected analytical applications.

2 Theory

2.1 Cavitation

2.1.1 Adiabatic processes

A consequence of the first law of *thermodynamics* is that energy cannot be created or truly destroyed, but it can be changed. This law is expressed in the first law of thermodynamics which states that when a system undergoes a thermodynamic cycles the net heat supplied to the system from the surroundings is equal to net work done by the system on its surroundings. This is shown in Equation 1.[39]

$$\Delta \mathrm{E} = \mathrm{Q} - \mathrm{W} \qquad \text{Equation 1}$$

Where:

ΔE = Change in energy of the system, J.

Q = heat, J

W = work, J

Equation 1 shows that the energy within a system can change by being lost as heat or work done by the system increasing the energy within the system but it is always changed and never destroyed. This concept is used in the General Energy Equation, shown in Equation 2:

$$\mathrm{Q} + (\mathrm{U} + \mathrm{PE} + \mathrm{KE} + \mathrm{pV})_{in} = \mathrm{W} + (\mathrm{U} + \mathrm{PE} + \mathrm{KE} + \mathrm{pV})_{out} + (\mathrm{U} + \mathrm{PE} + \mathrm{KE} + \mathrm{pV})_{stored} \qquad \text{Equation 2}$$

Where:

Q = heat, J.

U = internal energy (for example thermal energy, chemical energy etc), J.

PE = potential energy (energy resulting from something's position in a potential field, a potential being for example an electromagnetic or gravitational field), J.

KE =kinetic energy (energy from rotational/translational motion relative to a frame of reference.), J.

p = pressure, Pa.

V = volume, m^3.

W = work, J.

The general energy equation identifies the main different states of energy associated with a system and shows how they balance. This equation can be applied to a steady state flow system where no work is done by or on the fluid. These conditions are *adiabatic* and there is no change to the internal energy. Assuming this the general energy equation can be simplified to the following Equation 3:

$$(PE + KE + pV)_1 = (PE + KE + pV)_2 \qquad \text{Equation 3}$$

Where:

PE = potential energy, J.

KE = kinetic energy, J.

p = pressure, Pa.

V = volume, m^3.

Replacing the terms for potential and kinetic energy form the equation into the Bernoulli principle for a steady state flow system.

$$PE = mgh \qquad \text{Equation 4}$$

Where:

m = mass, kg.

g = gravity, N/kg.

h = height, m.

$$KE = \tfrac{1}{2}mv^2 \qquad \text{Equation 5}$$

Where:

m = mass, kg.

v = velocity, m/s.

Substituting Equations 4 and 5 into 3 results in Equation 6:

$$mgh_1 + \tfrac{1}{2}m{v_1}^2 + p_1V_1 = mgh_2 + \tfrac{1}{2}m{v_2}^2 + p_2V_2 \qquad \text{Equation 6}$$

Equation 6 shows that the sum of the energy terms in a steady state system equals a constant. This relates to Bernoulli’s principle which observes the total energy is a flowing stream is constant at a specific point in a tube. Bernoulli’s principle is based on the conservation of energy and relates all the energy terms to give a constant total in terms of energy in the flowing liquid. This means that an increase in velocity creates a decrease in pressure and vice versa.

It can be thought of as a series of energy terms which sum as shown in Equation 7:

$$C = p + KE + PE \qquad \text{Equation 7}$$

This can also be written for 2 different points within the same fluid system (Equation 8):

$$p_1 + KE_1 + PE_1 = p_2 + KE_2 + PE_2 \qquad \text{Equation 8}$$

Bernoulli's principle holds true as long as the flow rate and density are constant (incompressible fluids), and assumes that losses due to friction are negligible therefore conditions must be constant.

2.1.2 Hydrodynamic cavitation

Shear stress is a stress state where the material changes shape without changing volume. The shape of a Venturi orifice (See Figure 2-1) influences the shear stress exerted on a flowing liquid such as water. Whether a liquid cavitates or not depends largely on its tensile strength, the force required to pull something until it "breaks" in the case of water this breakage is classed as when a gas cavity forms in the liquid and the liquid "cavitates".[40] The tensile strength of a liquid is measured using a Berthelot-Bourdon tube method. This uses a glass tube, filled with the liquid under investigation which is sealed with minimal air left inside. The tube is then heated until the gas bubble dissolves into the liquid; the apparatus is then cooled which puts the liquid under tension so that it attains a "*metastable* state". When the tension in the liquid is increased sufficiently this disturbance disrupts the metastable state and the liquid cavitates.[40] Pure water has a very high tensile strength c.a. 27.7 MPa and will not cavitate easily as a result. However, completely pure water is very difficult to make and any contamination disrupts the hydrogen bonding between water molecules, thereby reducing the tensile strength.[7] Because these contaminations as well as dissolved gases act as nucleation sites for cavitation the stress required to rupture a liquid is not measured by the liquid's tensile strength but it's vapour pressure instead.[41]

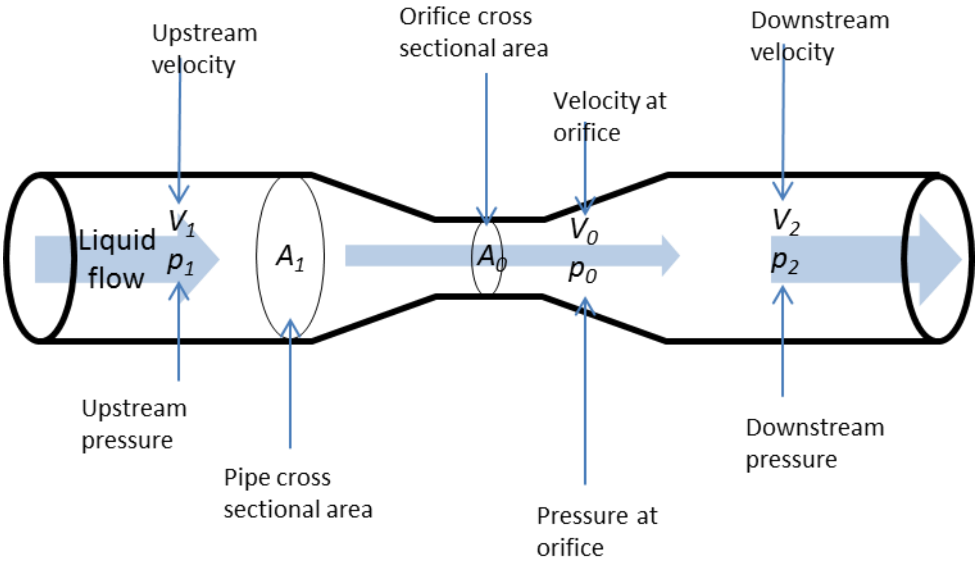

Figure 2-1 Hydrodynamic cavitation in a Venturi (image adapted from World Heritage Encyclopedia.[18])

Fluid dynamics holds that discharge coefficients are affected by the geometry of the pipes through which a liquid flows.[42] Hence, flow through a pipe can be calculated using Equation 9.[3]

$$Q = C_d A \sqrt{\frac{2\Delta p}{\rho}}$$ Equation 9

Where:

Q = flow rate, ml/min.

C_d = *flow coefficient*

A = cross-sectional area of flow path, m^3.

Δp = pressure different across the orifice, Pa.

ρ = density, kg/m^{-3}.

When equation 9 is used to calculate the flow through the Venturi problems arise. The flow coefficient depends upon the geometry of the pipe and the properties of the liquid. Equation 10 is the standard equation used to calculate the flow coefficient.[21]

$$C_d = \frac{Q}{A_0\sqrt{2(p_1-p_3)/\rho\left[1-\left(\frac{A_0}{A_1}\right)^2\right]}}$$ Equation 10

Where:

C_d = flow coefficient

Q = flow rate, ml $min^{-1.}$

p_1 = pressure upstream from orifice, Pa.

p_3 = pressure at in orifice, Pa.

ρ = density, kg $m^{3\ -1}$

A_0 = cross sectional area of orifice, m^3.

A_1 = cross sectional area of pipe, m^3.

The experimentally determined values for a flow coefficient for small bore orifices 0.3 mm-40 mm fall within the range 0.6-1.[43] However when the flow coefficient was calculated for a Venturi with an orifice size of 0.22mm with equation was calculated to be 37095724. This cannot be correct, therefore the model which was proposed by Schmidt and Corrandini to calculate the cavitating flow coefficient[17] (Equation 11) was used to calculate a flow coefficient for orifices sizes 0.22mm and 0.16mm of 0.9971 and 0.9974 which are within the range for expected values.

$$C_d = \sqrt{\frac{\frac{1}{2}\rho\left(\frac{m}{\rho A_0}\right)^2}{\Delta p}} \qquad \text{Equation 11}$$

Where:

C_d = cavitating flow coefficient

m = *mass flow rate*, kg/s.

Δp = change in pressure across the orifice, Pa.

ρ = density, kg/m^3

A_0 = cross sectional area of orifice, m^3.

Equation 12 which shows the flow rate through a Venturi can be calculated using the flow coefficient calculated using Equation 11:

$$Q = C_d A_o \sqrt{\frac{2\Delta \boldsymbol{p}}{\rho\left[1-\left(\frac{A_0}{A_1}\right)^2\right]}} \qquad \text{Equation 12}$$

Where:

Q = flow rate, ml/min

C_d =cavitating flow coefficient

A_o = orifice cross sectional area, m^3.

A_1 = "pipe" cross sectional area, m^3.

Δp = change in pressure across the orifice, Pa.

ρ = density, kg/m^3

The flow rate through the Venturi is used to calculate the cavitation number in Equation 15.

The change in pressure across the orifice is calculated using Equation 13, a variation on Bernoulli's principle.

$$\Delta p = \left(\frac{\rho\, C_1^2}{2}\right) . \left(\left(\frac{A_1}{A_0}\right)^2 - 1\right) \qquad \text{Equation 13}$$

Where:

Δp = change in pressure across the orifice, Pa.

ρ = density, kg/m^3.

C_1 = inlet velocity

A_1 = cross sectional area of inlet pipe, m^3.

A_0 = cross sectional area of orifice, m^3.

Using Equation 13 the change in pressure can be calculated as shown in the exemplar equation below calculated for water flowing through a 160 µm diameter Venturi at 100 mL min^{-1}:

$$\Delta p = \left(\frac{999.97 \text{ x } 0.236^2}{2}\right) . \left(\left(\frac{7.06858 \text{ x } 10^{-6}}{201062 \text{ x } 10^{-8}}\right)^2 - 1\right) \qquad \text{Equation 14}$$

The above Equation 14 has the values substituted in for water flowing at 100 ml min^{-1} through a Venturi with a restriction diameter of 160 µm and once calculated gives the following pressure change across the restriction:

$$\Delta p = 3435510\ P$$

This change in pressure at the Venturi is high and gives rise to the cavitation effect because this change in pressure can drop the pressure to below the vapour pressure of water which is 101325 Pa. When the pressure drops below the vapour pressure of the flowing liquid in this case water then cavitation is initiated.

The Cavitation Number σ_v is given by Equation 15:

$$\sigma_v = \frac{p_2 - p_v}{\frac{1}{2}\rho v_{th}^2} \qquad \text{Equation 15}$$

Where:

p_2 = exit pressure, Pa.

V_{th} = Q/A_{th} is the average velocity at the orifice throat, m/s. (A_{th} is the micro-Venturi throat area, m^3, Q is the flow rate, mL/min).

p_v = the vapour pressure of liquid, Pa.

ρ = the density of the incompressible liquid (water), kg/m^3.

σ_v = the cavitation number

The conditions under which cavitation inception occurs is different for each orifice size. The cavitation number which corresponds to the start of cavitation is called the cavitation inception number. Data available for micro-devices which have orifices of 20 – 60 µm i.d. have cavitation inception numbers clustered around 0.2-0.3. It has been observed that cavitation inception number increases with orifice size, for instance over the size range 0.1 -13 cm cavitation inception number increases from

0.15 to 3.0 respectively.[41, 44] Generally cavitation intensity increases with decreasing cavitation number[45] until the orifice becomes choked. The choking of an orifice is defined as the point where the exit pressure loses control over the flow rate and flow stops.[25]

2.1.3 Theoretical cavitation bubble temperature

Assuming that the expansion and collapse of the cavitating bubble behaves as a reversible adiabat then it is a simple matter to calculate the local temperature which arises as a result of the increase in pressure on collapse of the bubble, as follows:

For an ideal gas undergoing adiabatic expansion:

$$p_v V_v^{\gamma} = p_2 V_2^{\gamma}$$ Equation 16 [46]

$$\frac{p_v V_v}{T_v} = \frac{p_2 V_2}{T_2}$$ Equation 17 [46]

Where:

$\gamma = \frac{C_{p,m}}{C_{V,m}}$

$C_{p,m}$= heat capacity at constant pressure for a monatomic gas, J/K.

$C_{V,m}$= heat capacity at constant pressure for a monatomic gas, J/K.

T_v = temperature at vapour pressure of liquid, K.

T_2 = temperature inside bubble at exit pressure , K.

p_v = vapour pressure of liquid , Pa.

p_2 = exit pressure , Pa.

V_v = Volume of of bubble at vapour pressure, m^3.

V_2 = Volume of bubble at exit pressure , m^3.

Substituting Equation 17 into Equation 16 gives Equation 18:

$$p_{v\left(\frac{p_2}{p_v}V_2\frac{T_v}{T_2}\right)^{\gamma}}=p_2V_2^{\gamma} \qquad \text{Equation 18}$$

Simplify the equation to give Equation 19:

$$p_vp_2^{\gamma}p_v^{-\gamma}V_v^{\gamma}T_v^{\gamma}T_2^{-\gamma}=p_2V_2^{\gamma} \qquad \text{Equation 19}$$

Multiply out the volumes gives Equation 20:

$$p_vp_v^{-\gamma}T_v^{\gamma}=\frac{p_2}{p_2^{\gamma}T_2^{-\gamma}} \qquad \text{Equation 20}$$

Simplify Equation 19 to give Equation 21:

$$p_v^{1-\gamma}T_v^{\gamma}=p_2\,p_2^{-\gamma}T_2^{\gamma} \qquad \text{Equation 21}$$

Further simplify Equation 20 to give Equation 22:

$$p_v^{1-\gamma}T_v^{\gamma}=p_2^{1-\gamma}T_2^{\gamma} \qquad \text{Equation 22}$$

Therefore in order to calculate the theoretical temperature inside a cavitation bubble in water Equation 22 can be rearranged to:

$$T_2^{\gamma}=\frac{p_v^{1-\gamma}T_v^{\gamma}}{p_2^{1-\gamma}} \qquad \text{Equation 23}$$

Where

p_v = 2.34 x 10^3 Pa

T_v = 293.15 K

p_2 = 101325 Pa

T_2 = Unknown

Gamma can be calculated using the below Equation 24

$$\gamma = \frac{C_p}{C_v} = \frac{{}^{5}/_{2}R}{{}^{3}/_{2}\,R} = \frac{5}{3} = 1.67 \qquad \text{Equation 24}$$

Substituting in the values for water under standard conditions where the pressure drops to the vapour pressure of water gives Equation 25

$$T_2^{1.67} = \frac{p_v^{-0.67} T_v^{1.67}}{p_2^{-0.67}} \qquad \text{Equation 24}$$

$$= \frac{(2.34x10^3)^{-0.67}.\,(293.15)^{1.67}}{101325^{-0.67}}$$

$$= \frac{0.005539\,.\;13184}{0.0004427}$$

$$=164625$$

$$T_2 = \sqrt[1.67]{164625}$$

$$=1329\ K$$

The above calculation shows that water undergoing cavitation and adiabatic collapse of the cavitation bubble will generate temperatures in the region on 1329 K. The implication of this is that very high temperatures can be achieved within a collapsing cavitation bubble in the region required to create a plasma and emit photons.

In conclusion the calculations in this section have shown that the conditions which are generated within the Venturi are in theory sufficient to initiate and sustain cavitation. The calculations have also shown that very high temperatures can be generated inside the gas bubbled and it is this effect of potential plasma generation on the micro-scale which is under investigation in this research, to be exploited as a possible excitation source for analytical atomic emission spectroscopy

3 Instrument development

3.1 Objective

The first objective was to construct a micro-Venturi, fluid handling manifold, sample introduction and light detection system. The intention was to keep the experimental setup simple and built with maximum flexibility in mind to allow for changes to be easily made. The main apparatus required are a spectrometer, Venturi, sample introduction and fluidic manifold. The detection of light emitted will be performed initially using a photo multiplier tube and amplifier.

3.2 Venturi tube design

One of the key challenges was the fabrication of a Venturi tube. Initial design requirements were:

1. fused silica construction to allow transmission of UV radiation;
2. orifice of <250 µm to enable cavitation to occur at flow rated less than 100 mL min^{-1};
3. liquid connections able to withstand pressures in excess of 1000 psi;
4. orifice geometry optimised for cavitation.

3.2.1 Venturi Mk I

Several attempts were made in-house to manufacture a Venturi tube with the desired features:

Attempt 1: was to Embed a short length of micro-capillary tubing in polymethylmethacrylate resin while in a tubular mould. While it was possible to embed the length of capillary tubing it was not possible to tap the PMMA inorder to facilitate a high pressure liquid interface. Problems encountered included the PMMA cracking and the flow channel blocking.

Attempt 2: etching channels into a glass chip to make a microfluidic chip. Problems encountered included the difficulty in making a mask, not having in-house engineering experience of making micro-fluidic chips, the time and cost of out sourcing this capability.

After several unsuccessful attempts to make tubes in-house, and by external glassblowing services, a Venturi tube which met some, but not all, of the design requirements was fabricated by LabGlass (Anthony Wright, LabGlass Ltd, Cambridgeshire, UK) based on an Omnifit® LC column (Part No #006CC-03-05-FF, Kinesis, Cambridgeshire, UK) as shown in Plate 3-1. This met two of the initial design requirements, namely 2 and 3: a 160 µm i.d. orifice was obtained by collapsing the glass at the centre of the column; and PTFE tubing could be connected directly using ferrules and nuts, providing high pressure connections up to 69 bar. Unfortunately the Omnifit® columns could not be obtained in quartz so design requirement 1 was not met. Cavitating flow is heavily influenced by the geometry of the Venturi, especially the overall shape and imperfections in the glassware[17] however, despite not being deliberately optimised (design requirement 4) the highly symmetrical geometry of this design was found to be effective, with cavitation and associated CFL being detected, so this Venturi was used for the initial optimisation experiments. The purpose of these experiments was to maximise the light throughput achieved into the detector both on terms of CFL emission and the optical arrangement.

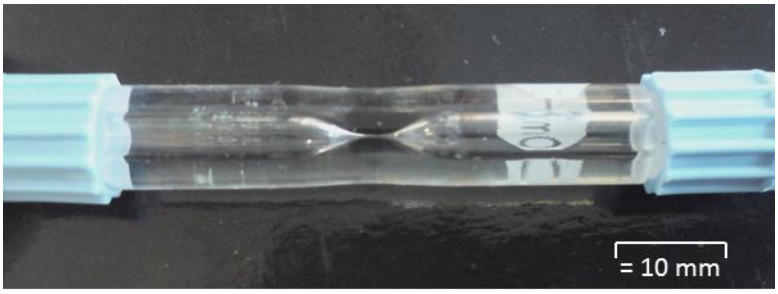

Plate 3-1 Modified Omnifit Venturi with an orifice of 220 µm i.d.

In operation, the pressure put on the fittings by prolonged use caused the glass threads to crumble (although the glass itself was not damaged by prolonged cavitating flow), so a second batch of Venturis, made by a different glass blower at the same company, was fabricated. These Venturis were non-symmetrical and resulted in a 90% reduction in CFL, suggesting that the geometry of the orifice has an important influence on the intensity of CFL.

3.2.2 Venturi Mk II

A second Venturi, which met design requirements 2, 3 and 4 was eventually fabricated by a different glassblower (Matthew Myles, University of East Anglia, Norwich UK). These were very symmetrical and had a nearly identical profile to the Mk I Venturi. The Ventruis fabricated by Myles were used in the experiments whose results are shown in this thesis.

3.2.3 Venturi Mk III

A third Venturi which met design requirements 1, 2, and 4 was fabricated by a prototyping company Multi-lab (Multi-lab QuartzTec Ltd. 5 Langlands Place, Kelvin South Business Park, East Kilbride, G75 0YF) as shown in Plate 3-2.

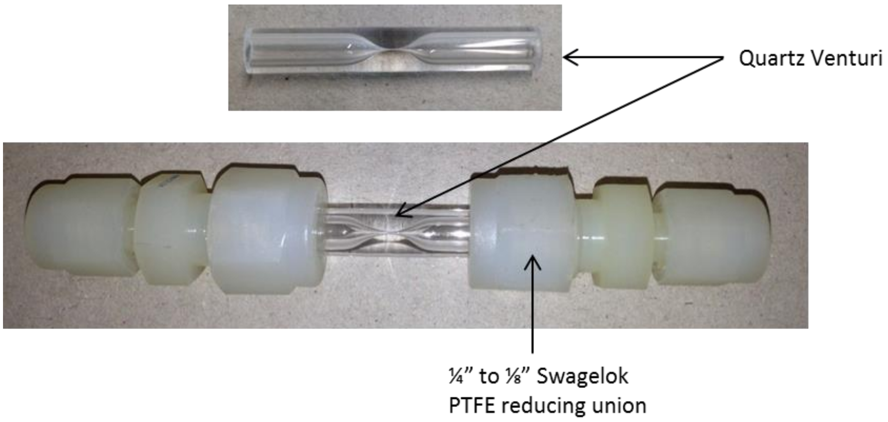

Plate 3-2. Quartz Venturi with a 220 µm i.d. orifice with and without fittings to allow liquid interface.

The Venturi was made from quartz therefore allowing potential UV emission to be transmitted; the orifice was 220 µm i.d. and the shape was based on the successful shape of the Mk II Venturi. Unfortunately Multi-lab were unable to fabricate threads to fit the high pressure connections. In order to overcome this ¼” to ⅛” Swagelok PTFE reducing unions were used (Figure 3.5). This enabled a liquid interface to occur, albeit at reduced flow rates due to leaks occurring at flow rates over 120 mL min^{-1}. However the venturi Mk III did allow the comparison between CFL observed through glass and through UV transparent quartz to be explored.

3.3 Optical system design

Initial design requirements of the optical system:

1. ensure only light from the Venturi cell was transmitted into the detector;
2. contain the optical arrangement optimised for light transmission;
3. flexible to allow integration of alternative detectors and alternative Venturis.

Given the extremely low levels of light detected via by CFL[16, 47] it was necessary to design an optical system capable of gathering the maximum amount of emitted light, while also minimising the amount of stray light in the system. After testing various prototypes, a final design was constructed (Machine Shop, University of Plymouth, UK) as shown in Figure 3-1 and Plate 3-3.

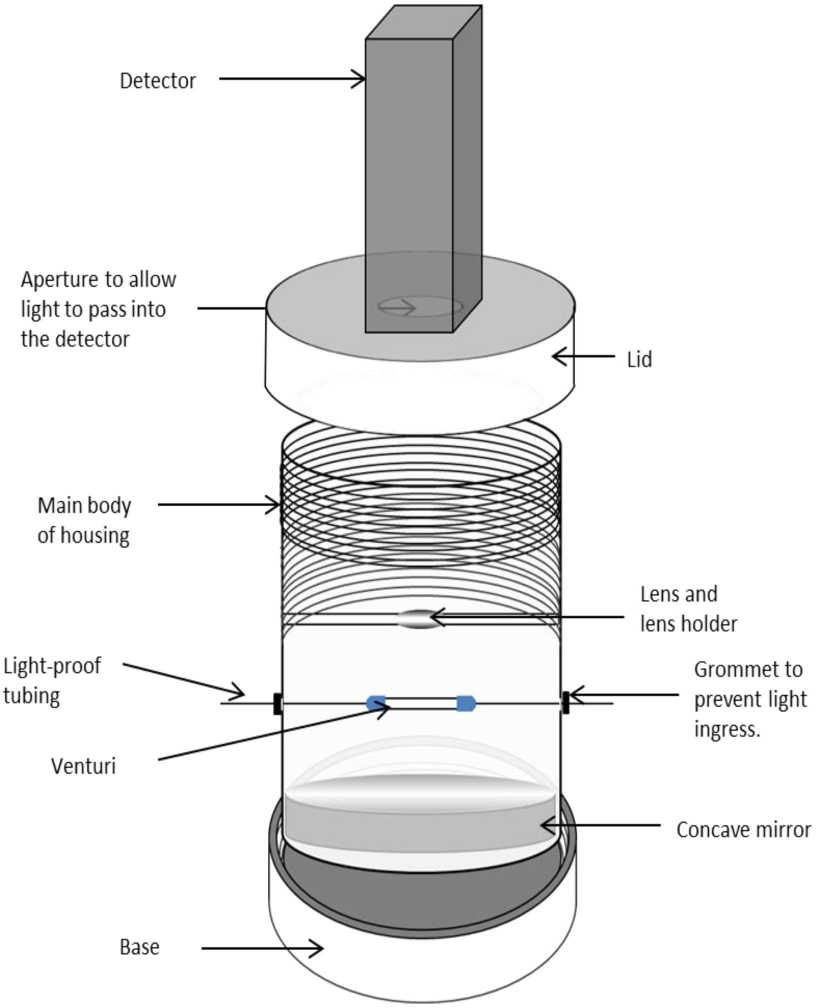

Figure 3-1 Cross section of optical system design

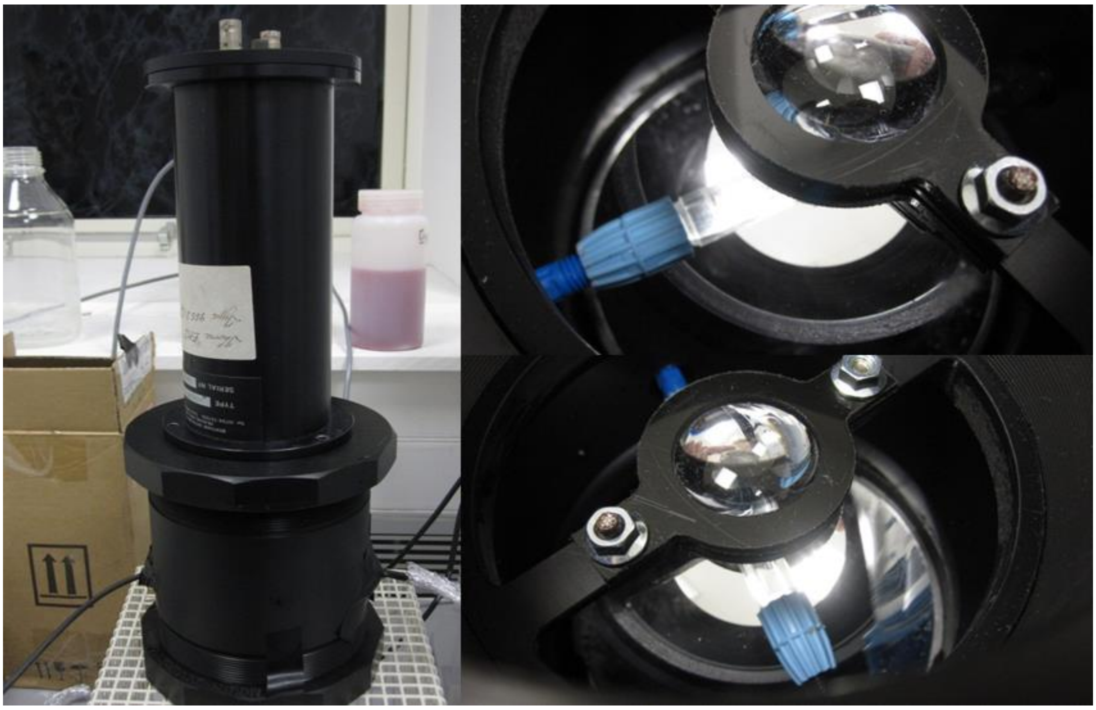

Plate 3-3 Optical system and detector also showing the Venturi and lens in situ

The optical system fulfilled all initial design requirements. It was machined from Delrin® (acetal homopolymer) this had good creep resistance, hardness and low thermal expansion. These qualities meant that the fine threads required to give the optical system a high level of flexibility could be machined into it easily. The optical system held in place the optimised optical arrangment.

The optical arrangment conisted of a concave mirror (f= 14.8 cm) and biconvex lens (f = 2.5 cm). The mirror was set at a fixed distance (9.8 cm) from the Venturi while the lens distance was adjustable to allow the focussing of the image onto the detector. The set up was optimised using an optical bench and an LED in place of the light emission from the Venturi. The optical arrangment is shown in Figure 3-.

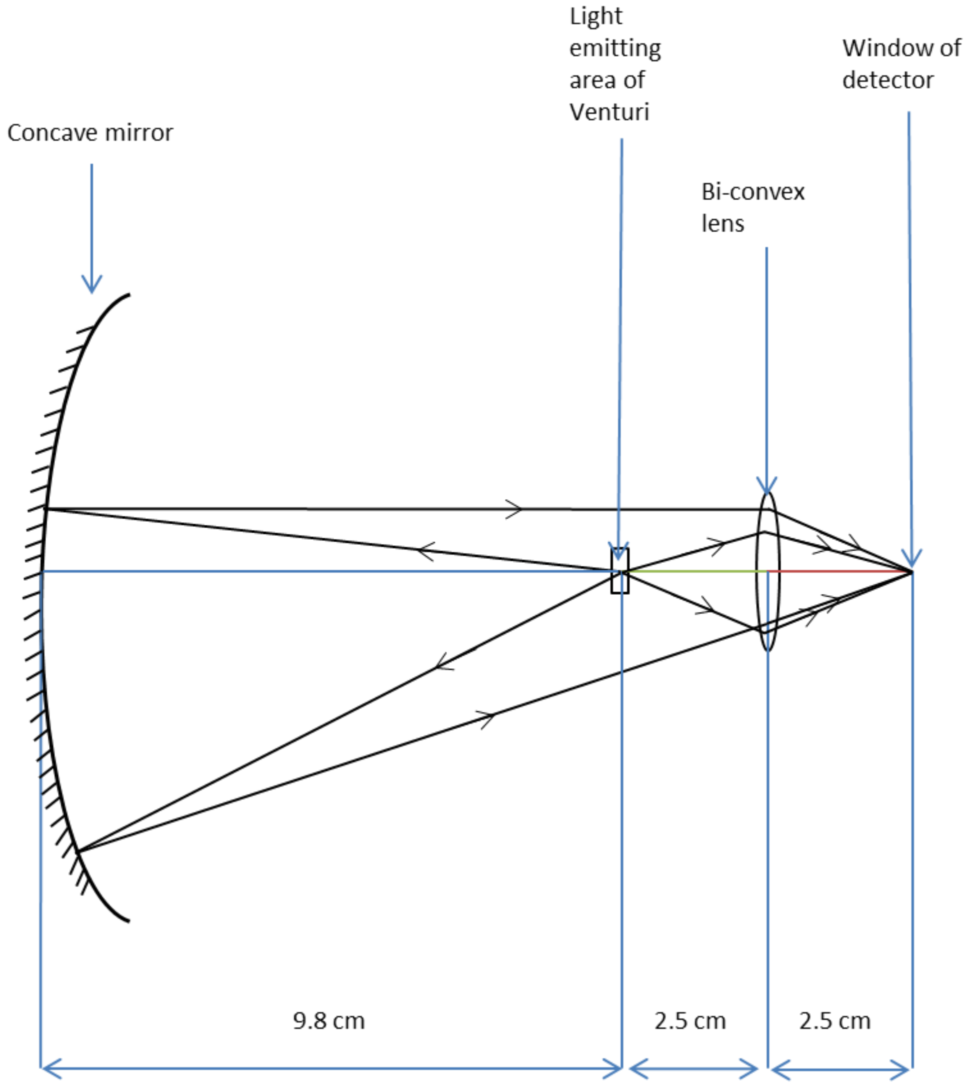

Figure 3-2 Ray diagram for optical arrangement.

The Venturi was held in place by the PTFE tubing, connecting the liquid handling manifold, via two holes in the side of the housing. This connecting tubing was coated in black heat-shrink to eliminate stray light total internal reflection along the tubing.

The housing was also adapted for experiments with liquids below ambient temperature by lining the inside with silica gel packs to prevent condensation on the Venturi (Plate 3-4).

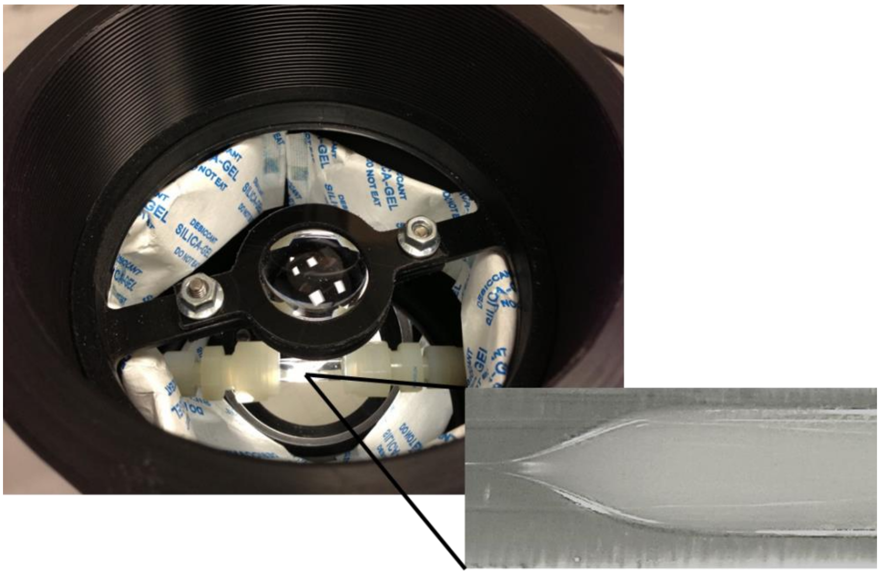

Plate 3-4 Housing with the quartz Venturi and silica gel packs.

3.4 Liquid handling manifold

The liquid handling manifold is shown schematically in Figure 3-; it comprised a 6-port injection valve and two high-flow preparative LC pumps.

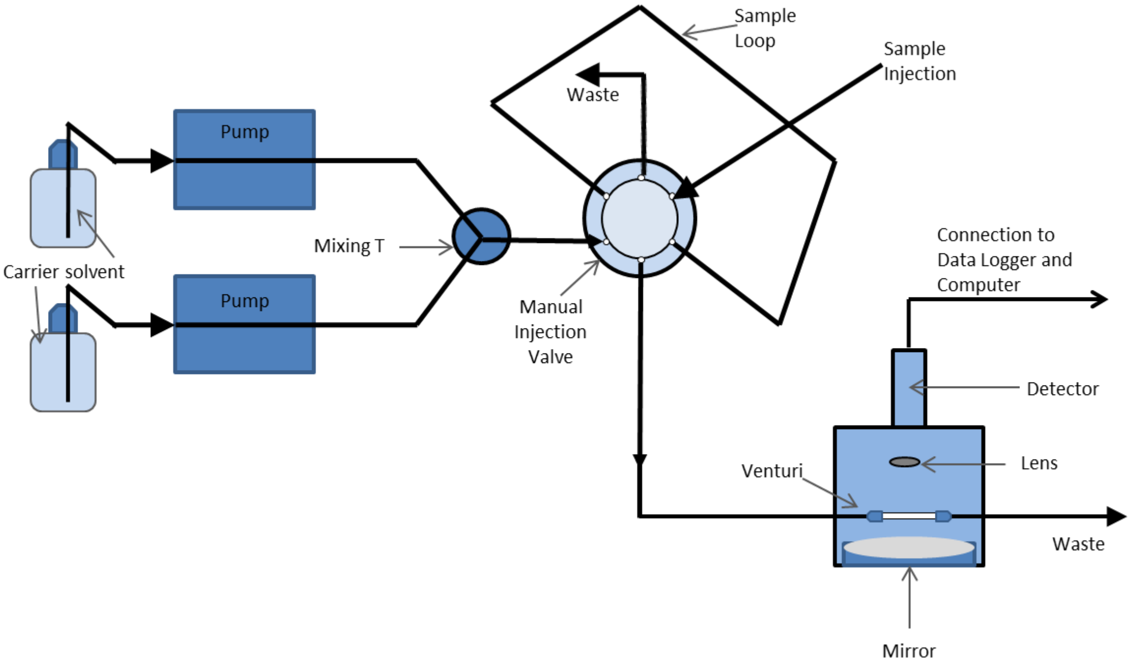

Figure 3-3 6-Schematic of system including 6-port injection valve configuration.

The 6-port injection valve was made of PEEK (Cheminert, Part No #C22-6184, Thames Restek UK Ltd, Units 8&16 Ministry Wharf, Wycombe Rd, Bucks, HP14 4HW) The valve could be fitted with 1.1 mm i.d. x 3.18 mm o.d. PTFE tubing and sample loops of varying sizes between 1 and 20 mL and could withstand backpressures of up to 17 bar. The injection valve arrangement allowed varying volumes of different liquids to be injected into the Venturi via a carrier of distilled deionised water (DDW, 18 MΩ). In order to achieve cavitation in Venturis with orifices between 160 and 250 µm i.d. liquid flow rates of between 20 and 120 L min^{-1} are necessary, with consequent pressures in the range from 2.5 to 25 bar. For example, Jarman and Taylor reported using a flow rate of 120 L min^{-1} through a Venturi with a 3/16 ” orifice[16] in order to achieve the cavitation effect. The micro-scale Venturi orifices used in this work did not require such high flow rates, however, it was still necessary to achieve substantial flow rates at high pressure, therefore two pumping methods which met the high pressure/high flow criteria were used namely positive head pressure and mechanical pumping.

3.4.1 Methods used to achieve high liquid flow rates

3.4.1.1 Positive head pressure

Initially a positive head pressure pump was constructed using a 2 litre expansion vessel from a central heating boiler (Antwort Part no #2181054 rated to 10 bar), shown in Plate 3-5.

Plate 3-5 Pressure vessel used as a method of introducing liquid under pressure to the Venturi.

The expansion vessel could be filled with DDW then pressurised up to 10 bar using a gas cylinder or bicycle pump via the Schrader valve. The major limitation of this system was that the head pressure was limited to 10 bar, hence limiting the flow rate through smaller orifices, and the internal pocket made of butyl rubber was prone to degradation. Nevertheless, this was a cost effective and successful method used for initial experiments. This set up that was used is shown in Figure 3-.

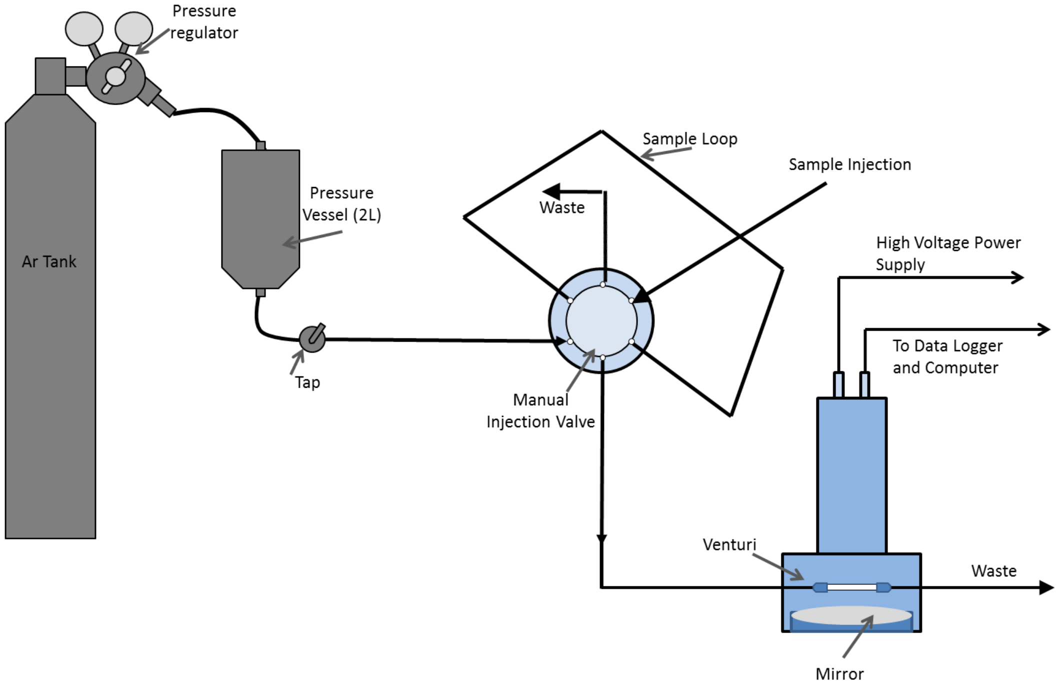

Figure 3-4. Schematic of positive head pressure setup.

3.4.1.2 Mechanical pumping

Mechanical pumping was achieved using two high flow preparative LC pumps (Gilson 306, Gilson scientific Ltd., Luton UK), each capable of pumping up to 100 mL min^{-1}, and plumbed together using a mixing T to give a combined maximum flow rate of 200 mL min^{-1} in 0.1 mL intervals (Figure 3-). The only drawback was that there was considerable pulsing, with consequent pulsing in the CFL signal.

3.5 Gas handling manifold

Previous studies have shown that the addition of noble gases to a cavitating liquid increases the light emission. [9, 10, 28, 34, 38] A gas handling manifold was constructed to enable controlled and reproducible dissolution of a known amount of gas in a liquid (Figure 3-5).

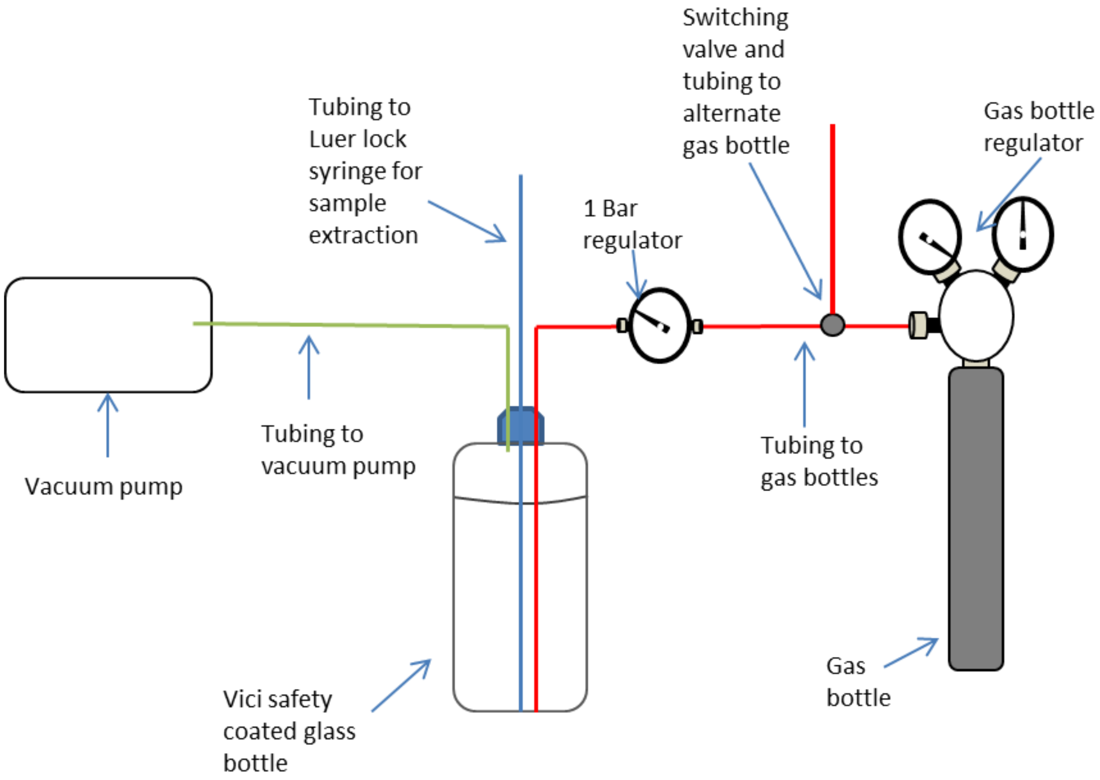

Figure 3-5 Schematic diagram of the gas handling manifold.

In operation, the gas handling manifold was maintained at a constant temperature in a water bath. The liquid under study was introduced into the coated safety bottle which was evacuated using the vacuum pump and the liquid sparged with helium to displace any dissolved gas. The helium sparge was turned off after 10 min and the vacuum pump was kept running until a pressure of -0.2 bar was obtained, whereupon the vacuum line was isolated and the vacuum pump turned off. The gas line was then switched so that the noble gas under study could be introduced at a pressure of 1 bar until the pressure in the system had equalized as evidenced by the cessation of gas bubbles emerging from the sparge line. Aliquots of liquid were removed from the bottle using the sampling line, via a quick stop Luer inline check valve, into a 5 mL Luer lock syringe and injected into the liquid handling manifold.

According to Henry's Law, the solubility of a gas is proportional to the partial pressure of the gas above the solution. The relationship described in Henry's law is shown below in Equation 25.[48]

$$c = p\,k \qquad \text{Equation 25}$$

Where:

c = concentration (mol L^{-1})

p = pressure (atm)

k = Henry's Law constant (different for each gas and solution (mol L^{-1} atm^{-1})

The method described above maintains a pressure of 1 bar of the selected gas above the solution. In general it is understood a greater mass of gas will dissolve in water with a lower temperature. This is due in part to lower temperature gases having less kinetic energy and being less likely to escape the solution once dissolved. The other reason is related to *Le Chatelier's Principle* because a gas dissolving is an exothermic process due to the formation of hydrogen bonds between the water and gas, therefore lowering the temperature favours the dissolution of the gas into water. The effect of temperature on the concentration of gas in solution is shown in Figure 3-62.

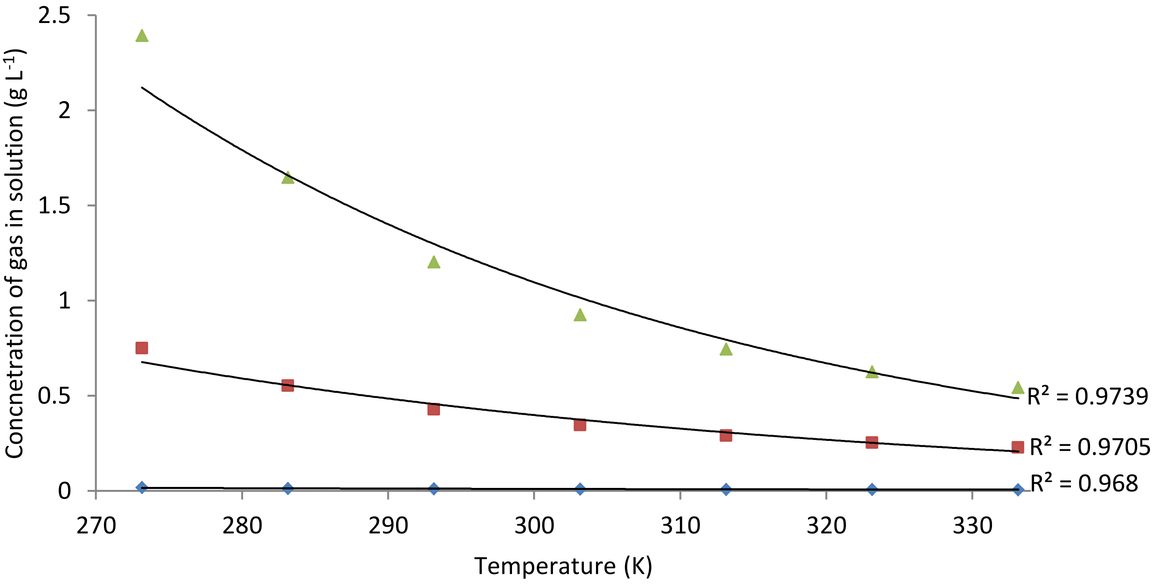

Figure 3-62. The effect of increasing temperature on maximum gas concentration in solution; ◆ Argon, ■ Krypton, ▲ Xenon. The values were derived from IUPAC solubility data.[49]

As can be seen in Fig 3-6, the higher the temperature the less gas was able to dissolve into solution due to gas interactions with the liquid it was dissolve in. Therefore in the experiments which were performed the samples were kept at low temperatures (3 °C) in order to maximise the volume of gas with a high heat capacity in solution which was expected to, in turn, increase the intensity of light emitted from cavitation.

The Henry's Law constants for the gases under investigation are shown in Table 3-1.

Table 3-1 Henry's law constants under standard conditions

Gas	Temperature K	Henry's law constant in water / mol dm-3 atm-1	Henry's law constant in water mol dm-3 atm-1
He	298	0.00038[50]	0.00071[49]
Ar	298	0.0014[50]	0.00255[49]
Kr	298	0.0025[50]	0.00450[49]
Xe	298	0.0043[50]	0.00790[49]

The values in Table 3-1 are for water at 298 K at atmospheric pressure. The constants are experimentally determined and therefore there is some disagreement between sources. The reasons for this include the experimental procedure followed to determine the constant, the analytical procedure followed, non-ideal solutions, and the effect of impurities. There is no official compilation of Henry's law data and the quality and age of the data can vary; therefore the values for this work were taken from a compilation which is currently awaiting publication.[51] Henry's Law constants can be used to calculate the solubility of the gas in liquid. The method used to regas the solutions isolated the solution and introduced a pure gas atmosphere above the solution at a pressure of 0.987 atm (1 bar). The predicted gas concentration in water under these conditions is shown in Table 3-2.

Table 3-2 Predicted gas concentrations in water at 298 K, column 1 uses data from *Wilhelm et al*.[50] column 2 uses data derived from IUPAC data.[49]

Gas	Gas concentration g L^{-1}	Gas concentration g L^{-1}
Helium	0.00146[50]	0.00280[49]
Argon	0.05519[50]	0.10053[49]
Krypton	0.19848[50]	0.37215[49]
Xenon	0.55715[50]	1.03526[49]

3.6 Detection and Data acquisition system

Initial requirements of the detection and data acquisition system were:

1. detect total light emission from CFL;
2. detect and differentiate the wavelengths of light emitted from CFL;
3. allow data to be continually logged on a computer.

Several different detectors were used to detect the CFL in different configurations, however, all were interfaced with an analogue to digital (Model ADC20 Picologger, Pico Technology, James House, Marlborough Road, Colmworth Business Park, Eaton Socon, St Neots, Cambridgeshire, PE19 8YP, United Kingdom) converter to allow data acquisition by computer and hence meet design requirement 3. The detector initially coupled with the optical system was a 2” diameter end-on photomultiplier tube (9558QB, Thorn EMI, ET Enterprises Limited, 45 Riverside Way, Uxbridge, UB8 2YF). This met design requirements 1 and 3. The PMT was operated at 1100 V with no additional gain settings. The picologger was set to log data every 100 ms.

A second detector which met design requirements 1 and 3 was the H10721P-110 (Hammatsu Photonics UK Limited, 2 Howard Court, 10 Tewin Road, Welwyn Garden City, HERTS, AL7 1BW) this detector was operated 2.7 mA and at 5 V with an optional +1.1 V to improve sensitivity, the optional additional voltage applied was 0.9 V.

In order to fulfil all design criteria it was necessary to interface a spectrometer with the optical system. Three different mini-spectrometers were investigated, namely: OceanOptics HR4000 (Part No. #HR4000, Ocean Optics Worldwide headquarters, Dunedin, Florida, USA); and two Hamamatsu mini spectrometers (Part No. #C9404MC and C10083CAH, Hamamatsu Photonics UK Limited, 2 Howard Court Tewin Road, Welwyn Garden City Hertfordshire, AL7 1BW, United Kingdom). In all cases it was necessary to use an optical fibre with a 3 mm solid UV transmitting core (#58458. 0.22NA UV/VIS Patchcord 1000 Micron fiber w/SMA Connector, Edmund Optics Ltd, 1 Opus Avenue, Nether Poppleton, York, YO26 6BL, UK) to transmit light between the optical system and the spectrometer which resulted in a high degree of *attenuation,* such that it was not possible to obtain a spectrum. In order to overcome this limitation the system was interfaced directly with a Hitachi F-4500 Fluorescence Spectrophotometer. The PMT was operated at 900 V with an excitation wavelength of 890 nm (to avoid interference with the signal detected from the CFL) and emission wavelengths set to 200-900nm. The slit width was 200nm (the maximum) and the scan rate was set to 30,000 nm/min.

3.7 Conclusions

The manufacture of a Venturi tube with a very small restriction was practically very difficult due to the ease with which the glass would collapse in on itself during the manufacturing process. Several approaches were therefore investigated. The best approach was found to be using a very experienced glass blower to make the restrictions. This resulted in several Venturis being fabricated for this research. The modified glass Omnifit tubes were the most adaptable and made part of the fluid handling manifold easily. However this meant that measurement of light emission in the UV was hampered. A quartz Venturi was fabricated; however this could not be reliably interfaced with the fluid handling manifold due to the lack of high pressure connections.

Other components for the system were sourced and resulted in a reliable high pressure system which could pump the carrier liquid and liquid samples through the Venturi while any light emission was monitored using a light tight housing and a low voltage PMT connected to a data logger and laptop to enable continuous data acquisition.

4 CFD model of cavitating flow

4.1 Objective

The second objective was to perform computational fluid dynamic modelling of the micro-Venturi to determine the effect of pressure and flow conditions on the liquid passing through the orifice.

4.2 Introduction

Computational fluid dynamics (CFD) is an engineering tool used to model a wide variety of flow conditions in liquids and gases, e.g. for modelling the interactions of helicopter propellers and the pressure field that they induce, or fluid flow down a plug hole. It is based on the principles of the conservation of energy, mass and force-momentum balance which combine to form the basis of the Navier-Stokes equations; these are partial differential equations which cannot be analytically solved. Because these equations cannot be solved an approximate solution must be obtained using a discretisation method whereby the continuous problem domain, e.g. a Venturi, is replaced with a discrete domain using a grid mesh. Each flow variable or unknown is then determined at each grid point using algebraic equations.

4.3 Stages of a typical CFD simulation

1. Drawing the geometry

   A Computer Aided Design (CAD) programme such as SolidWorks, is used to create a geometric model which accurately represents the physical object.

2. Creation of the mesh

The mesh identifies the discrete finite locations where the variables are going to be algebraically calculated. The most accurate results are generated using a fine mesh, but this increases the number of calculations, so the mesh needs to be tailored to the physical phenomenon under investigation. The reliability of the results generated from CFD are largely dependent on the suitability of the mesh.

3. Selection of model and parameters

The next step is to define the parameters such as fluid type, inlet flow rates, outlet conditions, temperatures for the simulation.

4. Calculation of variables.

The method of discretisation produces many algebraic equations which need to be solved. These equations are solved by an iterative process starting with a “best guess” for the variables before performing the calculations. This is repeated until a converged solution is determined to have been reached.

5. Determination of converged solution

A converged solution is reached when the sum of the residual values is low enough; this depends on the accuracy required from the process. A rule of thumb used in this research is that that the sum of residual values is less than 1×10^{-5}. Another check is to perform further iterations which result in negligible changes to the variable values.

6. Post processing

The results from the converged solution can then be presented in various ways depending on the parameter under investigation.

4.4 SolidWorks model

A simple Venturi was drawn using SolidWorks 13, (Figure 4-1) to mimic the conditions in the 160 µm i.d. Venturi used in cavitating flow experiments.

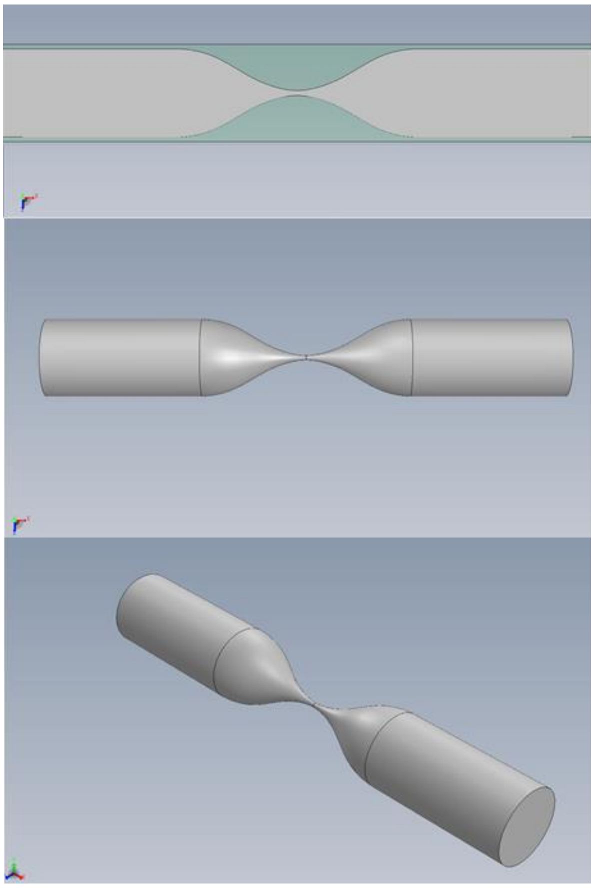

Figure 4-1 SolidWorks drawing of a Venturi with an orifice of 160 µm and initial pipe diameter of 3 mm.

4.5 Ansys CFD simulation

Ansys is a piece of engineering simulation software which can be used to simulate designs under real world conditions. In this research an Ansys simulation was used to analyse the flow regime in the Venturi and to assess the impact of the liquid interface on the pressure changes within the system.

The first stage of the simulation was to mesh the Venturi using the settings shown in Figure 4-2. The domain, which is defined as the Venturi, is discretised into the mesh where the governing equations were solved for each element. At each corner of the element the pressure, velocity, temperature and turbulence were solved, enabling maps of these physical properties to be produced. The tolerance of the residual target was 0.00001, which determined the level of residual error allowed in the solutions.

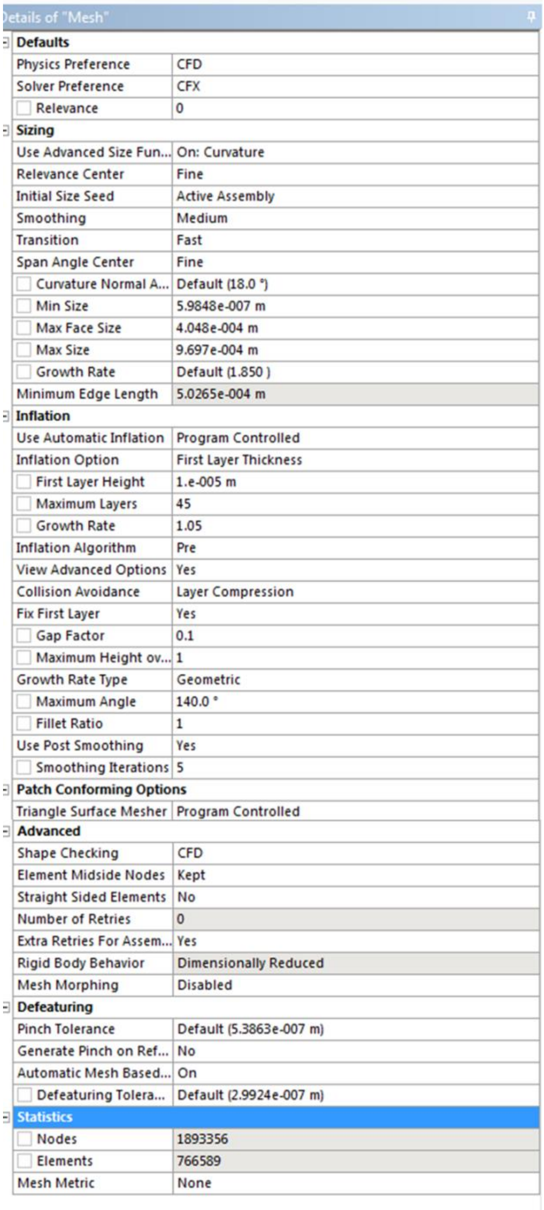

etails of "Mesh"

Defaults	
Physics Preference	CFD
Solver Preference	CFX
☐ Relevance	0
Sizing	
Use Advanced Size Fun...	On: Curvature
Relevance Center	Fine
Initial Size Seed	Active Assembly
Smoothing	Medium
Transition	Fast
Span Angle Center	Fine
☐ Curvature Normal A...	Default (18.0 °)
☐ Min Size	5.9848e-007 m
☐ Max Face Size	4.048e-004 m
☐ Max Size	9.697e-004 m
☐ Growth Rate	Default (1.850)
Minimum Edge Length	5.0265e-004 m
Inflation	
Use Automatic Inflation	Program Controlled
Inflation Option	First Layer Thickness
☐ First Layer Height	1.e-005 m
☐ Maximum Layers	45
☐ Growth Rate	1.05
Inflation Algorithm	Pre
View Advanced Options	Yes
Collision Avoidance	Layer Compression
Fix First Layer	Yes
☐ Gap Factor	0.1
☐ Maximum Height ov...	1
Growth Rate Type	Geometric
☐ Maximum Angle	140.0 °
☐ Fillet Ratio	1
Use Post Smoothing	Yes
☐ Smoothing Iterations	5
Patch Conforming Options	
Triangle Surface Mesher	Program Controlled
Advanced	
Shape Checking	CFD
Element Midside Nodes	Kept
Straight Sided Elements	No
Number of Retries	0
Extra Retries For Assem...	Yes
Rigid Body Behavior	Dimensionally Reduced
Mesh Morphing	Disabled
Defeaturing	
Pinch Tolerance	Default (5.3863e-007 m)
Generate Pinch on Ref...	No
Automatic Mesh Based...	On
☐ Defeaturing Tolera...	Default (2.9924e-007 m)
Statistics	
☐ Nodes	1893356
☐ Elements	766589
Mesh Metric	None

Figure 4-2 The settings used to generate a mesh for the 160 µm i.d. Venturi.

The settings shown in Figure 4-2 resulted in the mesh shown in Figure 4-3, inflation layers were used to ensure that enough detail was calculated at the walls of the Venturi where there was expected to be extensive interaction which needed to be modelled. This level of detail was extended to the orifice where fluid flow was expected to be complex.

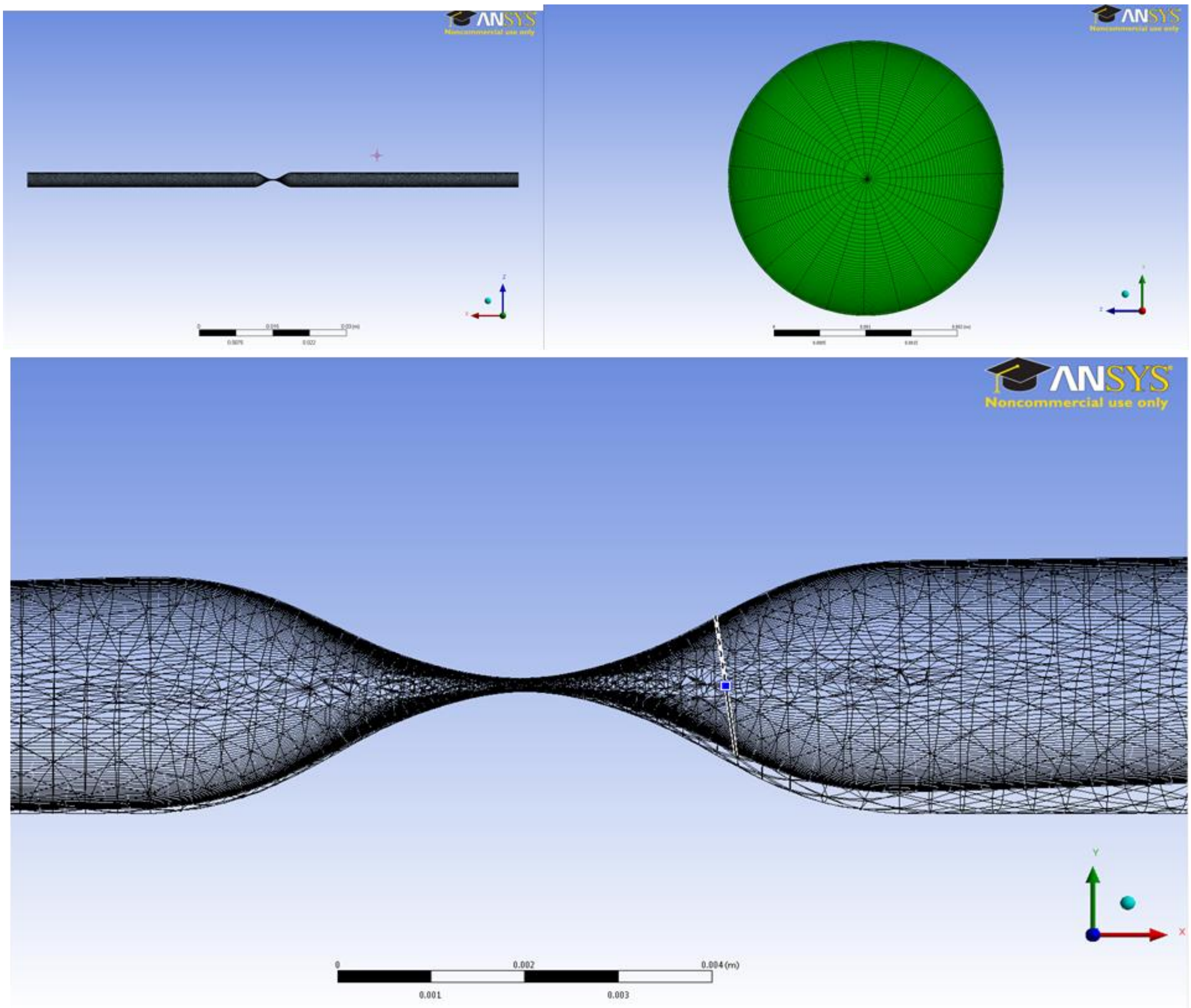

Figure 4-3 Rendered mesh for the orifice of the Venturi.

The solver was set to solve for water flowing through the Venturi at 160 mL min^{-1} using a shear stress transport (SST) model which is the optimal method for use in turbulent conditions. The conditions at the orifice are known to be turbulent because of a high calculated Reynold's number. This mesh gave results which enabled the temperature changes, turbulence and pressure changes inside the Venturi to be mapped as shown in Figure 4-5. A Y+ value is a dimensionless value used to describe how fine or coarse a mesh is, using the SST model a Y+ value of around 1 was required in order to map the boundaries of the Venturi sufficiently for the model to work. Using this mesh a Y^+ value of 1.01 was obtained, this indicated that the modelling of the boundary layer was modelled effectively.

The results from the CFD model were validated by using the Bernoulli equation to calculate the velocity at the orifice of the Venturi and comparing those results to those calculated by the model. The results of this comparison are shown Figure 4-4 and it can be seen that the results vary insignificantly indicating that the results generated by the model and the experimentally derived data are in agreement.

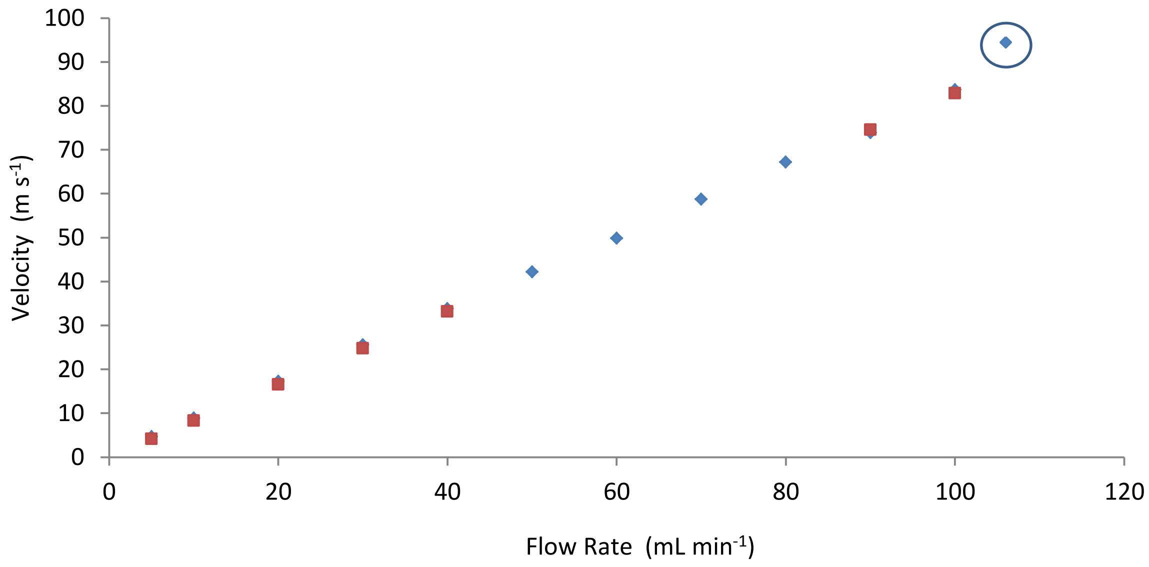

Figure 4-4 Comparison of calculated velocities at the orifice of the 160 µm i.d. Venturi: ◆ model values and ■ calculated values. The circled value is the start of predicted choked flow.

In the model the upstream pressure was set at the appropriate pressure for the flow rate under investigation, liquid flows from left to right in Figure 4-5. As can be seen from Figure 4-5 the model predicted lower pressures in the orifice as the flow rate was increased, which agrees with cavitation theory.

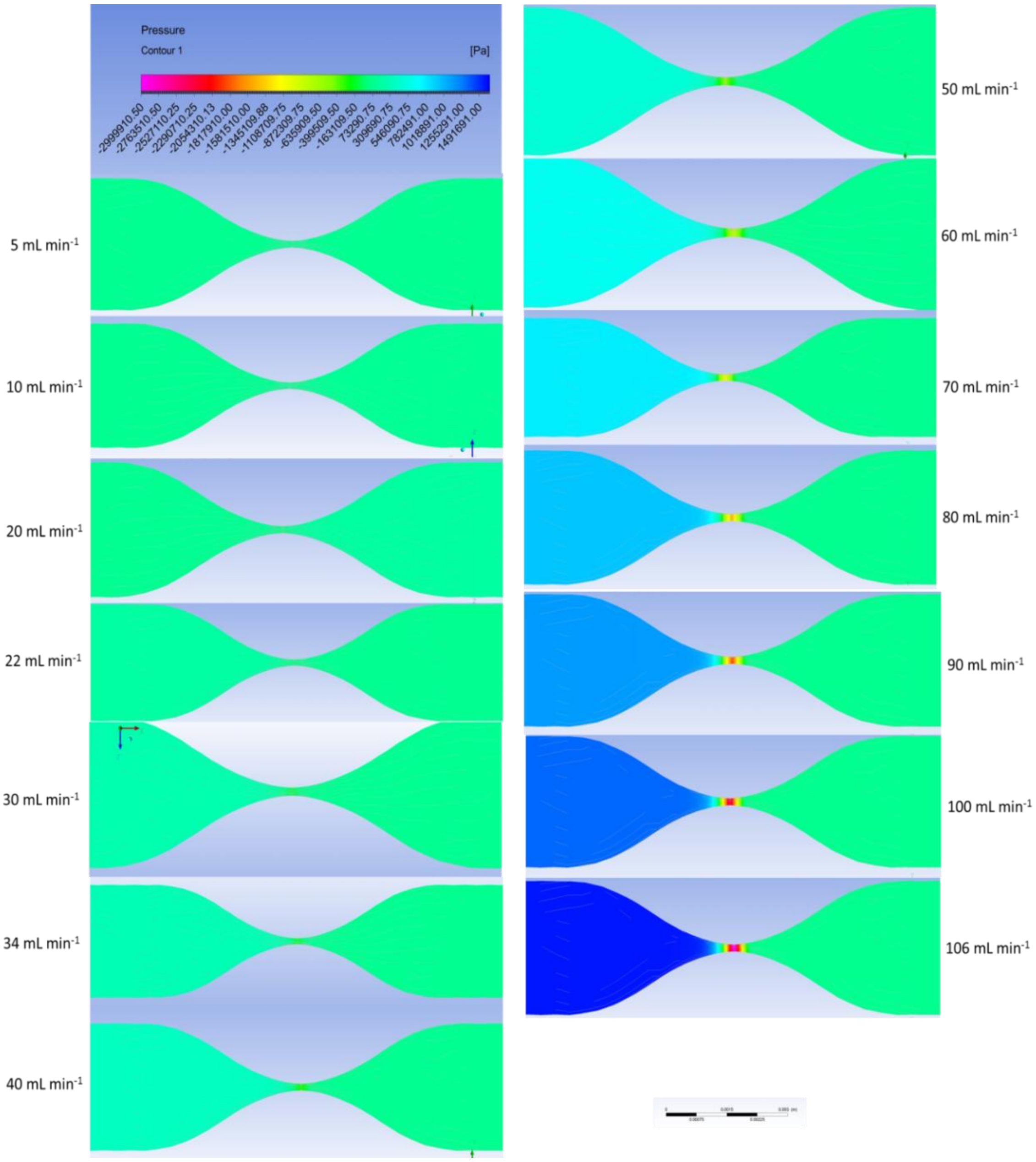

Figure 4-5 Modelling the effect of increasing flow rate on the pressure through a 160 µm i.d. Venturi using water at 276 K. The increase in flow rate promotes a decrease in pressure as indicated by the change in colours at the centre of the Venturi.

Between 22 and 106 mL min^{-1} the pressure in the orifice was predicted to be increasingly negative w.r.t. atmospheric pressure, indicating that cavitation would occur under these conditions. The negative solution results from the onset of multi-phase flow, which the current model is not sufficiently sophisticated to model with accuracy. However, the predicted trends were largely consistent with the empirical studies described here. For example, cavitation inception was observed to occur at 34 mL min^{-1} whereas the model predicted 22 mL min^{-1}, which is in reasonably good agreement given the difficulty of determining the exact point of inception by observation. The choking point was observed to occur at approximately 106 mL min^{-1} which was the upper limit at which the model could render successfully. It was not possible to make observations at flow rates above 100 ml min^{-1} due to the damage it threatened to cause the pumping system which struggled to cope with the back pressure.

The temperature of the fluid predicted by the model is shown in Figure 4-6, indicating that temperature dropped before passing through the orifice and increased again downstream. The temperature change remained small +/- 0.5 K over a wide range of modelled temperatures. It is unknown whether this change in temperature has a significant effect on the flowing liquid. However there was an observation that for liquid cycled through the Venturi during optimisation experiments the liquid did perceptibly increase in temperature.

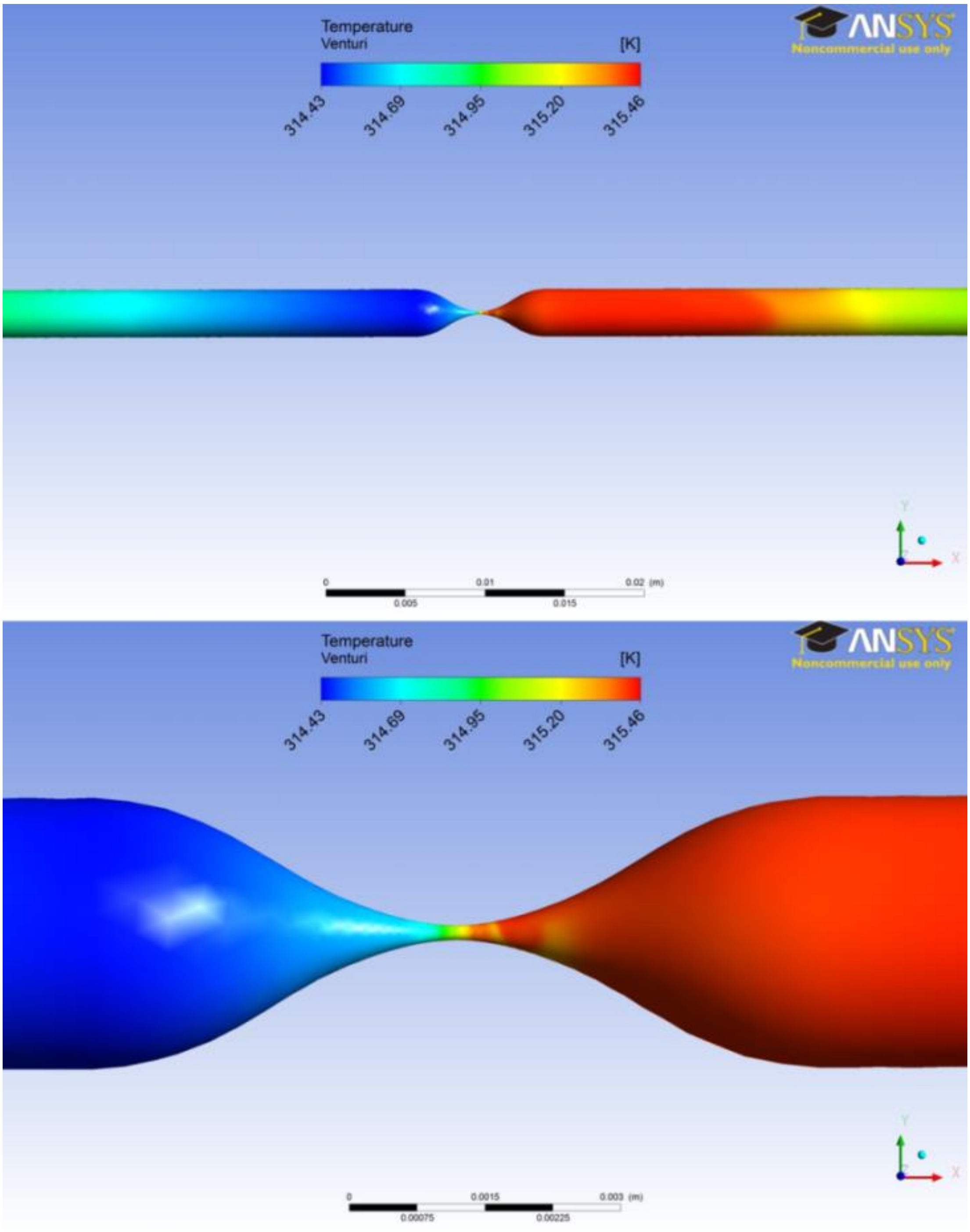

Figure 4-6 Temperature change across the orifice.

As the liquid flows through the orifice, the velocity increases and the pressure drops, as shown in Figure 4-7 as a series of streamlines. These streamlines show the fluid under laminar flow upstream of the Venturi orifice, then a large increase in velocity to 85 ms^{-1} as it passes through the orifice, and turbulent flow downstream of the orifice.

The velocity agreed well with the value of 83 m s^{-1} calculated using the Bernoulli equation.

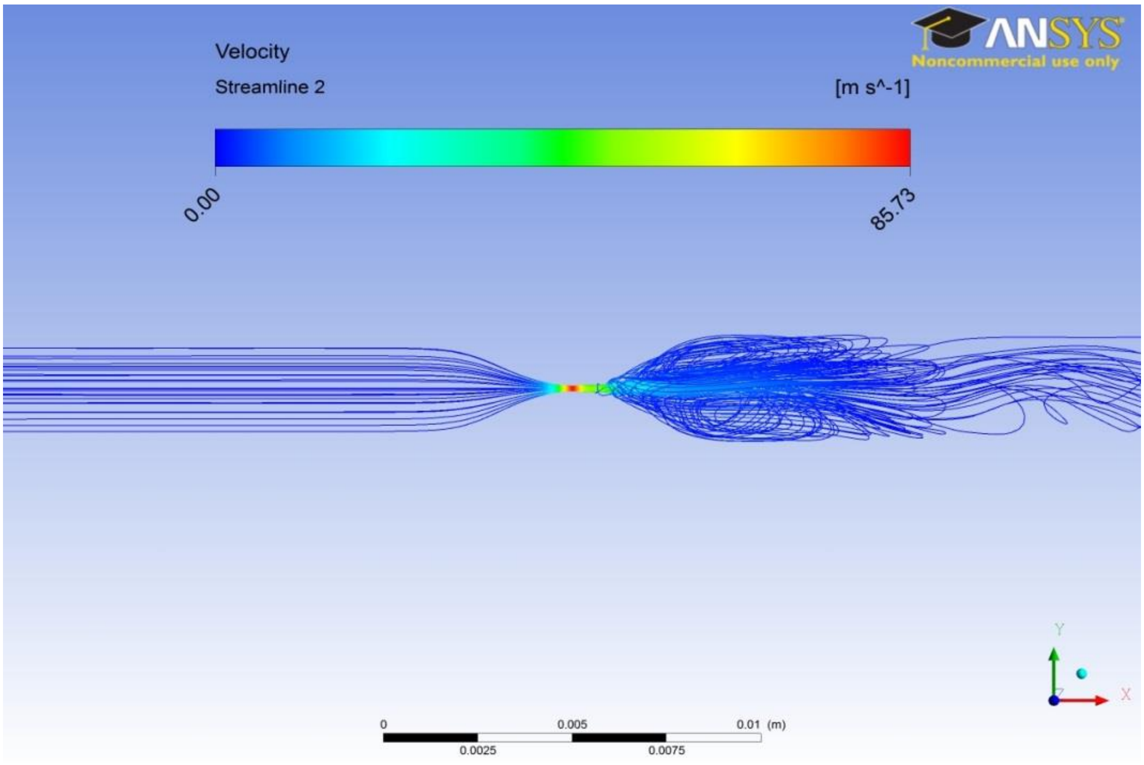

Figure 4-7 Streamline tracing the flow through a Venturi.

The point of maximum turbulence was estimated to be slightly downstream from the orifice as shown in Figure 4-8. This coincided with the area of CFL emission, determined by positioning a fibre optic at various points along the Venturi tube and monitoring the intensity of light using a coupled PMT. This result is expected because, under conditions of turbulent flow, the unstable pressure and velocity makes it more likely for cavitation, and potentially CFL under the correct conditions to be detected. The position of maximum light emission was determined during the early stages of this research when the experimental set up was being designed. It was determined that the detector had to accept light from a wide angle in order to maximise the intensity of light observed due to the scattering effect of the light off the water bubbles. Because of this the exact positioning of light emission was not determined. This could be identified in future research.

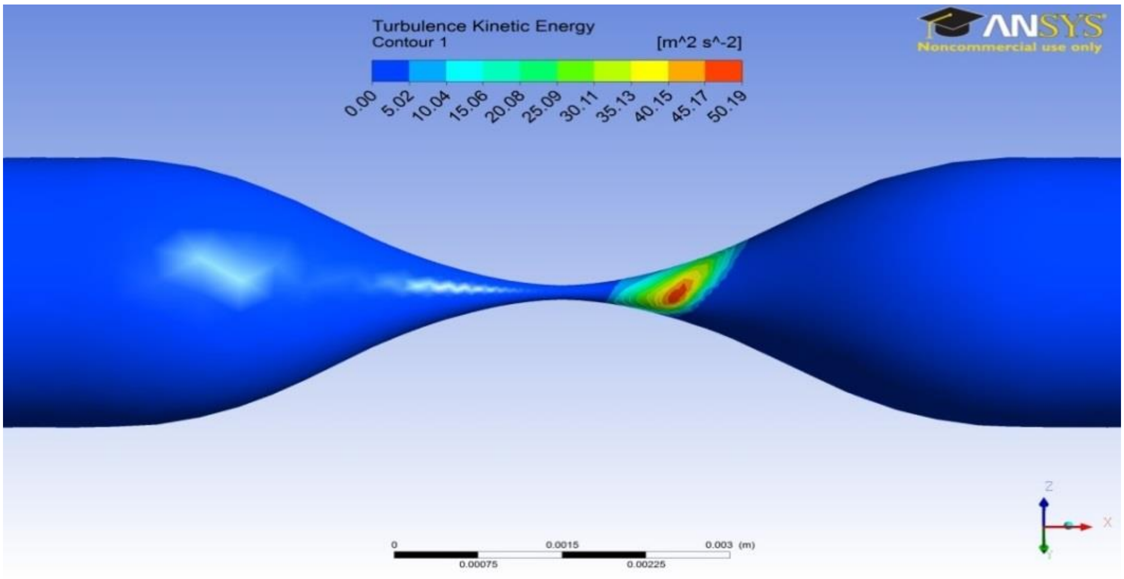

Figure 4-8 Turbulence in the Venturi.

4.6 Conclusions

Cavitation was modelled for water flowing through a 160 µm i.d. Venturi. The model was validated by comparing the predicted velocity, calculated using Navier-Stokes equations, with the velocity calculated using the Bernoulli equation. The results were found to be almost identical, hence verifying the model and the flow rates predicted for cavitation inception and choking. Pressures predicted using the CFD model were highly negative, suggesting that the model was insufficiently sophisticated to cope with cavitation inception. However, the pressure drops predicted before onset of cavitation compared favourably with the pressure changes calculated in Chapter 2 (Section 2.1.2), lending weight to the premise that the pressure changes would be sufficient to promote cavitation luminescence. The area of maximum turbulence predicted by the model coincided with the areas of maximum light emission observed experimentally in Chapter 5. A more in depth model could be of use to predict the conditions under which cavitation would occur, and could be expanded to categorise the type of cavitation, sheet, transient or super cavitation.

5 Cavitating flow luminescence and the effect of dissolving noble gases

5.1 Objective

Objective three was to investigate cavitating flow luminescence in the micro-Venturi with the specific focus of establishing the practical conditions under which optimal luminescence occurs. This will be based on work done previously by Jarman and Taylor in the 1960's,[1, 16] who achieved cavitation using tap water.

Results of the CFD modelling confirmed that cavitation should occur at the micro-scale, using a 160 µm Venturi orifice and liquid flow rates of between 40 to 106 mL min^{-1}. However, the CFD model could not predict whether CFL would occur so the next step was to test the system described in 3.

5.2 Cavitation flow luminescence in water.

The inception and progression of hydrodynamic cavitation occurring in a 160 µm i.d. Venturi using water at 298 K which has not been treated in any way is shown in Plate 5-1. Inception of cavitation was taken to be when visual and audible indicators were first observed. The inception of cavitation occurred at 35 mL min^{-1} giving a cavitation inception number of 0.234, which broadly agrees with work carried out by other researchers.[22] In Plate 5-1 the series of photographs taken with a USB microscope (VMS-004D – 400x USB Microscope, Veho Europe (HQ), PO box 436 Southampton, Hampshire, UK, SO30 9DH) demonstrates progression from laminar fluid flow, through de-gassing, to turbulent cavitating flow. The typical cavitation jet can be seen extending from the orifice into the main body of the Venturi as flow rate was increased.

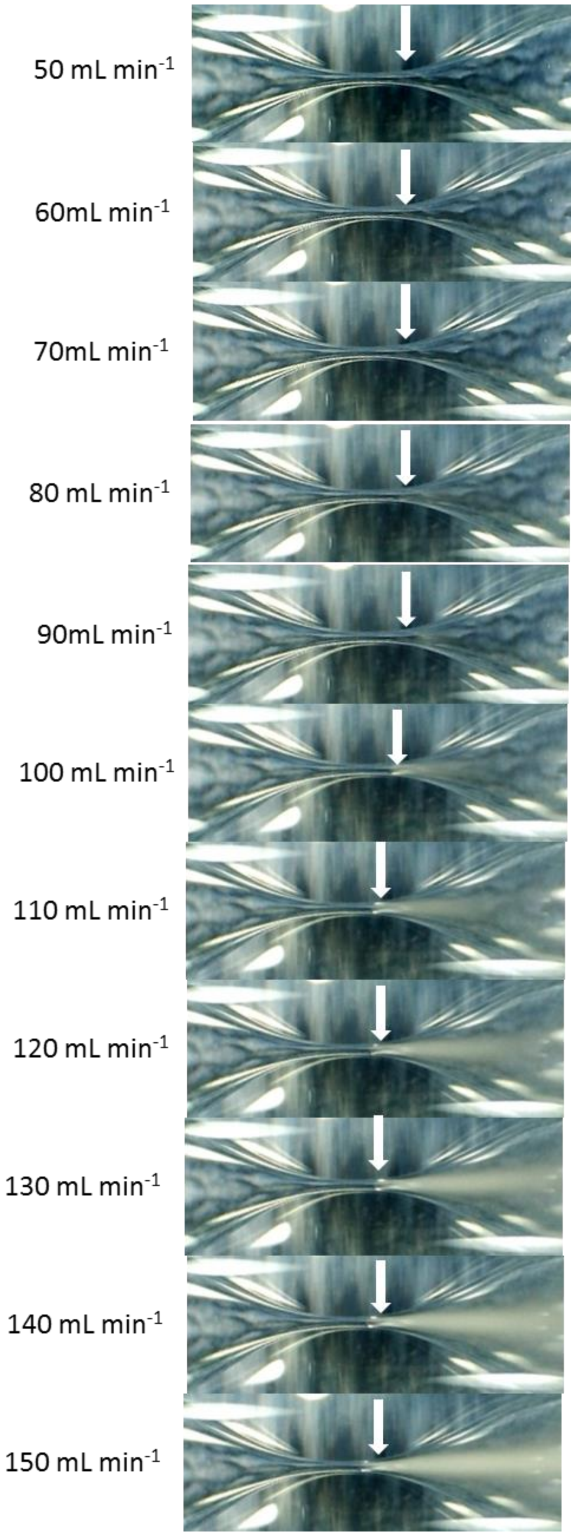

Plate 5-1 Photograph of a 220 µm i.d. Venturi orifice showing where cavitation occurs (solid white arrow) in water as flow rate increases. Note that the onset of cavitating flow occurs at 80 mL min^{-1} but is not distinctly visible in the picture until 100 mL min^{-1}. The photographs shown here are taken at 20x magnification.

Cavitating flow luminescence was observed at flow rates of 50 – 100 mL min^{-1} in a 160 µm i.d. Venturi, 70 – 150 mL min^{-1} in a 180 µm i.d. Venturi, 100 – 160 mL min^{-1} in a 200 µm i.d. Venturi and 100 – 160 mL min^{-1} in a 220 µm i.d. Venturi. An example of the raw data for a 5mL sample produced by the PMT is shown in Figure 5-1

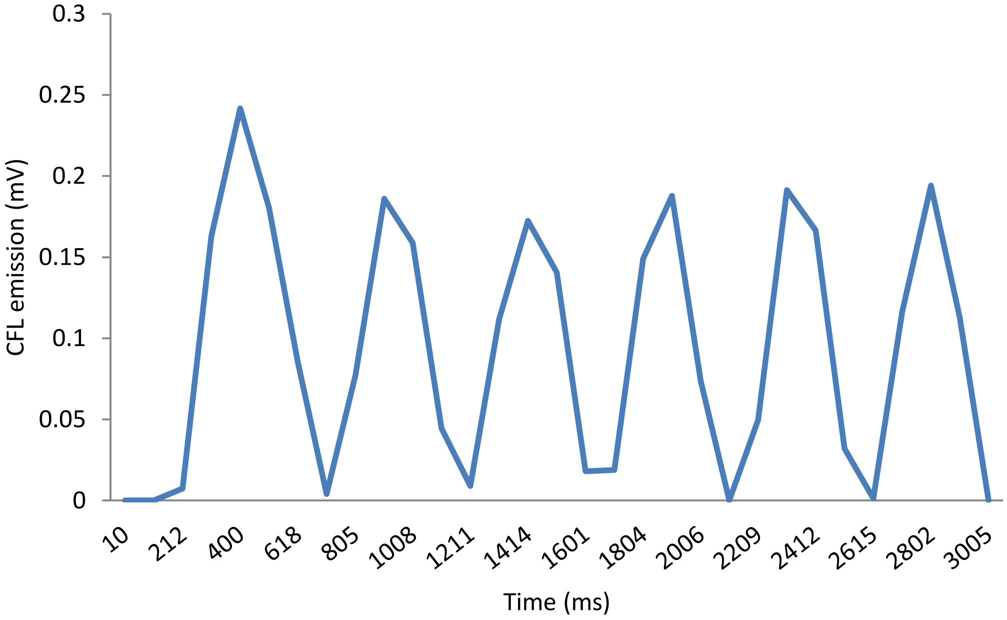

Figure 5-1 CFL emission raw data from a 5 mL sample of water at 276 K being pumped at 100 mL min^{-1} through a 180 µm i.d. Venturi. The pulsing from the pumps can be seen as noise in the signal. Due to the pulsing in the signal the peak height was not used, instead the total peak area for each sample was analysed.

This is the first time that CFL has been observed on the micro-scale. The CFL signal displayed a cyclical nature which corresponded with the pulsing of the pumps. The total area under the peaks of each 5 mL injection was integrated for quantitative comparisons. The data generated by integrating the total area was processed using Microsoft Excel and Minitab 16. Scatter graphs with error bars of ± 1 standard deviation were plotted using Excel (Figure 5-5, 5-6, 5-7, 5-8) and the significance of observed trends was tested using Minitab 16. The trends were identified and analysed using regression models (Figure 5-2 and Figure 5-3) and the significance investigated by producing p values and F values. A p-value of $p < 0.05$ was used as an indicator that the relationship observed was statistically significant. The F-value produced as part of the analysis of variance within the data set was used as an indicator that there was variance within the data set as expected for these experiments. A large F-value indicates a large variance and vice versa. The Anderson-Darling test is used to determine that the data comes from a normal distribution of data. An Anderson-Darling Normality Test was also carried out and a probability plot of residual values was plotted for each data set to check that the errors were distributed normally (residual values = expected values – experimental values). This produced a p value where $p > 0.05$ indicated a normal distribution (Figure 5-4) this will be referred to as the NPp value (Normality Plot p value).

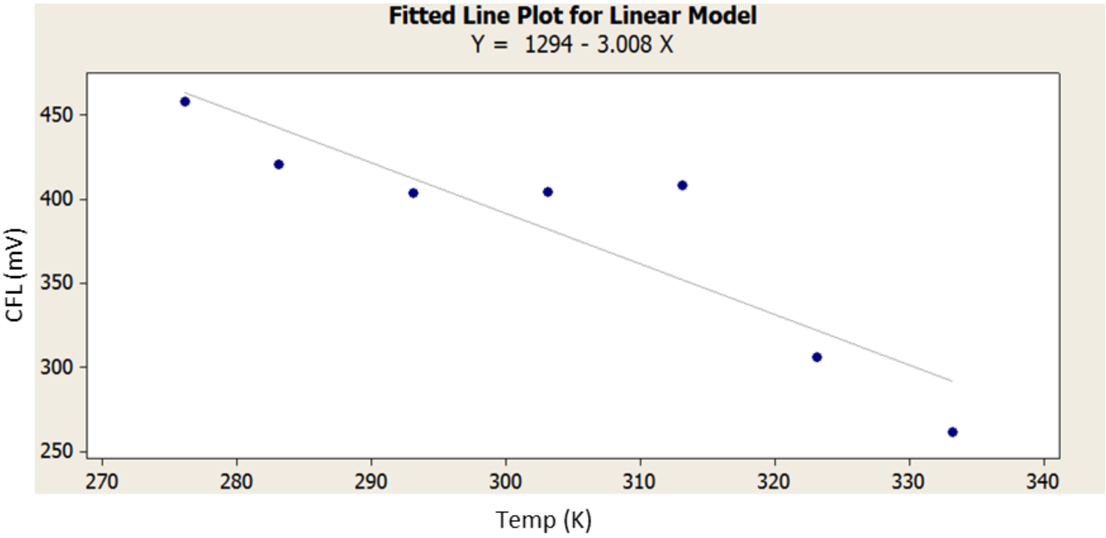

Figure 5-2 Scatter plot of the effect of increasing water temperature on CFL emission observed through a Venturi with a 220 µm i.d. orifice with water at 120 mL min^{-1}; linear regression model, df = 1, p = 0.005 and F = 22.071.

The effect of increasing temperature on CFL is shown in Figure 5-2 the data was generated using untreated DDW. The linear trend line was generated using regression analysis and chosen because a linear model gave the greatest R^2 value (smallest residuals) and smallest p value indicating that the linear relationship between temperature and CFL was more significant than the other potential relationships. Output from the Minitab 16 regression analysis tool is shown in Figure 5-3 this gives information about the data plotted and agreement of the model with the data. This was combined with a variance test and normality test to analyse the significance of the data collected.

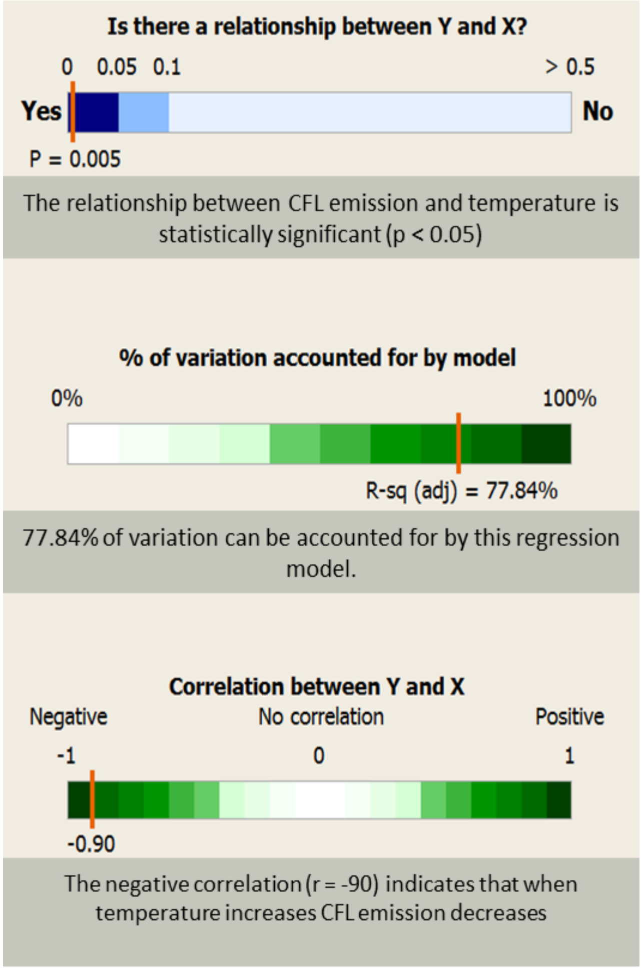

The relationship between CFL emission and temperature is statistically significant (p < 0.05)

77.84% of variation can be accounted for by this regression model.

The negative correlation (r = -90) indicates that when temperature increases CFL emission decreases

Figure 5-3 Output from Minitab 16 identifying the significance of the relationship between increasing temperature and CFL emission intensity from a Venturi with a 200 µm i.d. orifice. Red bars indicate the position of values generated by this analysis.

An Anderson-Darling normality test was performed on the residuals to determine whether the errors were normally distributed a p value of 0.189 (above 0.05 as required) shows that this was the case for the data in Figure 5-4.

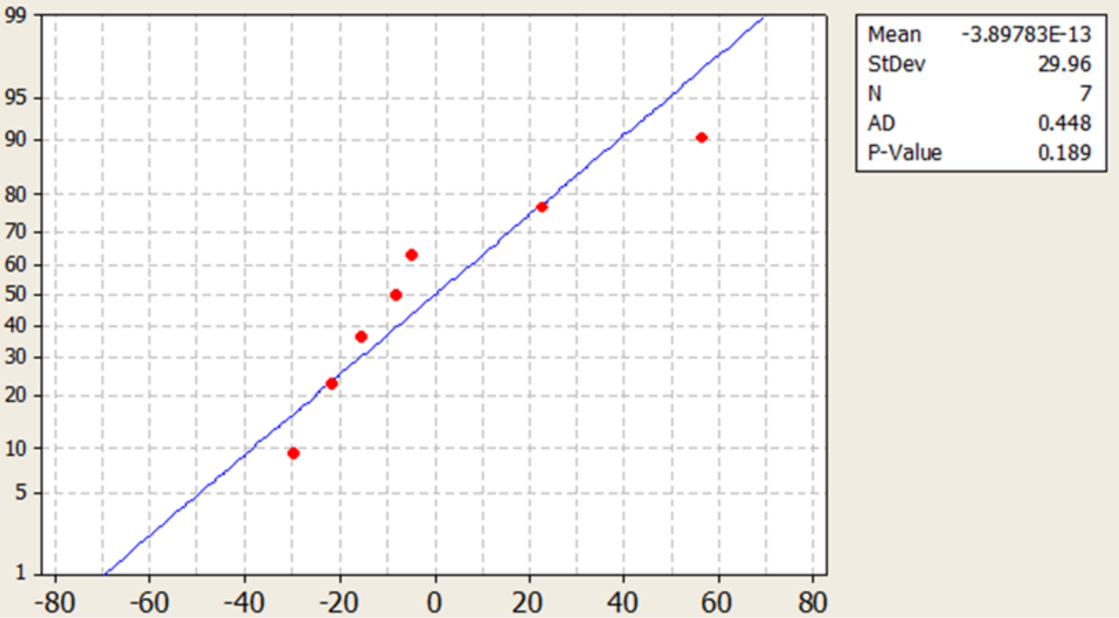

Figure 5-4 Anderson-Darling Normality Test probability plot of residual values showing normal distribution (p = 0.189) for the effect of increasing water temperature on CFL emission observed through a Venturi with a 200 µm i.d. orifice

The effect of temperature on peak area signal for CFL emission intensity in untreated DDW flowing through a glass Venturi tubes with orifice sizes of 200 µm i.d. and 220 µm i.d. and a quartz Venturi with an orifice of 210 µm i.d. is shown in Figure 5-5. These results show that increasing the temperature of the flowing liquid caused a decrease in the intensity of observed CFL due to the lower dissolved gas volume. This trend has statistical significance (all p values < 0.05). This holds true for the 2 different sized orifices (200 and 220 µm i.d.) as well as the two different Venturi materials (glass and quartz). It is also noted from these results that the quartz Venturi resulted in more CFL emission being detected. The shape of the quartz Venturi was closely modelled on the glass Venturi shapes produced. All Venturis had inlet and outlet angles of 20° therefore the change in geometry between the handmade glassware should be minimal. The error bars associated with the glass Venturi tubes are noticeably smaller than those for the quartz Venturi which was due to pressure fluctuations.

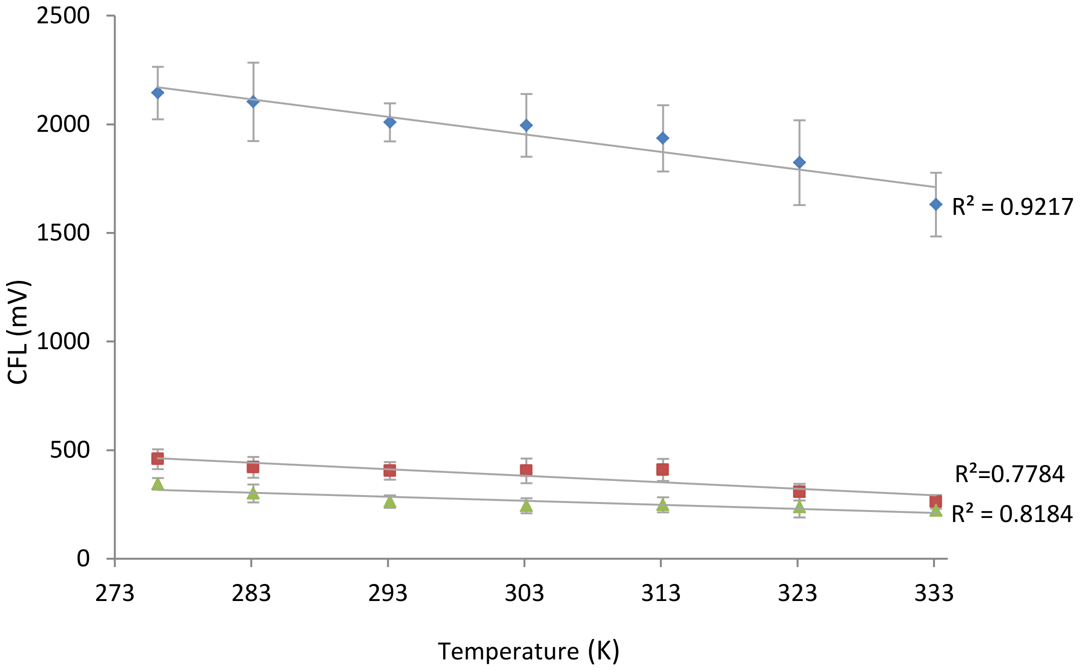

Figure 5-5 Effect of temperature on peak area signal for CFL emission in DDW at a flow rate of 120 mL min^{-1} passing through ◆ 210 µm i.d. quartz Venturi (df = 1, F = 58.59, p = 0.001, NPp = 0.659); ■ 200 µm i.d. glass Venturi (df = 1, F = 22.071, p = 0.005, NPp = 0.189); ▲ 220 µm i.d. glass Venturi (df = 1, F = 22.54, p = 0.005, NPp = 0.618). Experiments were performed without de-gassing or sparging with a noble gas. Error bars are ±1 standard deviation

It should also be noted that the F values for glass Venturis are similar (22.54 and 22.071). However the quartz Venturi F value is 55.9 which shows greater variance in these results. This is expected due to the pressure fluctuation experienced within the quartz Venturi as a product of the pressure fittings used to facilitate liquid interface. The glass Venturis did not experience this due to the high pressure connectors available for use with them. The results for the quartz Venturi still exhibited a statistically significant negative trend in spite of this.

The cavitation inception point for the four glass Venturi orifice sizes under investigation is shown in Table 5-1. The inception point was categorised as the point where visual and audible indicators of cavitation were experimentally identified.

Table 5-1 Cavitation inception flow rates and the corresponding orifice size in glass.

Orifice size (µm)	σ_i flow rate (mL min^{-1})
220	80
200	60
180	44
160	34

The relationship between orifice size and cavitation inception point is plotted in Figure 5-6, the data follows a significant quadratic trend as also noted by Mishra and Peles[52] on the micro-scale and macro-scale. The lack of varience on the data meant that error bars were too small to be seen on this graph.

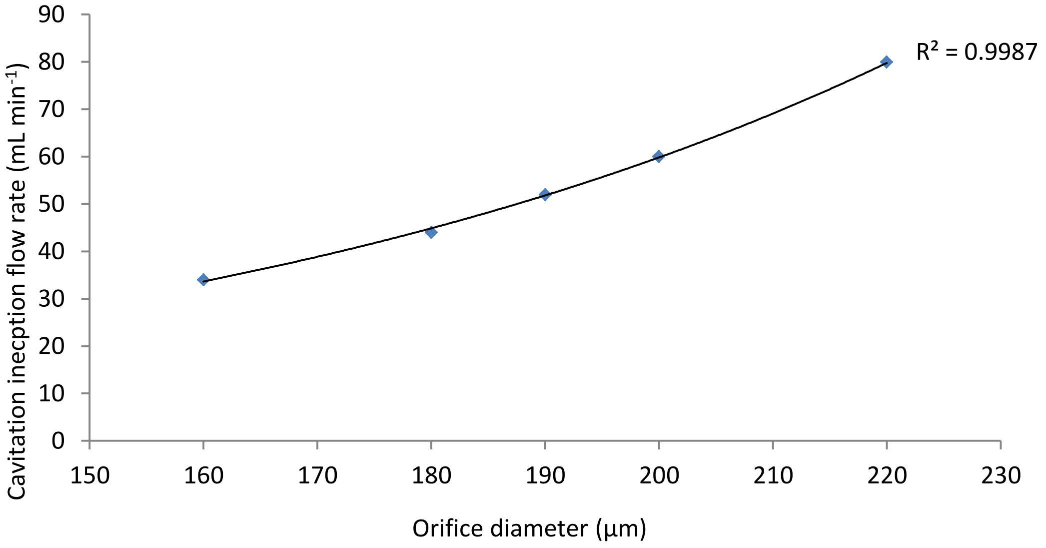

Figure 5-6 Relationship between orifice diameter and cavitation inception flow rate showing a quadratic relationship (df = 1, F = 94.11, p =0.01, NPp = 0.109).

The effect of flow rate and Venturi orifice i.d on CFL emission intensity in untreated DDW is shown in Figure 5-7. It has been established that once the flow exceeds the cavitation inception point then cavitation becomes increasingly destructive. [53] Therefore, with increasing flow rate and decreasing orifice size the cavitation should be more violent and it is expected that light emission would increase, which is confirmed by the results shown in Figure 5-7. Over the same range of flow rates the Venturi with the smallest diameter resulted in the most intense CFL (Figure 5-7). This is possibly due to the greater pressure change at the orifice, which has been observed in this work to increase the light emission up until the point at which choked cavitation is reached.

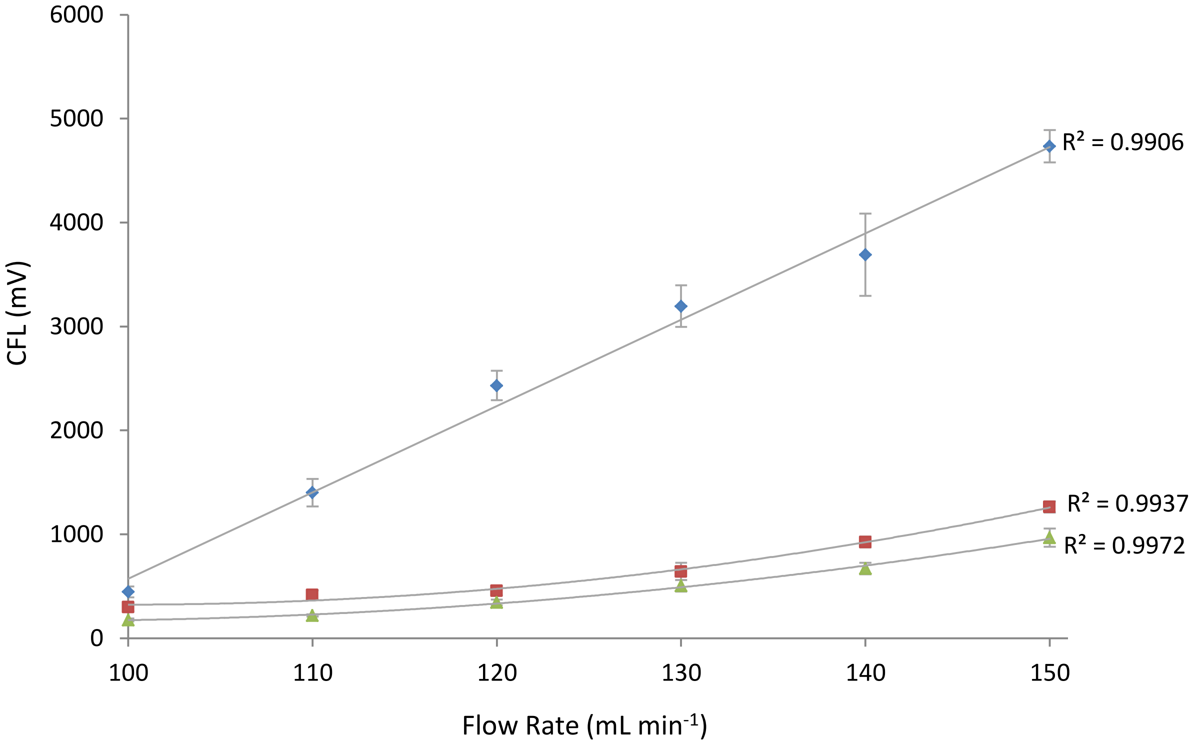

Figure 5-7 Effect of increasing flow rate through the Venturi on the peak area for CFL emission in water passing through ◆ 180 µm i.d. glass Venturi (df = 1, F = 423.08, $p < 0.001$, NPp =0.829), ■ 200 µm i.d. glass Venturi (df = 1, F = 44.58, p =0.003, NPp = 0.515), ▲ 220 µm i.d. glass Venturi (df = 1, F = 66.67, p = 0.001, NPp = 0.053). Experiments were carried out at 273 K and performed without de-gassing or sparging with a noble gas. Error bars are ±1 standard deviation

The effect of flow rate and temperature on CFL emission intensity in untreated DDW flowing through Venturis with orifice i.d.s of 160, 180, 200 and 220 µm i.d. is shown in Figure 5-8.

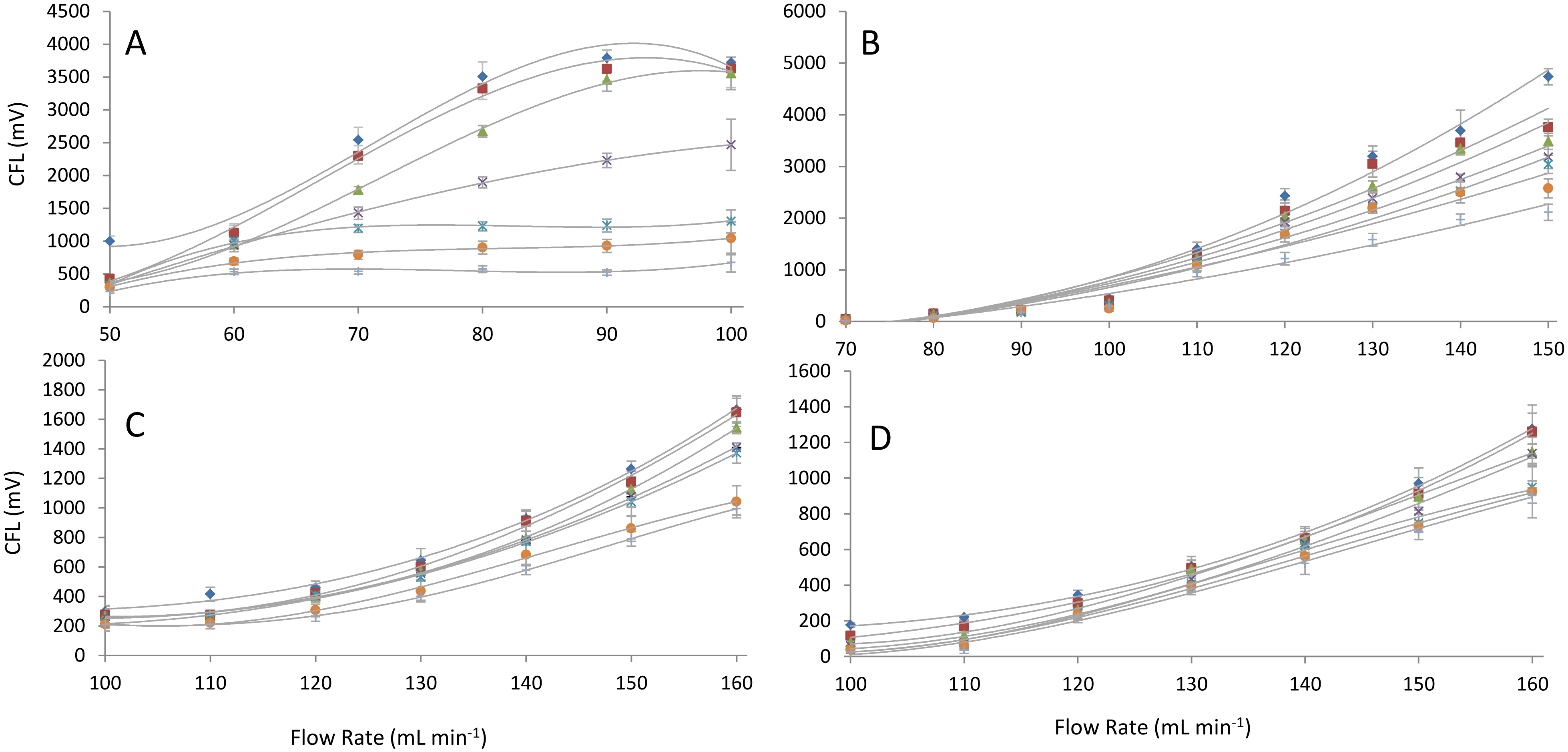

Figure 5-8 Effect of increasing temperature on peak area signal for CFL in water passing through glass Venturis with orifice sizes 160 µm i.d. (A), 180 µm i.d. (B), 200 µm i.d. (C) and 220 µm i.d. (D) at increasing flow rates, at the following temperatures: ◆ 276. K; ■ 283; ▲ 293 K; ×303 K; ✳ 313 K; ●323 K; + 333 K Experiments were performed without de-gassing or sparging with a noble gas. (All $p < 0.05$ and Nnp > 0.05) Error bars are ±1 standard deviation

The addition of solutes and/or noble gases to a cavitating liquid has been reported to increase the violence of cavitation and therefore CFL. [28, 33, 54, 55] The result of adding helium, argon, krypton and xenon is shown in Figure 5-9.

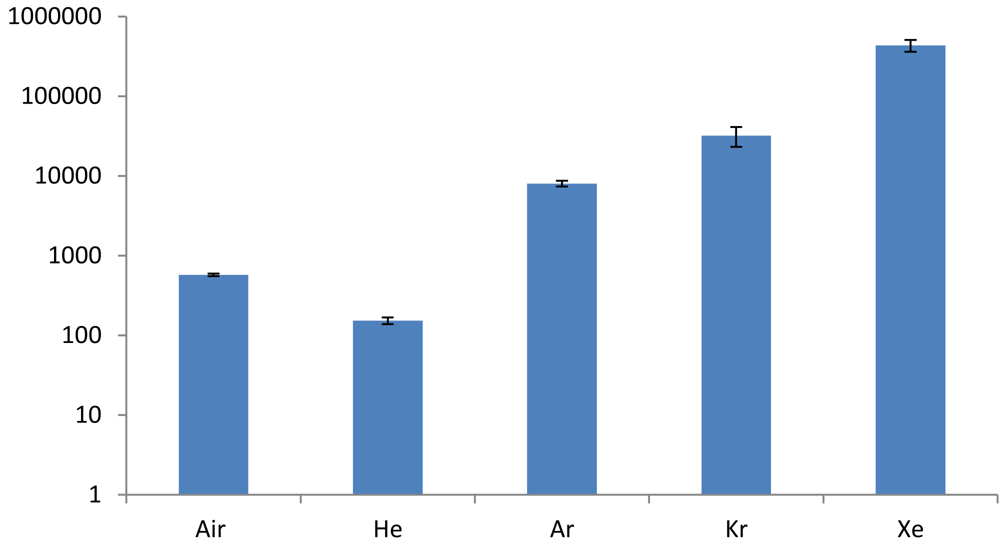

Figure 5-9 Effect of dissolving noble gases into water solutions at 276 K using the 220 µm i.d. Venturi at 160 mL min^{-1}. Error bars are ± 1 standard deviation

The addition of noble gases resulted in an increase in light emission from all samples except the sample sparged with helium. Physical constants of the noble gases used are given in Table 5-2. Typically, gases with higher ionisation energies and thermal conductivities would be expected to produce a plasma (assuming that one has formed) with higher thermal and excitation temperature. This trend was not observed however, with the intensity of CFL generally increasing with the solubility of the gas. It should be noted that, in order to account for the differences in solubility of the gases, the CFL data was normalised to the concentration of helium (0.000365 mol L^{-1}). The results of this are shown in Figure 5-10. These normalised results show that the increase in CFL emission was not due solely to the increase in solubility of the noble gas in solution, with argon and xenon having a greater effect on CFL emission. Hence, while solubility of the dissolved gas had a significant effect on CFL, the intensity of emission was also probably influenced by other physical properties. Unfortunately, without the ability to make spectroscopic measurements of line emission intensities it was not possible to determine the excitation temperature in the cavitation bubble, so the exact mechanism could not be determined.

Table 5-2 Physical constants for noble gases

Gas	Ionisation energy / eV	Henry's law constant in water / mol dm-3 atm^{-1}	Thermal conductivity / J K^{-1} m^{-1} s^{-1}
He	24.587[56]	0.00038[50]	0.141[56]
Ar	15.759[56]	0.0014[50]	0.0162[56]
Kr	13.999[56]	0.0025[50]	0.0086[56]
Xe	12.130[56]	0.0043[50]	0.0051[56]

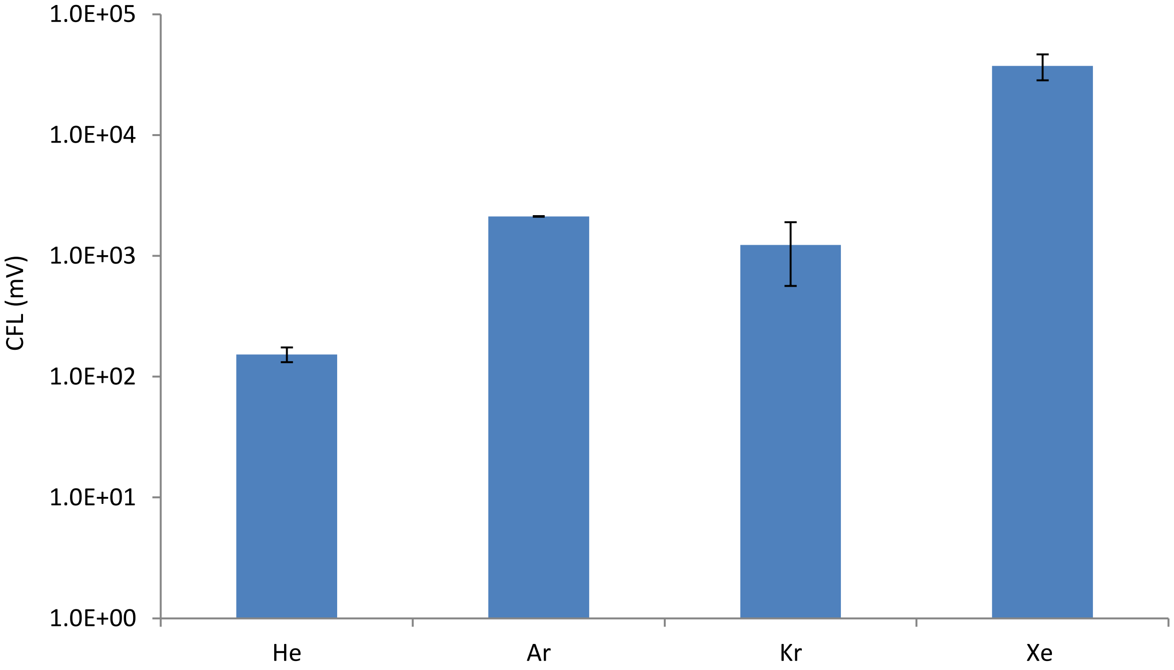

Figure 5-10 Normalised CFL emission using a 200 µm i.d. Venturi and a flow rate of 160 mL min^{-1} for noble gas solutions in DDW at 1 bar and 276 K. Error bars are ± 1 standard deviation.

In MBSL it has been noted that an increase in atomic weight corresponds to an increase in intensity and temperature inside the cavitating bubbles,[55] this could account for the increase in CFL observed here, however Didenko *et al.* [55] have not taken solubility of gases in solution into account, therefore the difference in increase in light intensity could have been due to a greater or lesser concentration of gas in solution. The results, which have been normalised in Figure 5-10, show that the increase was not due entirely to the increase in concentration of gas in solution, with argon, krypton and xenon having a greater effect of CFL than helium. A low resolution spectrum of CFL in DDW re-gassed with argon was obtained using 10 nm bandwidth filters spanning a range of 400 nm to 700 nm. These bandwidth filters were coupled with the photomultiplier tube as a detector. The results shown in Figure 5-11 indicate that the region of maximum emission was between 395 to 480 nm, which corresponds with a region of argon emission lines between 430 – 475 nm.

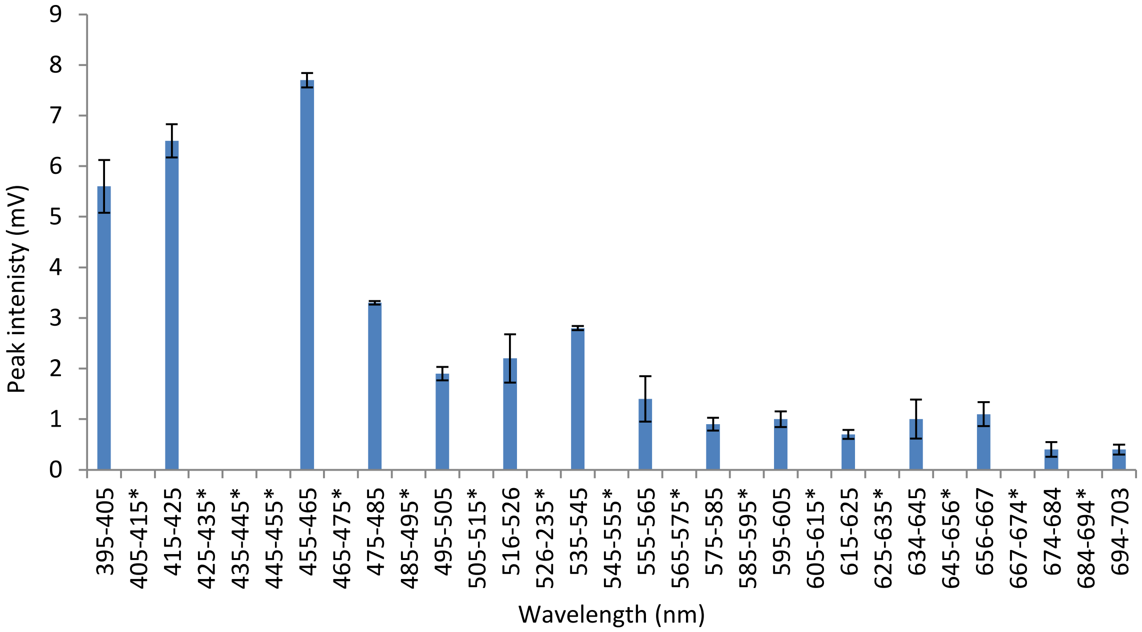

Figure 5-11 Low resolution spectrum of CFL emission from helium de-gassed and argon re-gassed DDW using a 180 µm i.d. Venturi at 100 mL min^{-1}. Error bars are ± 1 standard deviation. (Wavelength ranges marked with * indicate missing bandwidth filters.)

5.3 Scale effects

When applying classical hydrodynamic models developed on the macro-scale to orifice and pipe diameters on the micro-scale, the assumption of hydrodynamic similarity is made. Almost all empirical studies of cavitation base their comparisons on Reynolds and Cavitation numbers. However, in practise, deviation from similarity occur as a result of so-called *scale effects* caused by the viscosity of the liquid, dissolved gases and other constituent, bubble dynamics, geometry of the orifice and pipe, surface roughness, flow regime and turbulent motion. [57] Hence, one of the challenges of working with micro-Venturis, which are smaller than those typically investigated, and a variety of flowing liquids is that these scale effects are hard to predict and make comparisons of cavitation and Reynolds number of questionable validity. This partly explains why inaccurate orifice pressures were predicted by the CFD model as discussed in Chapter 4.

In order to investigate the size-scale effect the ratio of orifice to pipe diameter (β) was plotted against the cavitation inception number (σ_i) and the data compared with other researchers working with both micro-orifices and macro-orifices. The results of this comparison are shown in Figure 5-12, and suggest that there was a size scaling effect in play. The results show that for micro-scale experiments (orifice diameters <1 mm) there was no relationship between σ_i and β, whereas this was not the case for macro-scale experiments (i.e. those dealing with pipe and orifice diameters over 1 mm). It has been reported that this also holds true for cavitating choking number,[22] however this experiment could not be performed with the equipment used in this work due to the damage it would have inflicted on the equipment.

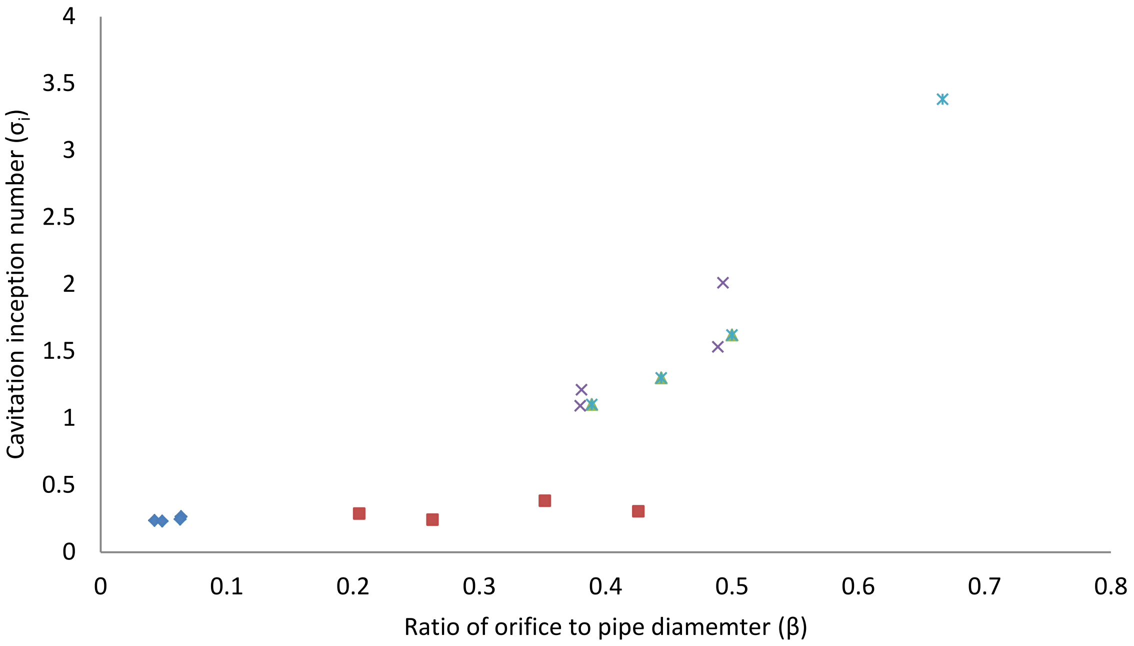

Figure 5-12 Relationship of orifice ratio and cavitation inception number exhibiting size scale effects. Data from × Tullis[49], ✳ Yan[58] and ▲ Ball *et al.*[59] was generated using macro-scale orifices. ◆ Experimental data and ■ Mishra and Peles[22] was generated using micro-scale orifices.

The relationship between orifice diameter and cavitation inception is shown in Figure 5-13, indicating that a logarithmic relationship exists such that the smaller the orifice the smaller the cavitation inception number.

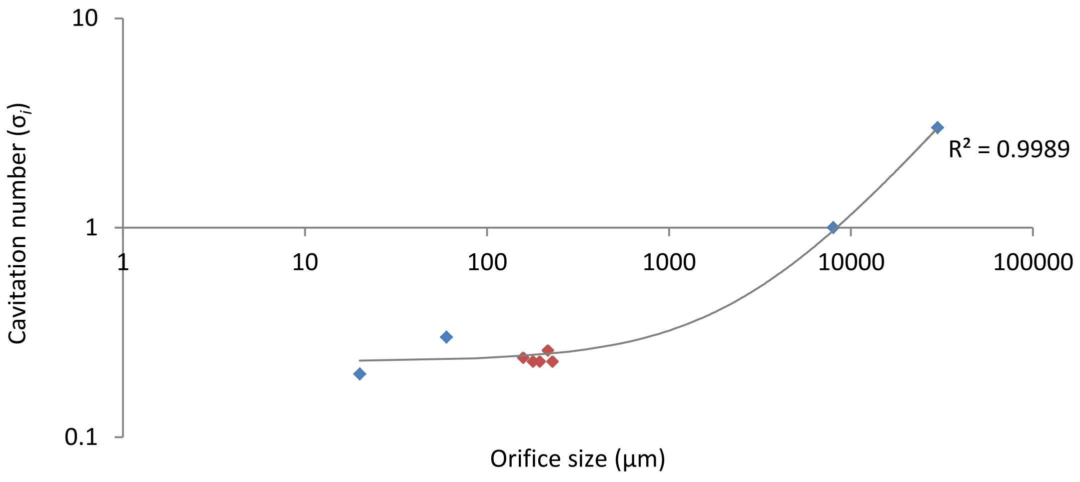

Figure 5-13 The correlation of cavitation and orifice size from other researchers data.[22] The experimental data points this research generated using deionised water are shown in red (df = 1, F = 6570.94, $p < 0.001$, NPp = 0.125).

Both Figure 5-12 and Figure 5-13 show that the cavitation inception number is different for different orifice sizes and also different orifice size to pipe size ratios, thus demonstrating size scale effects. Pressure and velocity scale effects have yet to be observed for hydrodynamic cavitation in micro-orifices.[25]

5.4 Conclusions

Cavitating flow luminescence was successfully generated in DDW for the first time using a micro-Venturi (orifice i.d. < 250 µm). Furthermore, the effects of various parameters on the intensity of CFL were investigated. The intensity of CFL was related to orifice diameter, temperature, flow rate (and hence pressure) and the nature of dissolved gases, with the most intense CFL observed at low temperature, high flow rate (pressure) and with highly soluble noble gases such as xenon. For the 160 µm i.d. Venturi, at temperatures below 293 K the CFL tended to plateau at higher flow rate, which was possibly due to the start of choked flow in the Venturi (Figure 5-8 A). At higher flow rates the back pressure exceeded the tolerance of the equipment, therefore confirming the presence of choked flow was not carried out to avoid damage to the pumps. The diameter of the Venturi orifice also influenced these trends, with CFL being easier to generate in Venturis with small diameters, likely due to the increased pressure differential across the orifice..

Size-scale effects were demonstrated for the micro-Venturi used in these studies, making it difficult to predict the exact behaviour for orifices of less than 1 mm in diameter.

More intense CFL was observed using quartz compared to a glass Venturi, suggesting that a significant proportion of the light was emitted in the UV part of the spectrum, however due to the instability of the equipment used to measure this further investigation is needed to quantify the extent to which CFL is increased. With a stable high pressure system the increase in CFL is likely to be higher than shown her due to the greater change in pressure at the orifice.

These results show that light is intense enough from micro-Venturis to be detected spectroscopically, and in further research will potentially lead to quantitative data being able to be produced.

6 Effect of solute and dissolved gases

6.1 Objectives

Objective four was to investigate the effect of dissolved gasses, solutes and solvents on CFL. Volatility and pressure are important to consider when inducing cavitation. Luminescence is increased with less volatile liquids, heat capacity and ionisation energy of dissolved gases. Heat capacity and the energy of ionisation of gases dissolved in the liquid stream play an important role in determining the excitation temperature in the plasma which is formed within the micro-bubble during the cavitation collapse. The solutes under investigation were: dimethyl sulfoxide (DMSO); isopropanol; diethyleneglycol and polyethyleneglycol. DMSO, diethylene glycol and polyethylene glycol are known to have low vapour pressures and therefore are expected to aid cavitation. For comparison isopropanol, with a high vapour pressure, was also tested with the expectation that lower light emission and cavitation will be observed. Gases under investigation were: helium; argon; krypton and xenon. The experiments were carried out using the 200 µm i.d. Venturi at a flow rate of 160 mL min^{-1} and temperature of 276 K because this was the combination of conditions which promoted the highest light emissions.

Objective five was to establish figures of merit for selected analytical applications but this proved difficult to achieve due to the low CFL emission intensity. Hence, this objective was changed to investigate the possible underlying mechanism of CFL in an attempt to prove that atomic emission was taking place.

6.2 Effect of fluid composition

6.2.1 Cavitation in dimethyl sulfoxide

The effect of dimethyl sulfoxide (DMSO) concentration on CFL emission is shown in Figure 6-1. As the concentration of DMSO was increased, so did the intensity of CFL. The trend followed a quadratic regression and increased until the mole fraction of DMSO reached 0.7. Between a mole fraction of 0.7_{DMSO} – 1_{DMSO} the temperature was increased to prevent freezing of the DMSO mixture, because temperature has been shown to affect CFL (through the increase in vapour pressure and associated drop in gas solubility in warmer liquids) this may explain the plateau observed in Figure 6-1.

The vapour-equilibrium curve for DMSO-water mixtures predicts that that the mole fraction of water in the vapour phase remains high (0.9) below a DMSO mole fraction of ≈0.68 in the liquid phase, and thereafter declines exponentially.[60] However, despite the disproportionate contribution of water to the vapour phase the overall vapour pressure of DMSO-water mixtures is very low,[57] because the vapour pressure – mole fraction curve for DMSO-water departs negatively from the ideal case[61].

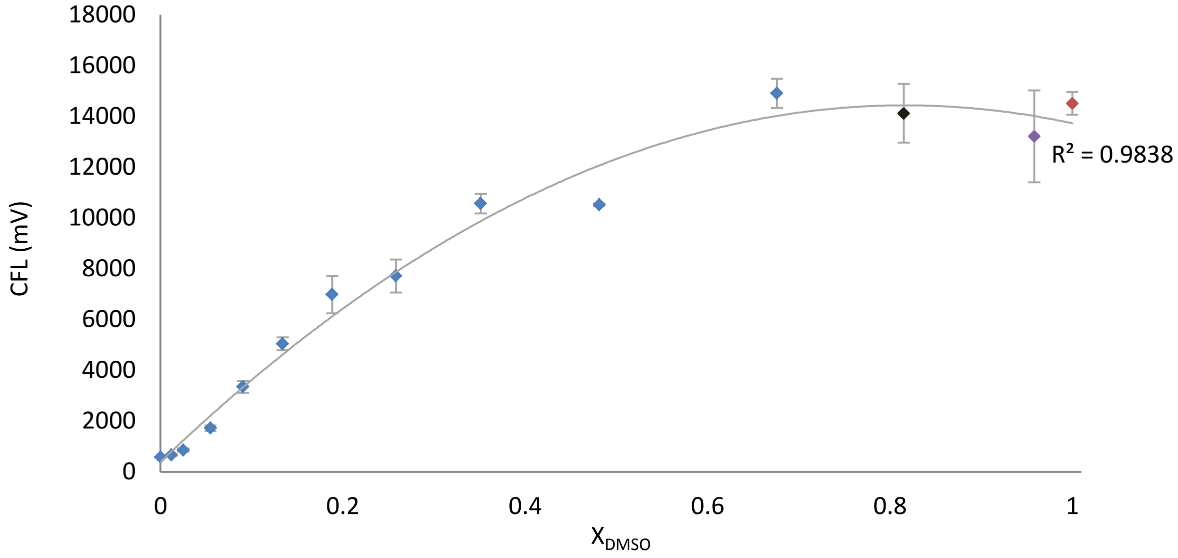

Figure 6-1 Effect of increasing DMSO concentration on the peak area for CFL emission using the 220 µm i.d. Venturi at 276 K with a flow rate of 160 mL min^{-1}, except for the data points in black, purple and red which were performed at 282 K, 285 K , and 292 K respectively due to their higher freezing points (df = 1, F = 58.59, $p < 0.001$, NPp =) error bars are ±1 standard deviation.

Assuming that the cavitation bubbles were formed from dissolved gas, one possible explanation for the enhanced CFL signal in the presence of DMSO is that the lower vapour pressure of this solvent resulted in less DMSO vapour being present in the cavitation bubbles, and hence less quenching of CFL.[28] For liquids with lower vapour pressures CFL intensity is influenced more by dissolved gases than by the liquid vapour itself.

The relationship between CFL emission and flow rate has been established previously for water, with higher flow rate causing more intense CFL emission. However, this might not be true for other fluids. The effect of flow rate on CFL for different concentrations of DMSO is shown in Figure 6-2.

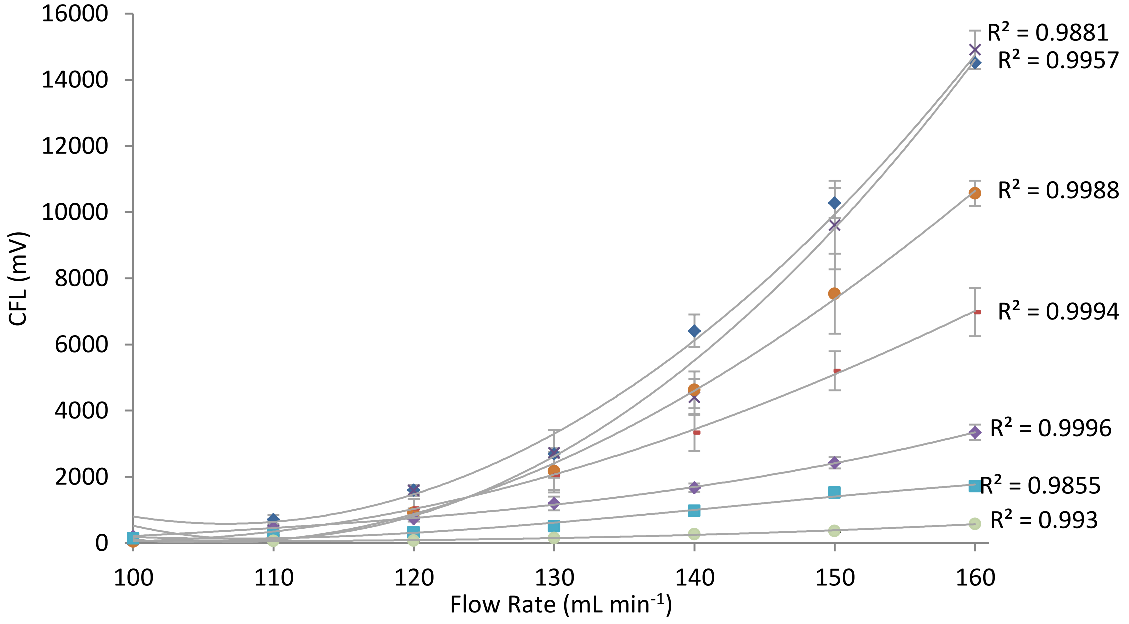

Figure 6-2 Effect of flow rate on peak area for CFL emission in different DMSO/water mixtures using the 220 µm i.d. Venturi at at 276 K except 1_{DMSO} which was performed at 292 K due to increased freezing point: ◆ 1.0_{DMSO} (df = 1, F = 58.59, $p < 0.001$, NPp =), × **0.68_{DMSO}** (df = 1, F = 58.59, $p < 0.001$, NPp =), ●0.35_{DMSO} (df = 1, F = 58.59, $p < 0.001$, NPp =), - 0.19_{DMSO} (df = 1, F = 58.59, $p < 0.001$, NPp =), ◆ 0.10_{DMSO} (df = 1, F = 58.59, $p < 0.001$, NPp =), ■ 0.05_{DMSO} (df = 1, F = 58.59, $p < 0.001$, NPp =), ● 0_{DMSO} (df = 1, F = 58.59, $p < 0.001$, NPp =). Experiments were performed without de-gassing or re-gassing with noble gases. Error bars are ±1 standard deviation.

In Figure 6-2 it can be seen that as flow rate and X_{DMSO} increased so did CFL emission. The exception to this general trend is the curve for 0.68_{DMSO}, the mole fraction with the lowest freezing point.[57, 60, 62] The general trend in Figure 6-2 can be explained by DMSO/water mixtures having lower vapour pressure than either of the pure solvents. The vapour pressure curve departs negatively from that predicted by *Raoult's law* because of hydrogen bond formation between water and DMSO (ΔH^o = -18.8 kJ mol^{-1}). This also corresponds with a point of very low surface tension[63] which may result in the cavitation bubbles imploding more easily. This decrease in surface tension may occur because in bulk liquids, for mole fractions above $0.6_{DMSO,}$ DMSO molecules tend to reside away from the surface due to competitive hydrogen bond formation between

DMSO and water, causing a localized decrease in concentration at the surface of the liquid.[63] This may also be true at the surface of the cavitation bubbles.

6.2.2 Cavitation in ethyleneglycols

The effect of two different ethylene glycols, namely PEG-200 polymer and diethylene glycol, on CFL emission is shown in Figure 6-3. Results were obtained using a 200 µm i.d. Venturi at a flow rate of 160 mL min^{-1} and 276 K. The maximum mole fractions that could be studied were $0.06_{\text{PEG-200}}$ and $0.11_{\text{diethyleneglycol}}$ because the back pressure exceeded the tolerance of the liquid handling manifold at higher concentrations. The vapour pressures of PEG-200 and diethylene glycol are <1.33 Pa and 0.799 Pa respectively and, similar to DMSO/water, the mixtures depart from ideality.

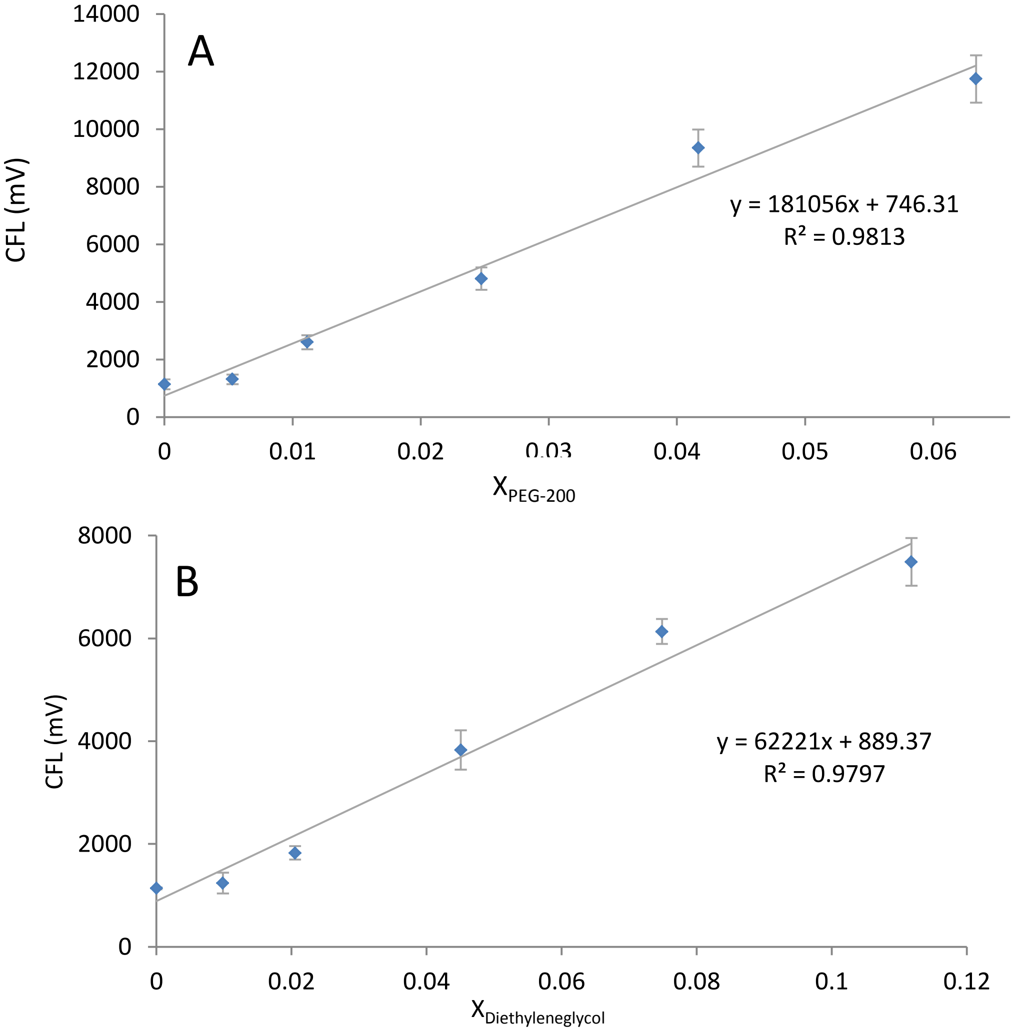

Figure 6-3 The effect of increasing solute concentration on CFL emission intensity in untreated solutions through a 220 µm i.d Venturi at a flow rate of 160 mL min^{-1} at 276 K. **A** PEG-200 (df = 1, F = 209.7, $p < 0.001$, NPp =0.089), and **B** Diethylene glycol (df = 1, F = 235.71, $p < 0.001$, NPp =0.515) error bars are ±1 standard deviation.

As can be seen in Figure 6-3, increasing solute concentration resulted in an increase in CFL emission in both solutes tested. This is again probably due to lower vapour pressure and reduced surface tension of the mixtures.

Figure 6-3 also includes the straight line equations for both ethylene glycol compounds. A (PEG-200) has a steeper gradient than B (diethylene glycol) showing that the longer chain molecule provides conditions which favour cavitation intensity as the light emission increases with concentration.

6.2.3 Cavitation in isopropanol

The effect of isopropanol concentration on CFL emission, using a 220 µm i.d. Venturi at a flow rate of 160 mL min^{-1} at 276 K, is shown in Figure 6-4. Isopropanol has a relatively high vapour pressure of 3599 Pa compared to DMSO and ethylene glycols. While fluids with a high vapour pressure are more likely to cavitate they are unlikely to produce CFL because of a potential quenching effect by the solvent on light emission. A high vapour pressure solvent has a higher concentration of the chemical inside the cavitation bubble; this effect can be used to degrade or promote chemistry to occur inside the cavitation bubble but reduces the light emission possibly due to energy transfer.[64, 65] This was largely borne out by the results which show that at very low concentrations of isopropanol CFL increased marginally, but then decreased. The initial increase may be due to a reduction in surface tension making cavitation bubbles implode more easily (isopropanol has a lower surface tension than water).

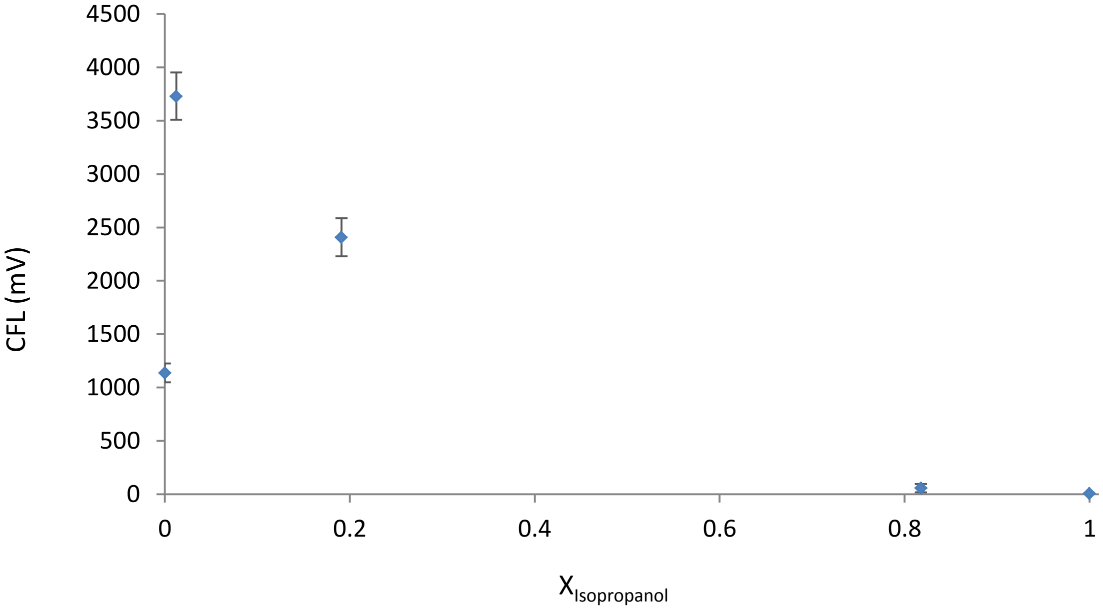

Figure 6-4 Effect of isopropanol concentration on peak area on CFL emission intensity in untreated solutions through a 220 µm i.d Venturi at a flow rate of 160 mL min^{-1} at 276 K. Error bars are ±1 standard deviation

6.2.4 Cavitation in solutions of Triton X 100

The effect of low concentrations of Triton X 100 (up to 5% V/V) on CFL emission using a 220 µm i.d. Venturi at a flow rate of 160 mL min^{-1} and 276 K. is shown in Figure 6-5. Triton X 100 reduces the surface tension of the water by disrupting hydrogen bonds between the water molecules and enhances the formation of cavitation bubbles.[66] Triton X 100 also has a low vapour pressure <133 Pa which could potentially lower the vapour pressure of the mixture, however, at the low concentrations studied here this is unlikely to have a significant effect. As can be seen in Figure 6-5, CFL emission increased slightly with increasing concentration. However the gradient is slight when compared to PEG-200 and diethylene glycol so while it does have an effect it is only slight.

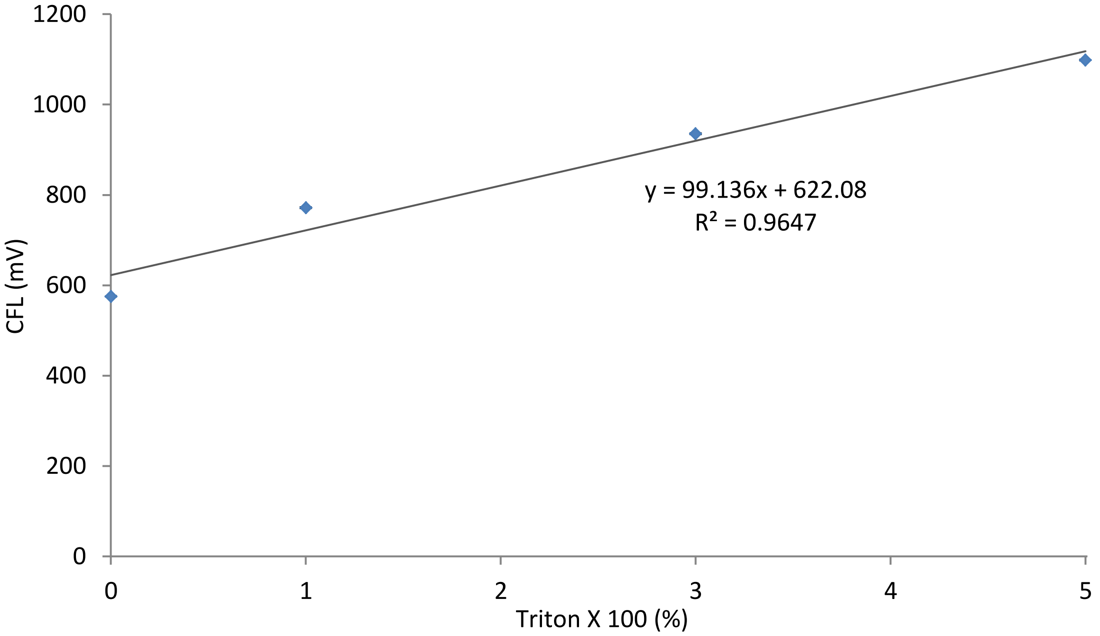

Figure 6-5 Effect of increasing concentration on peak area for signal CFL emission in different triton X 100/water V/V mixtures at 276 K through a 220 µm i.d Venturi at 160 mL min^{-1}. Experiments were performed without de-gassing or sparging with noble gases.

6.3 Effect of dissolved gases on cavitation

This section describes the effect of dissolved noble gases namely helium, argon, krypton and xenon on CFL emission. Noble gases have been shown to increase luminesce intensity in sonoluminescence.[9, 10] The presence of soluble gases increases the gas nuclei present in a solution and the higher the solubility of the gas (and hence higher gas concentration in solution) the more gas is present in the cavitation bubble, promoting a more violent collapse of the cavitation bubble. [37] This may be due to their higher *heat capacity* at *ionisation temperature* compared with diatomic gases which have a higher heat capacity at lower temperatures due to vibrational excitation. Also shown (Figure 5-9 and Figure 5-10) is that dissolving noble gases in water increased the CFL intensity, so the study was extended to examine the effect of this in conjunction with fluid composition.

Results for noble gas addition are shown in Figure 6-6; graphs A, B and C show that adding a noble gas to a solution of DMSO, PEG-200 or diethylene glycol increases the light emission observed. The intensity increased in the order Xe > Kr > Ar > He. Xenon promoted the maximum light emission observed for all the solutes including isopropanol.

Isopropanol behaved differently to the low vapour pressure solvents DMSO, PEG-200 and diethylene glycol. CFL emission initially increased with very low concentrations of isopropanol which is due to the disruption to the surface tension of the liquid but then quenched CFL as the concentration increased.

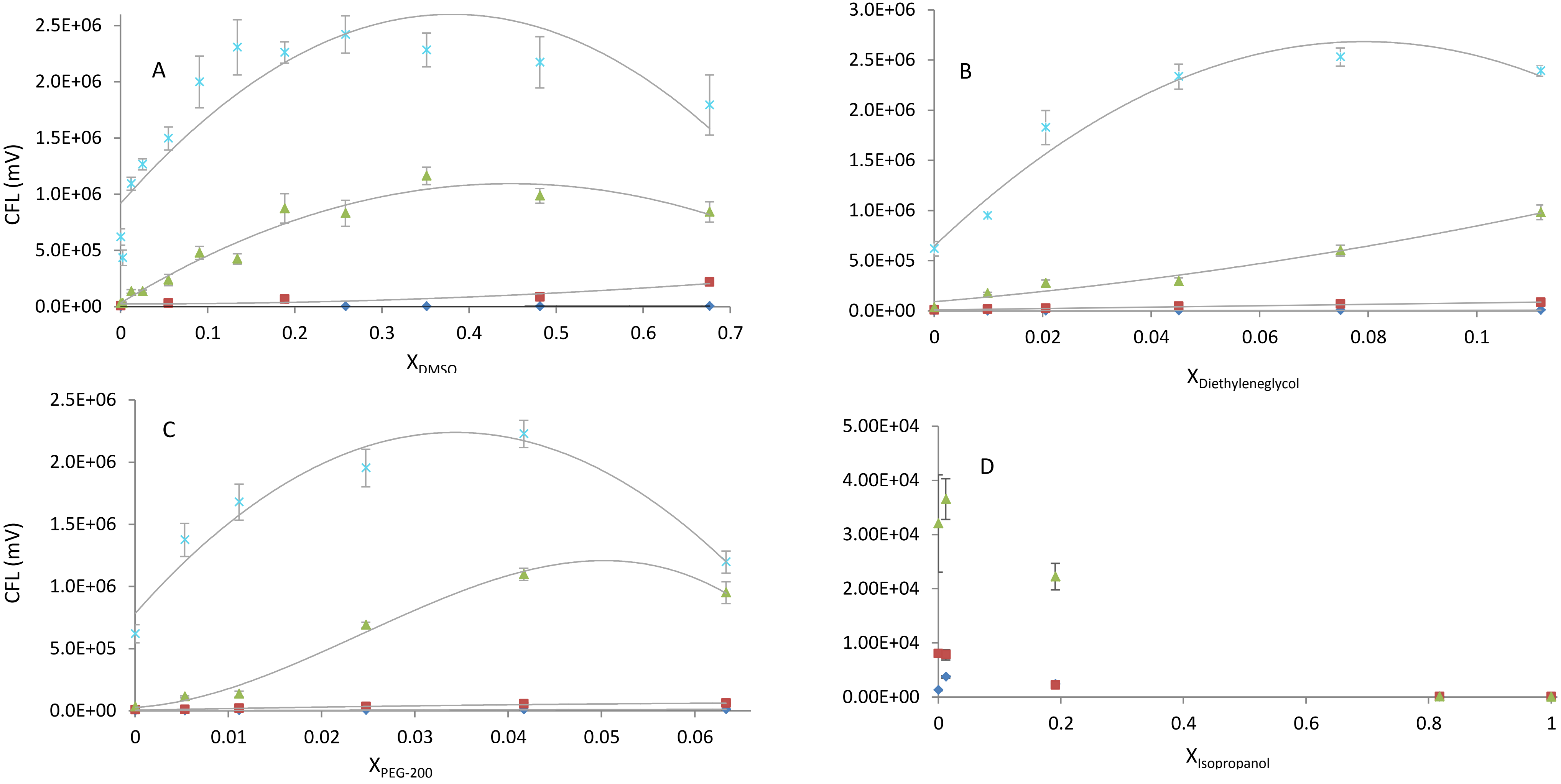

Figure 6-6 Effect of noble gas addition to various concentrations of solute concentrations (A) DMSO, (B) Diethyleneglycol, (C) PEG-200 and (D) Isopropanol using a 220 µm i.d Venturi with the solutions at 276.15 K: ◆ helium; ■ argon; ▲ krypton and × xenon (All data trends were significant and the errors normally distributed) Error bars are ±1 standard deviation.

6.4 Other factor affecting cavitation luminescence

6.4.1 Effect of nano-particles

The formation of a cavitation bubble is thought to originate at a nucleation site with the flowing liquid. Typically, in classical cavitation experiments this occurs at the liquid solid interface, e.g. the surface of a propeller or Venturi. Hence, it is reasonable to suppose that the prescence of solid particle suspended within the fluid could provide nucleation sites for bubble formation. To test this theory, solutions of 0.1 mg L^{-1} titanium dioxide (20 nm average diameter) were prepared in 5% Triton X 100 in DDW and ultrasonicated for 20 minutes prior to use.[67] Results are shown in Figure 6-7.

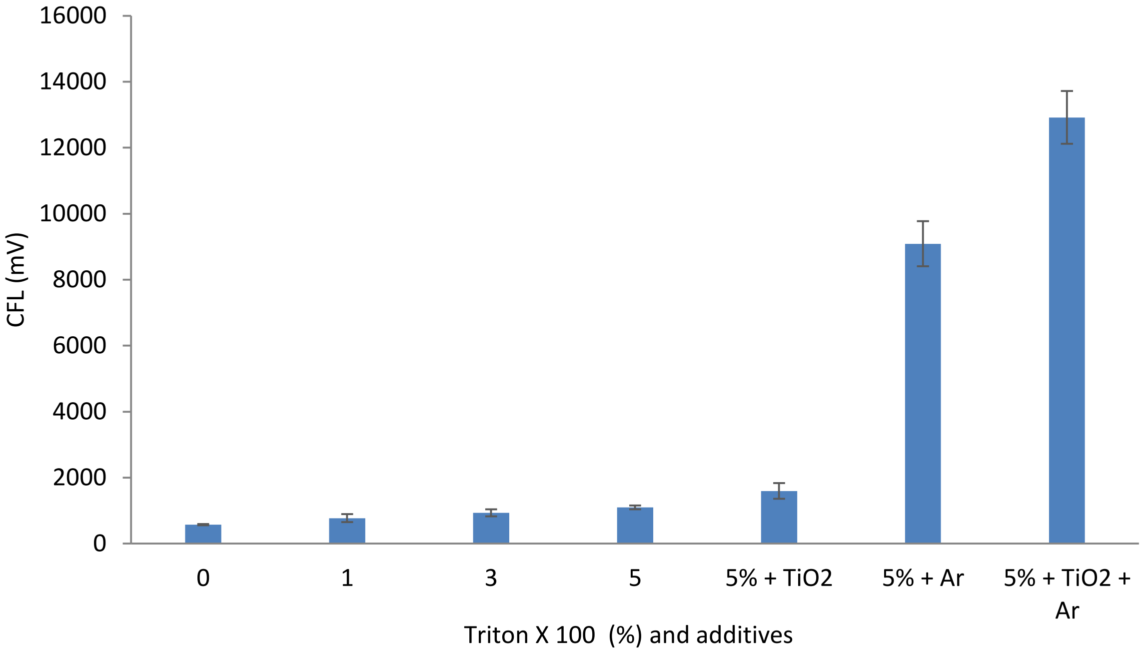

Figure 6-7 Effect of increasing concentration of triton X 100,addition of titanium nano-particles and sparging with argon on peak area signal for CFL emission in solutions passing through a 220 µm i.d Venturi at 160 mL min^{-1}. Error bars are ±1 standard deviation.

The effect of nano-particles on CFL shows that with the addition of triton x 100 and titanium sulphate nano-particles emission intensity increases. This increase is slight when compared to the addition of argon to the fluid with or without nanoparticles. These results show that the increase in nucleation sites increases CFL; however the increase is small when compared to the effect of adding argon to the cavitating fluid.

6.4.2 Light scattering

One of the problems encountered was distinguishing between stray light and CFL. Stray light was caused by *total internal reflection* along the PTFE tubing and into the housing. During cavitation the bubbles scattered this light in the direction of the detector giving rise to an apparent CFL signal shown in Figure 6-8. This signal did not exhibit the same pulsing effect as a true CFL signal because the light did not originate from the cavitating bubbles themselves, so was not linked directly to the CFL phenomenon *per se.* i.e., cavitation occurs even when CFL does not. CFL occurs when the bubble collapse is great enough to create a plasma and emit photons; however until this point is reached the cavitation bubbles form at the orifice momentarily and light can scatter when it refracts at the edge of the bubble.

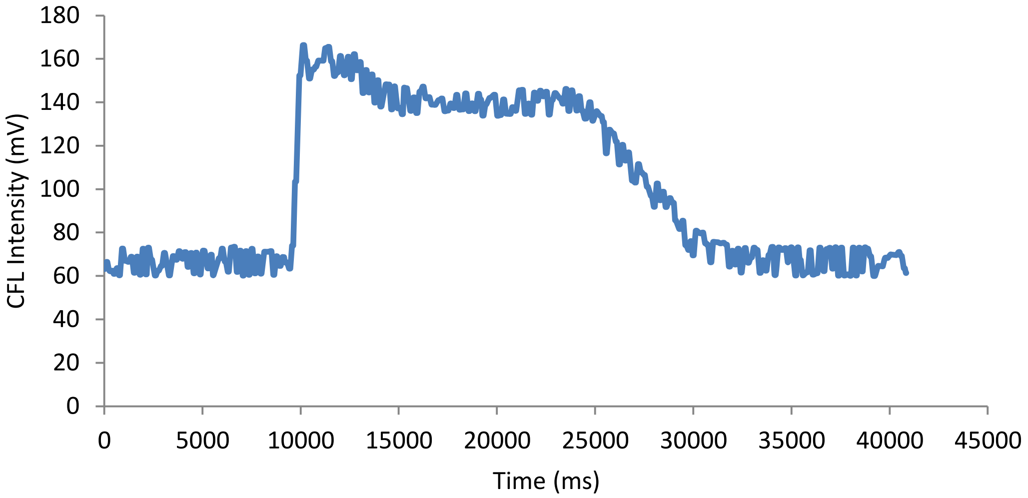

Figure 6-8 Light detected from light scattering form a solution of DMSO and water passing through a 220 µm i.d Venturi at 60 mL min^{-1}.

In order to eliminate stray light the housing and tubing were light-proofed and experiments were performed in a darkened room. Light was prevented from entering the housing by using black PTFE tubing and by constructing a housing from black polymer plastic as detailed in Section 3.2. Without these precautions it was not possible to differentiate between scattered light and CFL especially when the intensity differential between the scattered background light and the light levels observed purely from CFL.

6.4.3 Free radical reactions

In order for free radical reactions to occur it is first necessary to form the free radicals. In order to investigate this possibility, a degradation study was performed to determine whether DMSO degraded during cavitation, as this would be an indicator that free radicals were produced. A 50 mL sample of pure DMSO was cycled through the 160 µm i.d Venturi at 100 mL min^{-1} for 72 hours in order to concentrate any degradation products. The degraded solution was then analysed using electrospray ionisation mass spectrometry (ESI-MS) with results shown in Figure 6-9 No degradation of the analytical grade DMSO was observed so it is unlikely that any free radicals were formed, and consequently this was ruled out as a possible mechanism for CFL.

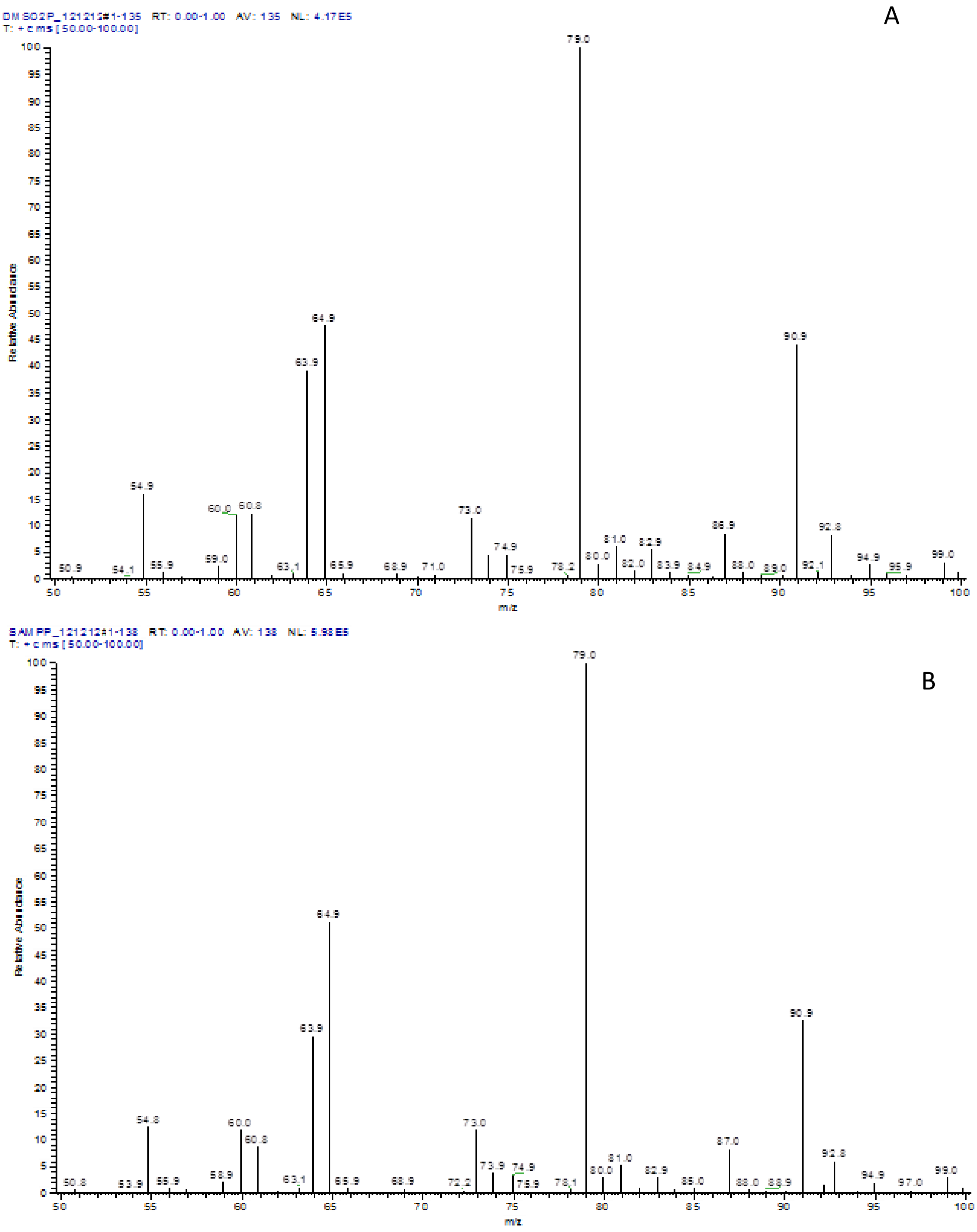

Figure 6-9 Mass Spectrum of (A) non-degraded DMSO sample (100 ppm in DDW) and (B) 72 h degraded sample (100 ppm in DDW)

6.4.4 Atomic / molecular emission

A possible explanation for CFL is molecular emission (fluorescence) from the flowing liquid itself. In order for this to occur the molecules must first be excited, either by another source of radiation, or by non-radiative means. Since non-radiative excitation of the compounds under study is unlikely, there must be some source of radiative energy which originates from either atomic or molecular excitation. Unfortunately, it was not possible to obtain a high resolution spectrum which is necessary to determine whether any atomic emission was present; because the intensity of CFL was insufficient to be detected using the available spectrometer equipped with a 1 mm UV transmitting fibre optic cable coupled with a 1cm collimator to collect light from a wide angle. However, a low resolution spectrum was obtained by using a series of 10 nm bandwidth interference filters spanning the range from 400 to 700 nm. Each filter was placed in turn between the lens and detector, and average CFL emission for ten replicate injection of a 5 mL sample was recorded. The results for pure DMSO are shown in

Figure 6-10 indicating maximum emission between 455 nm and 545 nm, i.e. in the blue and green areas of the visible spectrum.

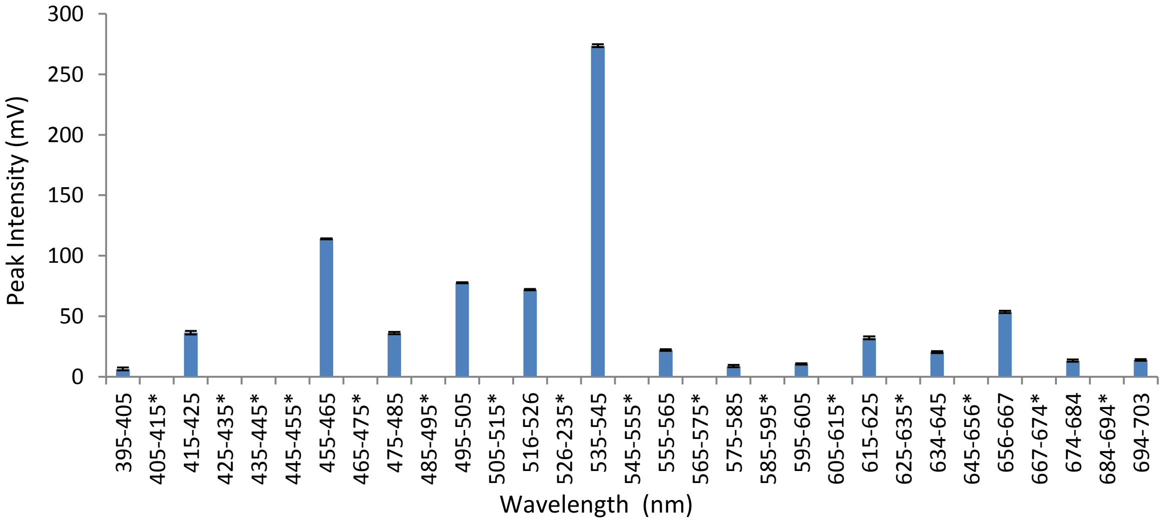

Figure 6-10 Low resolution spectrum of normalised CFL emission from pure DMSO using a 180 µm i.d Venturi at 100 mL min-1. Error bars are ±1 standard deviation. (Wavelength ranges marked with * indicated missing bandwidth filters.)

The UV-visible spectra for DMSO and PEGG-200 are shown in Figure 6-11, which shows that they both absorb in the UV.

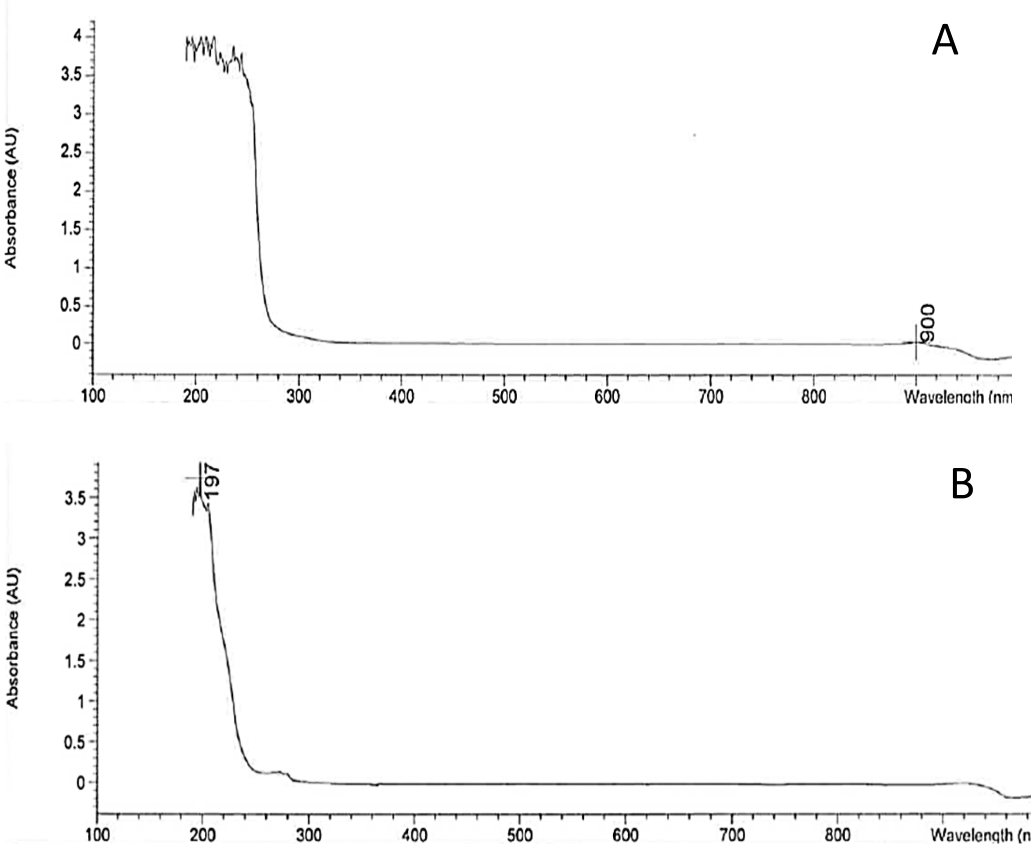

Figure 6-11 UV-Visible absorbance spectra from (A) DMSO and (B) Polyethylene glycol.

Both DMSO and PEG-200 absorb in the UV part of the spectrum indicating that, should they fluoresce, they must first be exposed to light with a wavelength less than 270 nm. The fluorescence spectra for DMSO and PEG-200 are shown in Figure 6-12 and it can be seen that molecular fluorescence from PEG-200 is significant between 300 – 390 nm and 540 – 690 nm with less intense emission at 490 nm. DMSO does not fluoresce. It can be concluded that, whilst it is possible that molecular fluorescence was observed for PEG-200 it was first necessary for there to be radiative excitation in the UV (λ_{ex} = 220 nm). In contrast, molecular fluorescence from DMSO was not observed therefore

CFL emission must occur by some mechanism that is not related to molecular fluorescence.

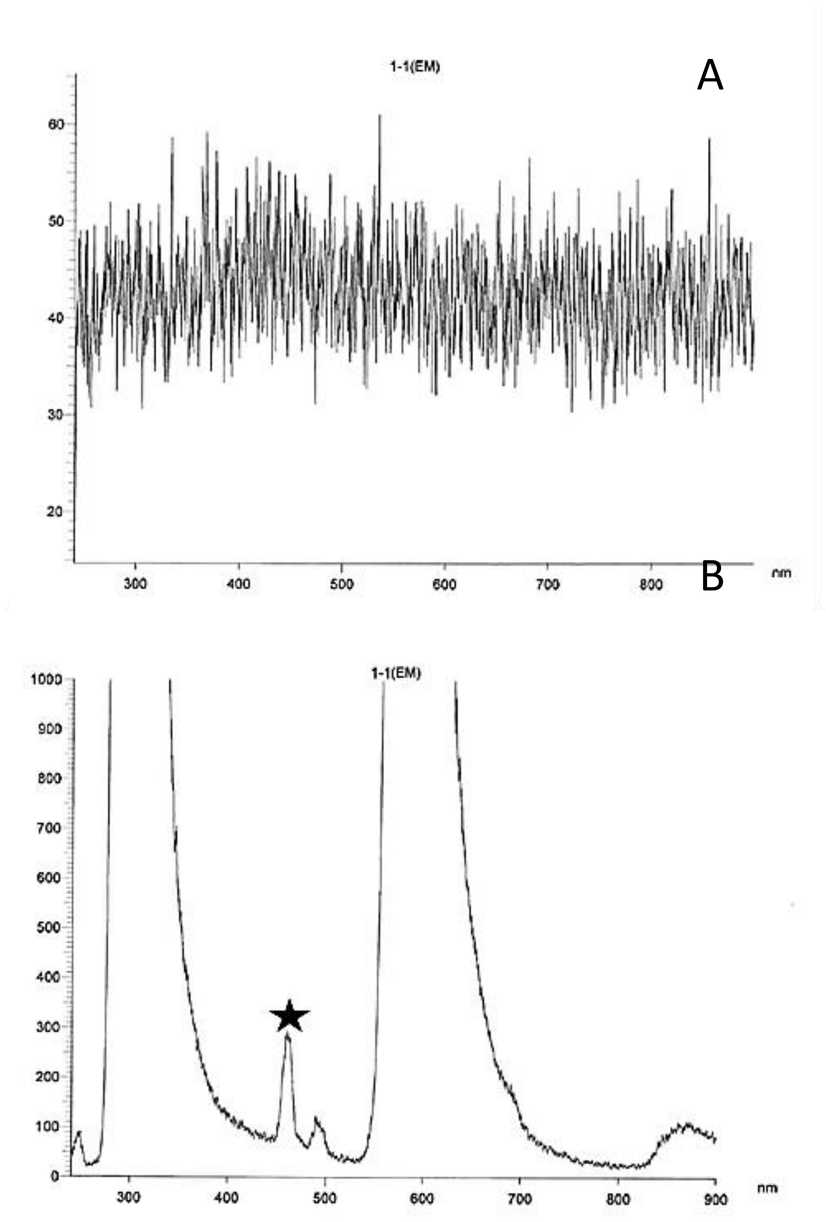

Figure 6-12 Fluorescence spectra of (A) pure DMSO exhibiting a lack of fluorescent emission and (B) Pure PEG-200 exhibiting fluorescent emission which occurs at 300 – 390 nm, at 490 nm and 540 – 690 nm. Both were exposed to an excitation wavelength of 220 nm. (There is second order excitation observed which is starred on the spectra.)

Finally, a Venturi was fabricated from quartz in order to determine whether this resulted in an increase in CFL from emission in the UV spectrum. Results in Figure 6-13 show a three-fold increase in signal when using a quartz Venturi, suggesting that there may have been emission in the UV. If this was indeed the case this must have originated from some processes occurring during CFL rather than molecular fluorescence or scattered light.

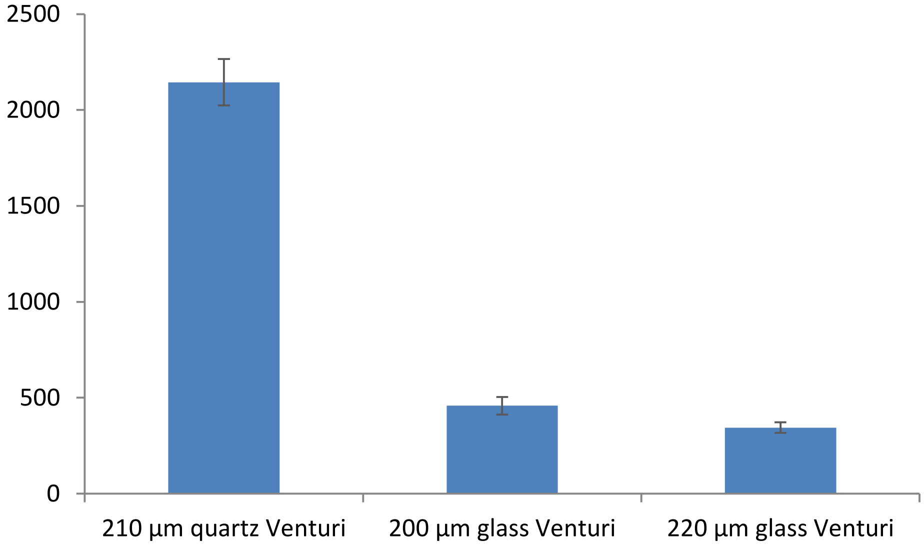

Figure 6-13 Effect of Venturi composition on CFL emission observed using DDW at a flow rate of 120 mL min^{-1} at 276 K. Error bars are ±1 standard deviation

6.5 Conclusions

The results showed that the addition of DMSO and ethylene glycols increased CFL when compared to water. This increase was attributed to the change in the properties of the cavitating liquid; by lowering vapour pressure and surface tension CFL was increased. It has also been shown with experiments using isopropanol that a liquid with a high vapour pressure decreases CFL due to quenching effects. These results show that the addition of noble gases significantly increased CFL emission in the order Xe > Kr > Ar > He for the solutions under investigation. The addition of both triton X

100 and titanium sulphate nano-particles caused a small increase in CFL. Triton X 100 reduced the surface tension of the liquid and the nano-particles provided nucleation sites for cavitation bubbles however the increase in CFL was small when compared to the effect of the addition of noble gases. It is likely that an ideal cavitating fluid with ideal CFL properties could be devised in order to boost the light emission from a micro-Venturi. A solvent with a low vapour pressure which allows a high degree of solubility of a noble gas would be worthy of further investigation.

The light emitted seemed to originate from CFL; other mechanisms or sources of light such as light scattering, molecular fluorescence and degradation effects were considered unlikely. The results suggested that light was emitted by a plasma formed in DMSO. Light was also generated via plasma formation and possibly molecular emission in PEG-200 and diethylene glycol. The CFL emission was intense enough using micro-Venturis to be analysed spectroscopically, however, limitation of the equipment being used here mean that the results generated are limited to proof of concept currently. Spectroscopic observation would allow the differentiation between atomic and molecular emission.

7 Conclusions and future work

7.1 Conclusions

The first stage in this research was to design and construct a high pressure system comprising of a micro-Venturi (orifice i.d. < 250 µm), optical system, liquid handling manifold, mechanical pump and detector and data acquisition arrangement to generate and observe CFL. The following conclusions can be drawn regarding this part of the research:

1. A micro Venturi tube was designed and went through several iterations before a successful manufacturing solution was found. Two types of micro Venturi were developed, one glass and one made from quartz. The glass Venturis were constructed by collapsing an Omnifit® LC Column to form the micro-orifice. This allowed high pressure liquid connections to be used in conjunction with a preparatory HPLC pump; this formed most of the liquid handling manifold. In order to introduce samples to the liquid stream a 6-way injection valve was also included in the system. The glass Venturi was the most robust and was used to generate the bulk of the data, but it was not possible to observe UV emission. This was subsequently achieved using the quartz Venturi but it suffered from poor high pressure connections so limited data were obtained.
2. An optical system was constructed from separate optical components including a photomultiplier tube, focussing mirror and bi-convex lens contained within a custom designed housing to eliminate stray light. The

detector was coupled with a data logger to allow for data collection every 100 ms.

3. The system allowed for CFL to be generated and observed in both DDW and a range of organic solvents for the first time. Initial studies were carried out using DDW and the intensity of CFL was related to orifice diameter, temperature and flow rate (and hence pressure). The most intense CFL was observed at low (276 K) temperatures and high (160 mL min^{-1}) flow rates (pressure). The diameter of the Venturi orifice also influenced these trends, with CFL being easier to generate in Venturis with sub-millimetre diameters. The Venturi medium was also investigated by comparing the results generated using glass and quartz Venturis. The emission intensity increased three-fold when using a quartz Venturi, suggesting that a significant proportion of light emission occurred at wavelengths below 300 nm, the UV part of the spectrum.
4. Noble gases were added to DDW resulting in an increase in CFL signal. It was found that xenon promoted the most intense emission when compared to krypton, argon and helium even when the results were normalised with respect to gas concentration. It is thought this is due to the increase in temperature within the collapsing bubble due to the presence of xenon. A lack of spectroscopic data means that this cannot be proven for CFL but it is known to occur in SBSL (single bubble sonoluminesnce) and MBSL (multibubble sonoluminescnce).[32,55, 68-70]
5. Studies of the addition of organic solvents were carried out and have shown that solutions of DMSO and ethylene glycols increase CFL when compared

with water. This increase is due to the change in the properties of the cavitating liquid; by lowering vapour pressure and surface tension, CFL was increased. As with water CFL was further increased with the addition of noble gases, significant increase of CFL emission in the order Xe > Kr > Ar > He was observed. The results could not be normalised with respect to gas concentration due to the lack of solubility data for organic solvents available. In addition to the low vapour pressure solvents isopropanol was investigated because it has a high vapour pressure, however, because of the high fraction of solvent present in the cavitation bubble due to its high vapour pressure, isopropanol decreased CFL. This reaffirms that low vapour pressure liquids are required to generate CFL.

6. The addition of nano-particles to seed nucleation sites for cavitation bubbles was investigated using titanium sulphate nano-particles. Triton X 100 was required to suspend the nano-particles in solution and both triton X 100 and titanium sulphate nano-particles independently caused a small increase in CFL. Triton X 100 reduced the surface tension of the liquid, enabling cavitation bubbles were able to form more easily. The increase in CFL was small when compared to the effect of the addition of noble gases.
7. In order to determine that the only source of light was from CFL, other mechanisms or sources of light such as light scattering, molecular fluorescence and degradation effects were ruled out. The results have shown that light is generated via plasma formation in DMSO and indicated that this method could have applications in atomic emission spectrometry.

Light has been generated via plasma formation and possibly molecular emission in PEG-200 and diethylene glycol.

In conclusion, the results generated for the first time in this research show that light is intense enough from micro-Venturis to be analysed spectroscopically as evidenced by the spectra generated using bandwidth filters. Further investigation would build upon this proof of concept to take CFL to the next level as a potential analytical method.

7.2 Suggestions for further work

The system constructed in this work was a proto-type and was useful for the investigation of CFL in a micro-Venturi. Apart from the glassware the system was constructed using off the shelf components or readily available technology. This process could be developed in a number of ways:

1. Simultaneous acquisition of a large spectral range and isolation of a specific spectral range would allow measurement of excitation and ionisation temperatures using the Boltzmann Plot method. This uses the ratio of two or more integrated line intensities to determine their temperature. It would also enable the isolation of single wavelengths for measurements of molecular and atomic spectra and would identify or rule out spectra from free radical reactions to elucidate possible mechanisms.
2. At present the ideal shape for a Venturi to generate light is unknown therefore the use of modelling software to investigate the optimal geometry

prior to a new Venturi design with tightly controlled parameters is recommended. In this research the use of UV transparent materials was not fully explored. However, the few results which were obtained indicated that there was emission in the UV so construction of Venturis in an optically transparent medium such as quartz is worthy of further investigation.

3. Cavitation occurs around bubble nuclei which weaken the tensile strength of the liquid, thus making it easier to manipulate into a cavitating state. In liquids which do not have numerous bubble nuclei alternative nucleation sites could be introduced to boost CFL. Further investigation into the use of polystyrene and metal nano-particles to seed nucleation sites and therefore CFL could be carried out.
4. During the course of this research it became apparent that the make-up of the cavitating fluid was very important to light emission. The characteristics of the fluid could be altered to boost CFL. The presence of noble gases has been shown to increase the intensity of light detected and this could be expanded to investigate how different concentrations of mono-atomic gases affect CFL to identify the optimal concentration to increase CFL observed. Low density and low vapour pressure liquids have been found to promote conditions favourable for CFL so the determination of an optimal cavitation fluid is necessary.

8 References

1. P. D. Jarman and K. J. Taylor, *British Journal of Applied Physics*, 1965, **16**, 675-682.
2. F. G. Hammitt, *Multiphase Fluid Flow-Theory And Practise*, 1977.
3. T. Koivula, presented in part at the Proc. of 1st FPNI-PhD Symposium, hamburg, 2000.
4. K. S. Kumar and V. S. Moholkar, *Chemical Engineering Science*, 2007, **62**, 2698-2711.
5. X. Wang and Y. Zhang, *Journal of Hazardous Materials*, 2008, **161**, 202 - 207.
6. A. T. J. Hayward, *J. Phys. D-Appl. Phys.*, 1970, **3**, 574-580.
7. G. Kuiper, *Journal*, 2012.
8. F. Caupin and E. Herbert, *Comptes Rendus Physique*, 2006, **7**, 1000-1017.
9. C. K. Su, C. C., B. Kappus and S. J. Putterman, *Physics of Fluids*, 2003, **15**, 1457-1461.
10. W. C. Moss, D. B. Clarke and D. A. Young, *Science*, 1997, **276**, 1398-1401.
11. P. Kobel, Obreschkow, D., de Bosset, A., Dorsaz, N., and Farhat, M., *Experiments in Fluids*, 2009, **47**, 39-48.
12. Q. D. Chen, L. M. Fu, X. C. Ai, J. P. Zhang and L. Wang, *Physical Review E*, 2004, **70**, 047301.
13. Q. D. Chen and L. Wang, *Chinese Physics*, 2004, **13**, 564-570.
14. T. G. Leighton, B. T. Cox and A. D. Phelps, *Journal of the Acoustical Society of America*, 2000, **107**, 130-142.
15. T. G. Leighton, W. L. Ho and R. Flaxman, *Ultrasonics*, 1997, **35**, 399-405.
16. P. D. Jarman and K. J. Taylor, *British Journal of Applied Physics*, 1964, **15**, 321-322.
17. D. P. Schmidt and M. L. Corradini, 1997, **7**, 603-616.
18. W. H. Encyclopedia, Venturi Effect, http://www.worldheritage.org/articles/Venturi_effect, (accessed 1st February 2015).
19. M. J. Ivanov, *Journal*, 2012, DOI: 10.5772/52493.
20. K. Sato, K. Hachino and Y. Saito, presented in part at the ASME Joint Fluids Engineering Conference, Honolulu, Hawaii, 10th July 2003, 2003.
21. C. Mishra and Y. Peles, *Physics of Fluids (1994-present)*, 2005, **17**, 113602.
22. C. Mishra and Y. Peles, *Journal of Microelectromechanical Systems*, 2005, **14**, 987-999.
23. C. Mishra and Y. Peles, *Physics Of Fluids*, 2006, **18**, 1036031 - 1036035.
24. R. Singh and Y. Peles, *Journal of Micomechanics and Microengineering*, 2009, **19**, 025009.
25. C. Mishra and Y. Peles, *Physics Of Fluids*, 2005, **17**, 17861-17876.
26. E. B. Flint and K. S. Suslick, *Journal of Physical Chemistry*, 1991, **95**, 1484-1488.
27. D. Lohse, *Nature*, 2005, **434**, 33-34.
28. Y. Didenko, W. B. McNamara and K. S. Suslick, *Nature*, 2000, **407**, 877-879.

29. N. C. Eddingsaas, *Mechanoluminescence and Sonoluminescence from Acoustic Cavitation*, University of Illinois at Urbana-Champaign, 2008.
30. D. J. Flannigan and K. S. Suslick, *Journal of Physical Chemistry A*, 2006, **110**, 9315-9318.
31. D. J. Flannigan and K. S. Suslick, *Acoustics Research Letters Online-Arlo*, 2005, **6**, 157-161.
32. D. J. Flannigan and K. S. Suslick, *Physical Review Letters*, 2005, **95**, 044301.
33. N. C. Eddingsaas and K. S. Suslick, *Journal of the American Chemical Society*, 2007, **129**, 3838-3839.
34. P. Wallace, K. McCallum, C. L. R. Barnard, C. Clement, J. Marshall and J. Carroll, *Measurement Science & Technology*, 2007, **18**, 740-746.
35. G. J. Posakony, L. R. Greenwood and S. Ahmed, *Ultrasonics*, 2006, **44**, E445-E449.
36. K. S. Suslick, W. B. McNamara and Y. Didenko, *Sonochemistry and Sonoluminescence*, 1999, 191-204.
37. Ta Yeong Wu, Ningqun Guo, Chee Yang Teh and J. X. W. Hay, *Advances in Ultrasound Technology for Environmental Remediation, Springer Science & Business Media*, 2013.
38. C. E. Brennan, *Cavitation and Bubble dynamics*, 1995, P. 20.
39. T. Benson, The First Law of Thermodynamics, http://www.grc.nasa.gov/WWW/k-12/airplane/thermo1.html, (accessed 16/12/13, 2013).
40. S. J. Henderson and R. J. Speedy, *Journal of Physics E-Scientific Instruments*, 1980, **13**, 778-782.
41. W. S. Lamb, *Cavitation and Aeration in Hydraulic Systems, BHRA*, 1987.
42. M. Hüning, *Journal of Turbomachinery*, 2010, **132**, 031017-031017.
43. A. Lichtarowicz, R. K. Duggins and E. Markland, *Journal of Mechanical Engineering Science*, 1965, **7**, 210-219.
44. R. E. A. Arndt and W. K. George, *12th Symposium on Naval Hydrodynamics*, 1979, 327-339.
45. V. S. Moholkar, P. S. Kumar and A. B. Pandit, *Ultrasonics Sonochemistry*, 1999, **6**, 53-65.
46. Peter Atkins and J. D. Paula, *Atkins' Physical Chemistry*, Oxford University Press, 8 edn., 2006.
47. F. M. Leighton T. G., Field J. E., Avellan F., *Journal of fluid mechanics*, 2003, **480**, 43-60.
48. W. Aeschbach-Hertig, F. Peeters, U. Beyerle and R. Kipfer, *Nature*, 2000, **405**, 1040-1044.
49. J. P. Tullis, *Hydraulics of Pipelines*, Wiley-Interscience, 1989.
50. E. Wilhelm, R. Battino and R. J. Wilcock, *Chemical Reviews*, 1977, **77**, 219-262.
51. R. Sander, *Atmos. Chem. Phys. Discuss.*, 2014, **14**, 29615-30521.
52. C. Mishra and Y. Peles, *Journal of Microelectromechanical Systems* 2005, **14**, 987-999.
53. M. Farhat, A. Chakravarty and J. E. Field, *Proceedings of the Royal Society A: Mathematical, Physical and Engineering Science*, 2011, **467**, 591-606.
54. Y. T. Didenko, W. B. McNamara and K. S. Suslick, *Abstracts of Papers of the American Chemical Society*, 1997, **213**, 118.
55. Y. T. Didenko, W. B. McNamara and K. S. Suslick, *Physical Review Letters*, 2000, **84**, 777-780.

56. E. Hywel Evans, Jeffery J. Giglio, Theresa M. Castillano and J. A. Caruso, *Inductively Coupled and Microwave Induced Plasma Sources for Mass Spectrometry*, Royal Society of Chemistry, 1995.
57. S. Martynov, D. Mason and M. Heikal, *Journal of Fluids Engineering*, 2006, **09**, 2006.
58. Y. Yan and R. B. Thorpe, *International Journal of Multiphase Flow,*, 1990, **16**, 1023-1045.
59. M. Sivakumar and A. B. Pandit, *Ultrasonics Sonochemistry*, 2001, **8**, 233-240.
60. Gaylord Chemical, DMSO physical properties, http://www.gaylordchemical.com/index.php?page=101b-dmso-physical-properties, (accessed 10th August 2012, 2012).
61. X. Q. Qian, B. X. Han, Y. Liu, H. K. Yan and R. L. Liu, *Journal of Solution Chemistry*, 1995, **24**, 1183-1189.
62. H. Lee, S. H. Park, Y.-K. Park, B. H. Kim, S.-J. Kim and S.-C. Jung, *Chemistry Central Journal*, 2013, **7**, 156.
63. S. A. Markarian and A. M. Terzyan, *Journal of Chemical & Engineering Data*, 2007, **52**, 1704-1709.
64. A. G. Chakinala, P. R. Gogate, R. Chand, D. H. Bremner, R. Molina and A. E. Burgess, *Ultrasonics Sonochemistry*, 2008, **15**, 164-170.
65. V. G. Deshmane, P. R. Gogate and A. B. Pandit, *Chemical Engineering Journal*, 2008, **145**, 351-354.
66. E. Camerotto, S. Brems, M. Hauptmann, A. Pacco, H. Struyf, P. W. Mertens and S. De Gendt, *Journal of Applied Physics*, 2012, **112**, 114322.
67. G. Federici, B. J. Shaw and R. D. Handy, *Aquatic Toxicology*, 2007, **84**, 415-430.
68. K. R. Weninger, C. G. Camara and S. J. Putterman, *Physical Review Letters*, 1999, **83**, 2081-2084.
69. D. J. Flannigan and K. S. Suslick, *Nature*, 2005, **434**, 52-55.
70. K. J. Taylor and P. D. Jarman, *Australian Journal of Physics*, 1970, **23**, 319-&.